

POLITECNICO DI TORINO

**Corso di Laurea Magistrale
in Ingegneria Energetica**

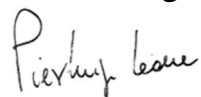
Tesi di Laurea Magistrale

Carbon Dioxide Pipeline Transportation & Network



Relatori

prof. Pierluigi Leone



Marco Cavana



Candidato

Andrea Terenzi



Luglio 2018

Abstract

Effective transportation of carbon dioxide has been identified as a significant challenge for a large-scale deployment of the Carbon Capture and Sequestration (CCS). Pipelines are considered the most cost-effective and safest option to transport large amounts of CO₂ over long distances. The development of integrated pipeline networks may enable a faster large-scale development of the CCS exploiting the economies of scale. The aim of this study was to evaluate pressure and temperature profiles in carbon dioxide pipelines and identify key parameters affecting transport.

A one-dimensional, steady state, non-isothermal, multi-component model for natural gas network was adapted for carbon dioxide. The model is composed of two loop cycles, the fluid-dynamic (flow equation) and the energy problem (energy equation). The physical properties of pure CO₂ have been calculated for dense ($T < 304.25$ K and $p > 73$ bar) and supercritical phase ($T > 304.25$ K and $p > 73$ bar).

The pipeline outlet pressure and temperature were calculated for an Australian network connecting single sources to single storage sites. The outlet temperature was found to reach the soil value for onshore pipes and sea water value for offshore pipes in almost all cases apart from those which are very short (less than 100 km). The outlet pressure was shown to be strictly related to the ambient and inlet temperature, flow-rate, length and diameter of each pipeline. The pressure drop was shown to increase as the inlet temperature increases due to higher level of turbulence during the transport.

The temperature profile along the pipeline for the Latrobe Valley to Gippsland was also assessed. It was found that the pipeline inlet temperature affects the profile due to the heat transfer between the trunk and the environment. The pressure profile along the pipeline was found to be linear and was higher in the onshore trunk where temperature differences between the fluid and the environment are high.

An assessment of pipeline networks was also undertaken providing a booster station at the Junction (Latrobe Valley and South New South Wales to the Gippsland Basin; South-Eastern Queensland). The results show that the pumping duty (kW) is approximately 37% higher when booster stations are not used.

An analysis to understand the effect on the inlet pressure with variable flowrates was carried out using two sources from the South-Eastern Queensland Hub Network (Tarong North and Millmerran). The inlet pressure for Tarong North was shown to be usually higher than for Millmerran due to the longer pipeline length and smaller diameter.

Acknowledgments

Professor Dianne E. Wiley (University of Sydney, AUS), Professor Minh Ho ((University of Sydney, AUS), Professor Pierluigi Leone (Politecnico di Torino, ITA) and Marco Cavana are thanked for the support given in this work as supervisors.

Professor Paul Fennell and Dr. Solomon Brown are thanked for helpful comments related to this work. They thank EP/PO26214/1 (UK CCS Research Centre 2017) for facilitating their involvement.

Contents

Abstract	0
Acknowledgments.....	1
Contents	2
List of Figures	4
List of Tables	6
1. Introduction.....	7
1.1. Carbon Capture and Sequestration (CCS).....	9
1.2. CO ₂ capture.....	10
1.3. CO ₂ sequestration	12
1.4. CO ₂ transportation	13
1.5. CCS in Australia.....	14
1.6. Thesis Objectives	16
2. Literature Review.....	17
2.1. Existing long-distance CO ₂ pipelines.....	17
2.2. Existing pipeline models	20
2.3. Transport Regulations	21
2.4. National codes and standards in Australia	22
2.5. Projects under proposal	23
2.6. Pipeline transportation network.....	25
2.7. Optimal conditions for CO ₂ transportation	28
2.8. Recent Techno-Economic studies about CO ₂ transportation	29
2.9. Equation of State for CO ₂ modelling	33
2.10. Models for CO ₂ heat transfer.....	35
2.11. Depressurization and fracture control.....	38
2.12. Leakage.....	39
3. Methodology	40
3.1. Model Development.....	40
Natural Gas Network	40
Flow equation.....	41
Energy Equation.....	41
Flow equation solution.....	42
Energy equation solution	42
Adapting the model for CO ₂ transportation	43
Model Validation	48
Optimal discretization scheme analysis	49

3.2.	Case studies	51
	Australian Network.....	51
	Understanding pipeline pressure and temperature profile	55
	Network evaluation	55
	Sensitivity Analysis.....	62
3.3.	Economic assumptions	63
	Compression and pumping cost estimation	63
	Pipeline cost estimation	64
4.	Results.....	65
4.1.	Australian Network Results.....	65
4.2.	Temperature and pressure profile along the pipeline	68
4.3.	Latrobe Valley and South New South Wales to Gippsland Basin	70
4.4.	South-Eastern Queensland to the Surat Basin.....	75
4.5.	Effects on pressure due to variable flow-rates: Tarong North and Millmerran to the Surat Basin 82	
4.6.	Sensitivity analysis	85
	Effects of diameter, flow-rate and length.....	85
	Effects of inlet pressure, inlet temperature and heat transfer coefficient.....	88
	Effects of soil temperature	92
5.	Conclusions.....	94
6.	References.....	97
	APPENDIX A: Matlab model.....	101
	APPENDIX B: Network model validation	109

List of Figures

Figure 1) Observed Global mean temperature [1]	7
Figure 2) Causes of CO ₂ emission by fossil fuels [4]	8
Figure 3) Carbon dioxide concentration records [3]	8
Figure 4) Carbon Capture and Storage (CCS) system (The Australian, 2017).....	9
Figure 5) Overview of CO ₂ capture processes and systems [5].....	11
Figure 6) CCS projects in Australia [17]	15
Figure 7) Canyon Reef Carriers Pipeline (Adapted from Kinder Morgan CO ₂ Company).....	17
Figure 8) Bravo Dome Pipeline (Adapted from Kinder Morgan CO ₂ Company)	18
Figure 9) Cortez Pipeline (Adapted from Kinder Morgan CO ₂ Company).....	19
Figure 10) Weyburn Pipeline (Adapted from EnCana Corp.'s)	19
Figure 11) Prescribed standards and codes for CO ₂ pipeline transportation (Global CCS Institute)	21
Figure 12) APGA: Australian Pipelines & Gas Association published the AS2885.....	22
Figure 13) Latrobe Valley Project, Australian Government - Department of Resources, Energy and Tourism (2012)	23
Figure 14) Location of the South West Hub project adapted from [70]	24
Figure 15) Location and facilities description of the Gorgon Project adapted from [71].....	24
Figure 16) CO ₂ transportation infrastructures adapted from Mallon et al. [6]	26
Figure 17) Phase diagram for pure CO ₂ (DNV, 2010)	28
Figure 18) Pipeline route scheme [29].....	30
Figure 19) Multi-criteria applied to two transportation technologies for CO ₂ [31]	30
Figure 20) Network length, cumulative investment cost and number of countries involved evolution in time [26].....	31
Figure 21) Locations of three CO ₂ capture plants, CO ₂ hub terminal, and storage site [72]	32
Figure 22) Deviation of saturated pressure as a function of the reduced temperature T_r adapted from Kim [9]	33
Figure 23) Maximum deviation of CO ₂ density in different phase [25]	34
Figure 24) Density of supercritical CO ₂ for different Equations of State compared to experimental data [24]	34
Figure 25) Temperature sensors added in CO ₂ pipeline [34].....	35
Figure 26) Diagram of the structure of the supercritical CO ₂ in the pipeline [47]	39
Figure 27) CO ₂ jet flow during the leakage process [47]	39
Figure 28) Algorithm flow-chart: fluid-dynamic and thermal problems [14]	40
Figure 29) Joule-Thomson coefficient for CO ₂ as a function of pressure and temperature (NIST Webbook).....	46
Figure 30) Computational time to reach the convergence	49
Figure 31) Temperature Relative Error with respect to 200-node discretization	50
Figure 32) Pressure Relative Error with respect to 200-node discretization	50
Figure 33) Network component types and the operations permitted for each component [11].....	51
Figure 34) Sources and Sinks - Eastern Australia.....	53
Figure 35) Sources and Sinks - Western Australia	53
Figure 36) Pipeline scheme: Latrobe Valley & South NSW to Gippsland.....	56
Figure 37) Transport infrastructure with booster station at the Junction.....	58
Figure 38) Transport infrastructure without booster station at the Junction.....	58
Figure 39) Location of sources and sinks of the hub network described by the CO ₂ CRC [10].....	59
Figure 40) Tarong North & Millmerran to Surat	61
Figure 41) Tarong North CO ₂ captured yearly profile (2010)	61
Figure 42) Millmerran CO ₂ captured yearly profile (2010).....	62

Figure 43) CO ₂ transportation infrastructure adapted from Mallon et al. [6]	66
Figure 44) Latrobe Valley to Gippsland: Temperature and Pressure variation along the pipeline ...	68
Figure 45) Pressure drop over the length using the input parameters of the Latrobe Valley to Gippsland pipeline	69
Figure 46) Pressure and temperature profiles in trunk A, B and C with booster station at the Junction	70
Figure 47) Pressure and temperature profiles in trunk A, B and C without booster station at the Junction	70
Figure 48) Component contribute (%) to the transport infrastructure cost without Booster Station.	73
Figure 49) Component contribute (%) to the transport infrastructure cost with Booster Station	74
Figure 50) Description of the modelled pipeline network as reported by Fimbres et al. [11]	75
Figure 51) Pressure profile in the modelled Hub Network with a fixed value of diameter (450 mm for pipelines 1-7 and 850 mm for pipeline 8)	77
Figure 52) Pressure profile in the modelled Hub Network with the estimated value of diameter by CO ₂ CRC [10]	78
Figure 53) Component contribute (%) to the total infrastructure cost [A\$m] 2017 with a fixed diameter value (450 mm for trunk 1 to 7 and 850 mm for trunk 8)	81
Figure 54) Component contribute (%) to the total infrastructure cost [A\$m] 2017 with an estimated diameter value by the CO ₂ CRC [10]	81
Figure 55) Yearly flow-rate profiles in 2010 for Tarong North and Millmerran	82
Figure 56) Yearly inlet pressure profiles for Tarong North and Millmerran depending on the flow-rate of the two power plants	83
Figure 57) Effects of nominal outer diameter on the outlet pressure in a 1000 km pipeline with a flow rate of 5 Mt/y	85
Figure 58) Effects of flow-rate on the outlet pressure in a 1000 km pipeline with a diameter of 650 mm	86
Figure 59) Effects of onshore pipeline length on the outlet pressure with a diameter of 650 mm and flow-rate of 5 Mt/y	86
Figure 60) Pressure drop with inlet temperature equal to 298,15 K and $U_{\text{onshore}}=3.69 \text{ W/m}^2\text{K}$	88
Figure 61) Pressure drop with inlet temperature equal to 323,15 K and $U_{\text{onshore}}=3.69 \text{ W/m}^2\text{K}$	88
Figure 62) Pressure drop with inlet temperature equal to 298,15 K and $U_{\text{onshore}}=0.1 \text{ W/m}^2\text{K}$	89
Figure 63) Pressure drop with inlet temperature equal to 323,15 K and $U_{\text{onshore}}=0.1 \text{ W/m}^2\text{K}$	89
Figure 64) Pressure drop with inlet temperature equal to 298,15 K with different values of U_{onshore}	90
Figure 65) Pressure drop with inlet temperature equal to 323,15 K with different values of U_{onshore}	90
Figure 66) Temperature drop with inlet temperature equal to 323,15 K with different values of U_{onshore}	91
Figure 67) Temperature and pressure variations along the onshore length with different values of soil temperature	92

List of Tables

Table 1) CCS benefits and challenges summary	Error! Bookmark not defined.
Table 2) Average sea water temperature (Global Sea Temperature).....	44
Table 3) Carbon Dioxide critical properties used by Fimbres et al. [11] for property calculations ..	45
Table 4) Constant parameters for supercritical and liquid phase for the Joule-Thomson coefficient calculation [77]	45
Table 5) Input data for the three pipelines analysed by OLGA	48
Table 6) Comparison with OLGA: inlet temperature equal to 298,15 K	48
Table 7) Comparison with OLGA: inlet temperature equal to 323,15 K	48
Table 8) Input data for the discretization scheme analysis	49
Table 9) Source hubs and storage sites for case study [10]	52
Table 10) Pipeline database for the Australian network [10]	54
Table 11) Input Data: Latrobe Valley to Gippsland	55
Table 12) Input data in case of booster at the Junction.....	57
Table 13) Input data in case of absence of booster at the Junction.....	57
Table 14) Carbon dioxide emission sources described by Fimbres et al. [11]	59
Table 15) Data and equation coefficients for pipeline diameter as a function of distance and flow-rate for steel grade X70 [10]	60
Table 16) Input data used for modelling the Hub Network described by Fimbres et al. [11]	60
Table 17) Input data for the sensitivity analysis	62
Table 18) Unit pipeline cost $C_{u,onshore}$ estimated from data reported by the CO2CRC [10]	64
Table 19) Results for outlet temperature and pressure with inlet temperature at 298,15 K and 323,15 K.....	67
Table 20) Pumping duty (kW) calculated with $\rho=630 \text{ kg/m}^3$ and $\eta_p=0,75$	72
Table 21) Pipeline capital cost (A\$m)	72
Table 22) Compressors, pumps and booster cost calculation (A\$m)	72
Table 23) Pressure and temperature results for the Hub Network with a fixed diameter or the optimal diameter for each pipeline.....	76
Table 24) Compressor cost calculation [A\$m] 2017 with $P_{initial}=0,1 \text{ MPa}$ and $P_{cut-off}=7,38 \text{ MPa}$	79
Table 25) Pumping Duty (kw) and pump cost calculation [A\$m] 2017 with $P_{cut-off}=7,38 \text{ MPa}$, $\rho=630 \text{ kg/m}^3$ and $\eta_p=0,75$	79
Table 26) Pipeline cost calculation [A\$m] 2017 for the Hub Network with fixed or estimated diameter value.....	80
Table 27) Inlet pressure [bar] in Tarong North and Millmerran calculated with the yearly average flow-rate [Mt/y].....	84
Table 28) Results comparison between modelling as a network or as single pipelines	109

1. Introduction

Carbon dioxide (CO₂) is a combustion by-product of fossil fuels (oil, natural gas, coal) used for electricity production, transportation, heating and industrial applications. It is also released when solid organic waste and wood are burned.

CO₂ is the most important anthropogenic greenhouse gas (GHG) contributing to global warming. Each year, 6 billion tons of CO₂ are released in the atmosphere contributing to the greenhouse effect by absorbing infrared radiation produced by solar warming. Global warming refers to the increase in the average temperature of the Earth's near-surface air and oceans in recent decades and it is foreseen to continue.

As can be seen in Figure 1, global average surface temperature has risen about 1 °C to 1.2 °C since 1850 and it will likely rise further 1.1 to 6.4 °C during the 21st century (IPCC, 2007).

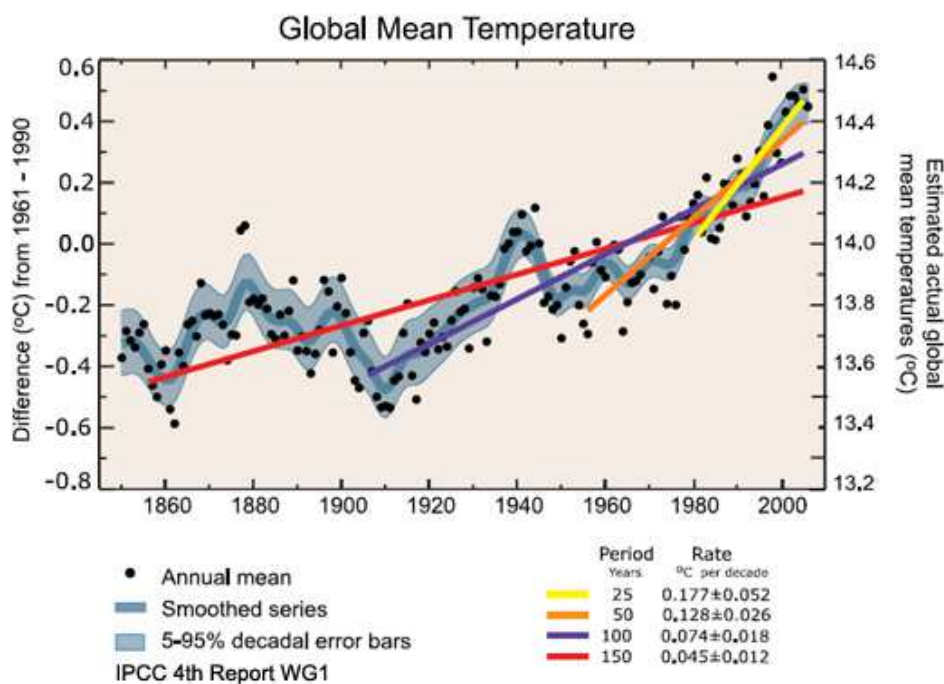


Figure 1) Observed Global mean temperature [1]

It may be noted that carbon dioxide emission and world energy consumption are correlated. It has been reported that the Earth's CO₂ concentration levels have increased from 280 ppm in 1750 to 380 ppm in 2003 (Ehleringer et al., 2005), as can be seen from Figure 3. Carbon dioxide emissions are forecasted to rise to about 44,000 million metric tons by 2030 (IEAGHG, 2009). The largest amount of CO₂ related to human activities is from flue gases due to the combustion of fossil fuels in power plants, as indicated in Figure 2. The largest contribute is represented by coal (43%) followed by petroleum products (36%) and natural gas (20%).

Carbon dioxide emissions from fossil fuel combustion

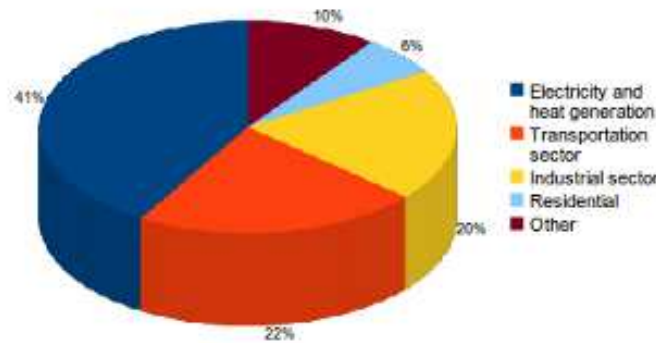


Figure 2) Causes of CO₂ emission by fossil fuels [4]

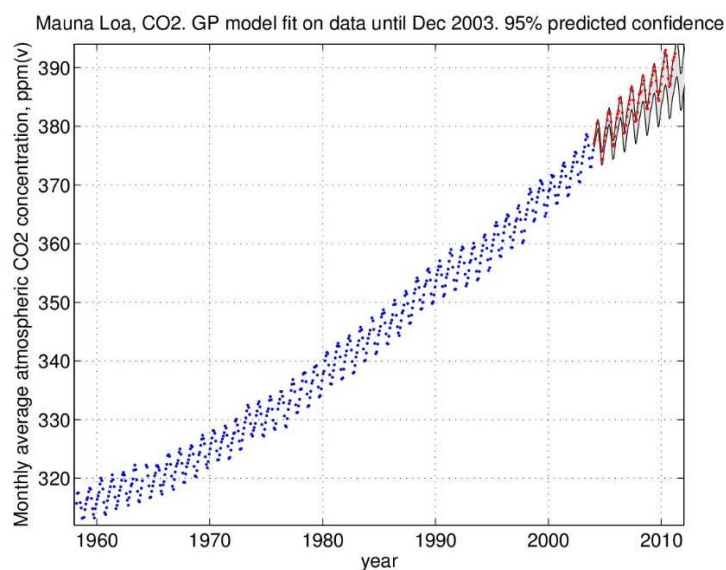


Figure 3) Carbon dioxide concentration records [3]

As reported by the Global CCS Institute (2006), gaseous, liquid and solid carbon dioxide in pure form is generally used for:

- Carbonated beverages;
- Aerosol propellants;
- Recharging/ conservation of natural mineral water, wine and beer;
- Enrichment of air in greenhouses;
- Chemical industry;
- Shielding gas for welding;
- Mineral carbonation;
- Fire extinguishers;
- Gas analysis as carrier gas;
- Dry ice for refrigeration;

- Water treatment;
- Fracturing and acidizing oil wells;
- Tertiary oil recovery.

Other interesting uses include the following:

- Biological/Chemical conversion of CO₂ to fuel or other chemicals;
- Use of CO₂ as a heat exchange fluid or working fluid;
- Cushion gas for Compressed Air Energy Storage (CAES);
- Use of CO₂ as a solvent, fumigant, propellant or inert gas.

1.1. Carbon Capture and Sequestration (CCS)

After 20 years of progress, CCS has been proven in many applications and it is now considered as an important and integral part of global energy and climate strategies, as stated by the International Energy Agency [59]. Underground storage of gases from fossil fuel-fired power plant (coal, natural gas and other sources), industrial furnaces, cement plants etc. is a method for limiting environmental pollution. CCS will be essential in delivering the ambitions of the Paris Agreement and limiting future temperature increases to well below 2°C. The method has the potential for immediate, worldwide deployment where there is compatibility between CO₂ availability from sources and CO₂ sequestration acceptability. In any case, CO₂ must be transported and processed to acceptable compositional level suitable for pipeline transmission.

In a typical CCS facility, as can be seen from Figure 4, CO₂ is processed, dried to reduce the water content to acceptable levels and then compressed. Dry CO₂ is transported from a central processing facility to metering and dispatch stations. It is then transported through a pipeline system consisting of various pumps and valves to designated locations, usually for injection purpose and storage.

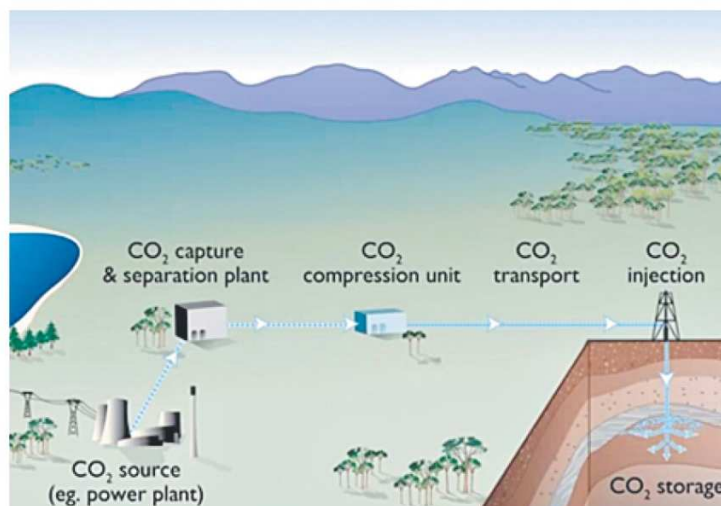


Figure 4) Carbon Capture and Storage (CCS) system (The Australian, 2017)

CCS has moved forward significantly over the past 20 years, with important developments in technology and project experience. In 2016, the International Energy Agency outlined some key points over this time:

- Significant progress has been made but policy support is needed to provide a financial incentive for investment;
- Long-term commitment and stability in policy frameworks is still critical;
- Early opportunities for CCS deployment must be cultivated finding a combination of economic factors and government policies;
- CO₂ storage must be a priority: access to geological storage is potentially the most significant impediment to widespread CCS deployment;
- The availability of CCS in the future depends on present investment on oversize pipelines;
- Community engagement is essential. Successful deployment of CCS will involve improved efforts to ensure the transmission of public information about the potential of the technology;
- Governments and industry should exploit CCS retrofitting opportunities: enhanced oil recovery can generate net emissions reductions and yield storage of CO₂;
- Differentiated business models for CO₂ capture, transport and storage could address some of the challenges faced by integrated projects;

1.2. CO₂ capture

CO₂ capture is particularly interesting in the case of coal-fired power plants as they produce the higher level of carbon dioxide emissions. It is divided, according to the International Energy Agency (2016), into four different groups, as shown in Figure 5:

➤ **Post-Combustion capture**

A mixture of fuel and air is blasted into a boiler and ignited generating steam for a turbine and flue gases that will pass through several “cleaning” processes to remove fly ashes, sulphur and other impurities. The gas stream is cooled down and the CO₂ is separated using either chemical absorption, membrane, adsorption or cryogenic technologies, or a mixture of them.

➤ **Pre-Combustion capture**

An air separation unit produces a stream of almost pure oxygen which flows into the gasifier reacting with pulverized fuel to form Syngas. Steam is then added in a shift reactor converting carbon

monoxide to hydrogen and CO₂. CO₂ is then captured from the gas stream using absorption, membrane or adsorption technologies and, after dehydration and compression, is ready for transportation. In addition, hydrogen becomes the fuel to be burned in the power plant.

➤ Oxy-fuel combustion capture

It consists of burning fuel in a mixture of pure oxygen and recirculated flue gas instead of air having only CO₂ and water as products. This process increases the CO₂ concentration in flue gas making the processing phase before transportation more efficient. It deploys an air separation unit that removes nitrogen from the air using a selective membrane.

➤ Other industrial separation processes

Other several methods may be used. One of the most common is the direct air capture. It consists of removing CO₂ directly from the ambient air. Combining direct air capture with raw materials including fuels, plastics, and even pharmaceuticals with super-porous molecular structures known as covalent organic frameworks with catalysts could act as a carbon dioxide removal technology and utilization of secondary products.

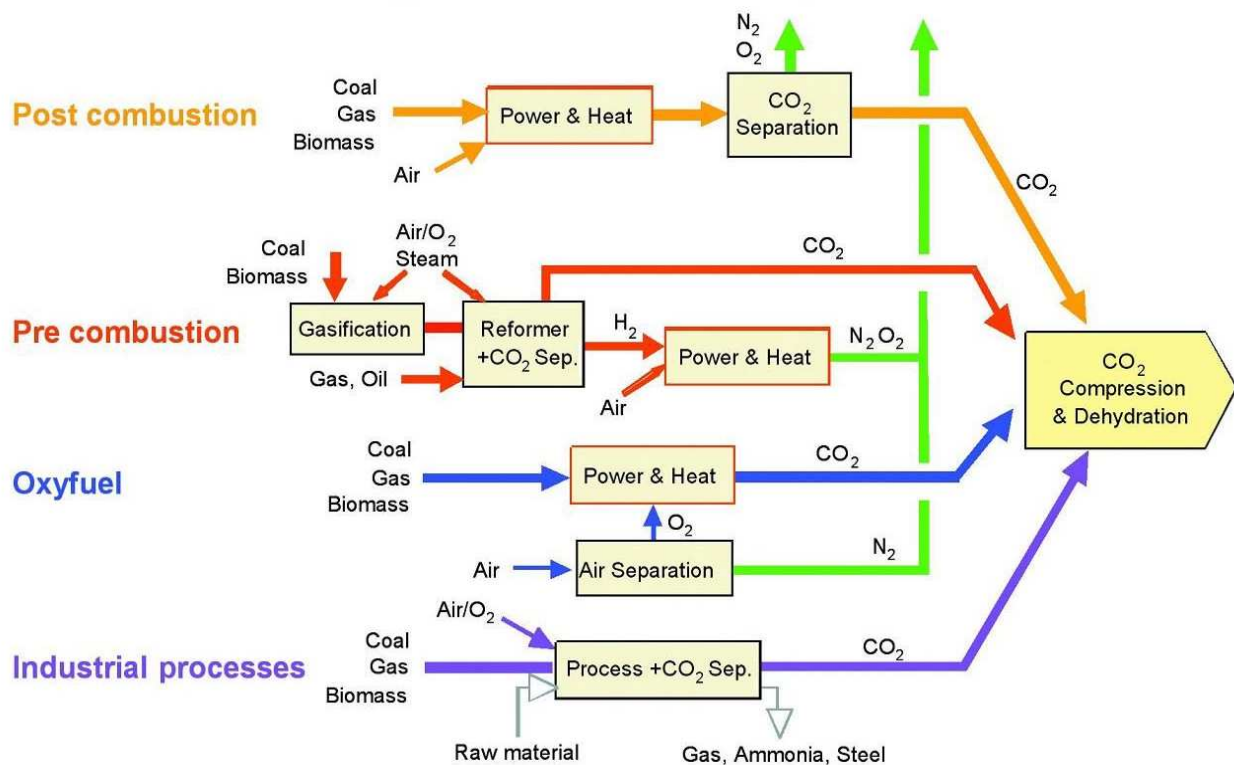


Figure 5) Overview of CO₂ capture processes and systems [5]

1.3. CO₂ sequestration

The geological sequestration of CO₂ can occur by either physical or chemical trapping mechanisms, which control the storage density and leakage potential. The main trapping systems, reported by the IPCC (2007), are:

- **Physical/adsorption trapping:** Molecules are immobilized or trapped at near-liquid-like density on micropore wall surfaces of coal organic matter, kerogen or minerals.
- **Hydrodynamic trapping:** CO₂ occupies the pore space of the rock layer.
- **Solubility trapping:** CO₂ dissolves in water or reacts with it to form carbonic acid.
- **Mineral trapping:** Dissolved CO₂ undergoes chemical reactions with silicate minerals resulting in the formation of a stable solid carbonate mineral phase.

Potential reservoirs for CO₂ storage include:

- Deep saline aquifers;
- Deep un-mineable coal seams;
- Depleted gas fields;
- Depleted oil fields.

Depleted oil and gas reservoirs have several attractive features as storage sites including:

- Proven traps;
- Known geology;
- Least exploration costs;
- Numerous existing sites;

The main challenge for CO₂ sequestration will be matching identified sources with candidate storage reservoirs in terms of injection and geological parameters. In fact, the successful sequestration will require proper site selection using accurate subsurface information, monitoring and verification program, as well as a reasonable legal and regulatory framework. Storage safety can be also enhanced using mitigation measures to stop or control CO₂ releases. Geological storage follows five main steps:

1. A rigorous characterization of the storage site and surrounding area;
2. The construction of geological model of the storage site and surrounding area;
3. Simulation of CO₂ injection into the storage reservoir;
4. Risk assessment and management process;
5. Monitoring program.

1.4. CO₂ transportation

As stated by the IPCC [1], CO₂ can be transported as liquid, solid, dense or supercritical phase. CO₂ must be processed into a form with higher density and lower viscosity in order to transport large quantities efficiently. The various methods for CO₂ transportation are:

- **Ship Transportation**

Generally, CO₂ transportation by ship is very cost effective due to large loading capacity. Ships with a capacity up to 1500 m³ have been used so far. CO₂ can be fully pressurized (high pressure) to prevent phase change at ambient temperature conditions, fully refrigerated (low temperature) to keep it as a liquid or solid under atmospheric pressure or semi-refrigerated and semi-pressurized combined conditions to be kept as a liquid ($T < 304,25 \text{ K}$ and $p > 73 \text{ bar}$). Typically, the offshore transportation involves liquefaction plant, refrigeration cycle, storage, loading on the ship and offloading into a depleted gas field.

- **Truck and Railway Transportation**

Liquified CO₂ can be transported by road or railway tank trucks stored in cryogenic vessels. These forms of transportation provide much lower capacities compared to ships or pipelines. Technically, CO₂ is transported as a liquid, at a temperature of 253 to 243 K and pressure of 17 to 200 bar. The tanks have an inner vessel which is surrounded and supported by an outer one while the space between the two is filled with a natural material that provides insulation.

- **Pipeline Transportation**

Pipelines for the transportation of pure CO₂ have been used since the early 1970s in the enhanced oil recovery (EOR) industry and they are the most widely used transport mode for. Currently, 2400 km of CO₂ pipelines are operating with a total capacity of transporting 44 Mt per year. Typically, pipeline systems are composed of a separation unit, processing including dehydration, compression and metering, pipeline transportation and injection systems. Major existing CO₂ pipelines are presented in section 2.1.

1.5. CCS in Australia

Although Australia is responsible for approximately 4% of global CO₂ emissions, it has one of the highest rate of emissions per-capita of the OECD countries. In 2010, Australia emitted 17.7 tons of carbon dioxide for every inhabitant, compared with a global average of 4.83 per person (The World Bank, 2017). These statistics can be attributed to Australia's relatively high level of socioeconomic development and comfort, reliance on coal and other fossil fuels as energy sources.

Coal-fired electricity, which has high emission intensity, provides around 80% of Australia's total electricity and causes one-third of national total GHG emissions (Australian Trade Commission, 2012). Australia's net total CO₂ emissions were 373.34 Mt in 2014 (International Energy Agency, 2017). Moreover, emissions are expected to increase by 24% above year 2000 levels by the 2020s, due to increased emissions from the growing sectors and increased economic activity (Garnaut, 2011). Therefore, it is evident that CCS deployment can contribute to decrease CO₂ emissions within the sectors with the higher contribution such as electricity and industrial processes. As a part of the Cancun Agreement, Australia has guaranteed to reduce its emissions by 5% relatively to year 2000 levels by 2020 (Garnaut, 2011).

The key points for commercial development of CCS in Australia are its cost, the risk of leakage from storage reservoirs and the high additional energy requirement, known as the energy penalty, associated to its processes. In fact, approximately 30% more coal is required to produce an equivalent amount of electricity if CCS is implemented in a pulverized coal power plant with respect to an equivalent plant without CCS (Spath and Mann, 2001). Currently, there are many demonstration and proposed CCS projects, as shown in Figure 6.

Currently, commercial-scale CO₂ transport pipelines are not operating in Australia. Transmission pipelines used for natural gas transport from production fields to distribution centres cover over 20,000 kilometres across Queensland, Victoria, New South Wales, South Australia, Tasmania and the ACT (ACCC, 2010). These pipelines typically have design specifications and operating conditions not suitable for CO₂ to be transported.

The geographical relationships between large major CO₂ sources and potential storage sites will influence the cost of CO₂ transport. If a large CO₂ source has no appropriate nearby sink, its potential for CCS may be limited by the cost of transmission infrastructures. Seiersten (2001) claimed that approximately 20% (120 million tonnes per year) of Australia's CO₂ emissions can be avoided from ten hubs.

In Table 1, major benefits and future challenges for CCS in Australia have been reported to highlight possible areas of development and advantages of this technology.

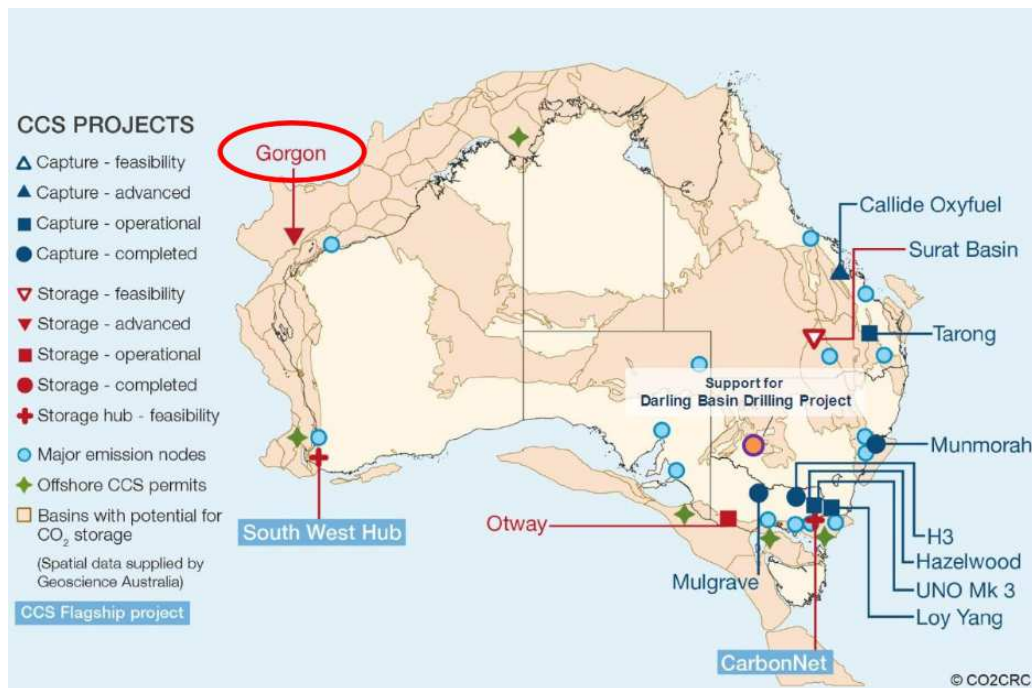


Figure 6) CCS projects in Australia [17]

Benefits	Challenges
Fossil fuels are capable of dispatching electricity whenever there is demand	Cost of CCS will make coal-fired electricity more expensive than wind power
Australia has significant deposits of coal allowing economic benefits for years to come without significant environmental impacts	Leakage from underground or undersea reservoirs
CCS can be used to capture CO ₂ from high-emission industrial processes such as the making of certain chemicals, steel and cement	Scarcity of potential sites and capacity compared to volumes of greenhouse gas needed to be sequestered
CCS has a great impact in reducing greenhouse gas emissions during the transition to sustainable energy supplies.	Existing power stations unlikely to be able to have carbon capture technology retrofitted
	CCS currently requires up to 30% more coal than conventional plants to cover the energy needs of CCS
	Infrastructure requirement would take years to build
	Government investments on CCS research and demonstration projects have been largely cut

Table 1) CCS benefits and challenges summary

1.6. Thesis Objectives

The three main objectives of this thesis are:

- Evaluate the pressure and temperature profiles along the length of carbon dioxide pipelines, for single trunks or hub networks highlighting the main differences in the two cases;
- Analyse the heat transfer between pipeline and the environment (soil for onshore pipelines and sea water for offshore transportation) for different ambient values and pipeline inlet temperatures;
- Identify key parameters which affect the transport in terms of variations in inlet pressure and temperature.

2. Literature Review

In this section, the state of art concerning carbon dioxide transportation through pipeline has been deeply analysed. The majority of the CO₂ pipeline systems is dedicated to enhanced oil recovery (CO₂-EOR), connecting natural and industrial sources of CO₂ with EOR projects in oil fields. Existing long-distance pipelines used for EOR and pipeline models are firstly presented to demonstrate the real development of the CCS technology and research.

The current international and Australian regulations for pipeline transport are commented to comprehend the risks and the current rules. Then, some projects under proposal were described to understand the challenges that must be overtaken to build CO₂ pipeline networks. Furthermore, some recent techno-economic studies are analysed in detail to show how and which parameters affect the transport of carbon dioxide and the cost of the infrastructure. In addition, various models about CO₂ properties calculation and operating conditions are analysed to understand the optimal condition for the pipeline transport.

2.1. Existing long-distance CO₂ pipelines

Canyon Reef

The first large CO₂ pipeline used for Enhanced Oil Recovery in the USA was the Canyon Reef Carriers, built in 1970 by the SACROC Unit in Scurry County, Texas (Figure 7). It is 352 km long with a 16-inch diameter (406 mm) and it has a capacity of 4.4 Mt per year. It is owned by the Shell Oil Company processing gasification plants in the Texas Val Verde basin.



Figure 7) Canyon Reef Carriers Pipeline (Adapted from Kinder Morgan CO₂ Company)

Bravo Dome Pipeline

The 20-inch (508 mm) Bravo Pipeline (Figure 8), owned by Occidental Permian, Kinder Morgan CO₂ and XTO Energy, runs 350 km to the Denver City Hub (Colorado) and has a capacity 7.3 Mt per year. Major delivery points along the line include the Slaughter field in Cochran and Hockley counties, Texas, and the Wasson field in Yoakum County, Texas. It was built in 1984 for the enhanced oil recovery in the Bravo Dome area.



Figure 8) Bravo Dome Pipeline (Adapted from Kinder Morgan CO₂ Company)

Cortez Pipeline

Built in 1982 to supply CO₂ from the McElmo Dome in South East Colorado, the 30-inch (762 mm), 803 km pipeline transports approximately 20 Mt per year to the CO₂ hub at Denver City, Texas. The line starts near Cortez, Colorado, and crosses the Rocky Mountains, where it is interconnected with other CO₂ lines in the Permian Basin previously described (Bravo Dome pipeline). Currently, the Cortez pipeline could handle the emissions of three coal-fired power stations. The Cortez Pipeline (Figure 9) passes through two built-up areas, buried at least 1 m deep and marked on its way to ensure the residents about the pipeline location and safety issues.



Figure 9) Cortez Pipeline (Adapted from Kinder Morgan CO₂ Company)

Weyburn Pipeline

This 330 km, 13-inch (330 mm) diameter system has a capacity of 40 Mt per year in the Great Plains Synfuels Plant near Beulah, North Dakota to the Weyburn project in Saskatchewan for the enhanced oil recovery (Figure 10). It is the world's largest carbon capture and sequestration system as an international collaborative scientific study to assess the technical feasibility of CO₂ storage in geological formations. The project began in 2000 and runs until the end of 2011 collecting data from the actual CO₂-enhanced oil recovery operations in the Weyburn oil field.



Figure 10) Weyburn Pipeline (Adapted from EnCana Corp.'s)

2.2. Existing pipeline models

In this section, some existing models which describe the flow of carbon dioxide in pipeline are presented.

The development of the dynamic two-fluid (gas and liquid) model *OLGA* was started in the early 80s by Statoil in order to meet the two-phase modelling challenges specific to CO₂ pipeline transportation and it's today considered an industry standard for such applications. Today, *OLGA* can solve a three-phase mixture of gas, oil and water and it can handle impurities.

LedaFlow is a transient multiphase flow simulation tool developed in the early 2000s by Total, ConocoPhillips and SINTEF. The *LedaFlow* model is mainly developed for three-phase oil-gas-water mixtures and it is generally applicable for multiphase flow CO₂ transport.

TACITE is a transient multicomponent, multiphase flow simulation tool developed by Elf Aquitaine/Total in the early 1990s. The tool has been developed mainly for simulating natural gas transport. It uses closure relations and thermodynamics based on flow regimes and tabulated properties.

PipeTech is a transient multicomponent simulation tool developed and maintained by professor Haroun Mahgerefteh at Interglobe Ltd. The main focus of *PipeTech* is the simulation of transient behaviour related to accidental depressurization and catastrophic failure of pipelines. The tool is used by the petroleum industry for safety assessment.

Aursand et al. [27] developed a pipeline and fluid flow model showing the difference in fluid dynamics and crack arrest properties of a pipeline pressurized with natural gas (methane) and pure CO₂. The results showed that CO₂ pipelines may be more susceptible to fracture propagation than hydrocarbon pipelines. Therefore, the steel grade and dimensions must be selected carefully. The phase transition of carbon dioxide during depressurization was considered as a crucial factor for a safe and cost-effective transportation.

2.3. Transport Regulations

The design and operation of CO₂ pipelines are subjected to codes and regulations. CO₂ in gaseous and refrigerated liquid forms is classified as a non-flammable, non-toxic gas. In solid form (dry ice), it is classified as a dangerous substance by the UN Recommendations on the Transport of Dangerous Goods. Operational aspects of pipelines are divided into three areas: daily operations, maintenance and health, safety and environment. Overall operational considerations include training, inspections, safety integration, public education, damage prevention programs, communication, facility security and leak detection. Concerning the pipeline design, construction and operation, the major international regulations, reported by Mohitpour et al. [2], are:

- ISO 13623: Petroleum and natural gas industries – pipeline transportation systems;
- ASME B31.4: Pipeline transportation systems for liquid hydrocarbons and other liquids;
- ASME B31.8: Gas transmission and distribution piping systems.

Various international conventions are applied to CO₂ transportation. The most significant of them are the UN Law of the Sea Convention, the London Convention, the Convention on Environmental Impact Assessment in a Transboundary Context (Espoo Convention) and the Convention for the Protection of the Marine Environment of the North-East Atlantic (OSPAR). The Espoo convention covers environmental assessment seeking to ensure the acquisition of adequate information about measures to mitigate harm in developed projects. It promotes the cooperation between States to find the optimal solution concerning environmental assessment of CO₂ pipelines and storage sites.

Major standards and codes for CO₂ pipeline transportation were reported by the Global CCS Institute (Figure 11).

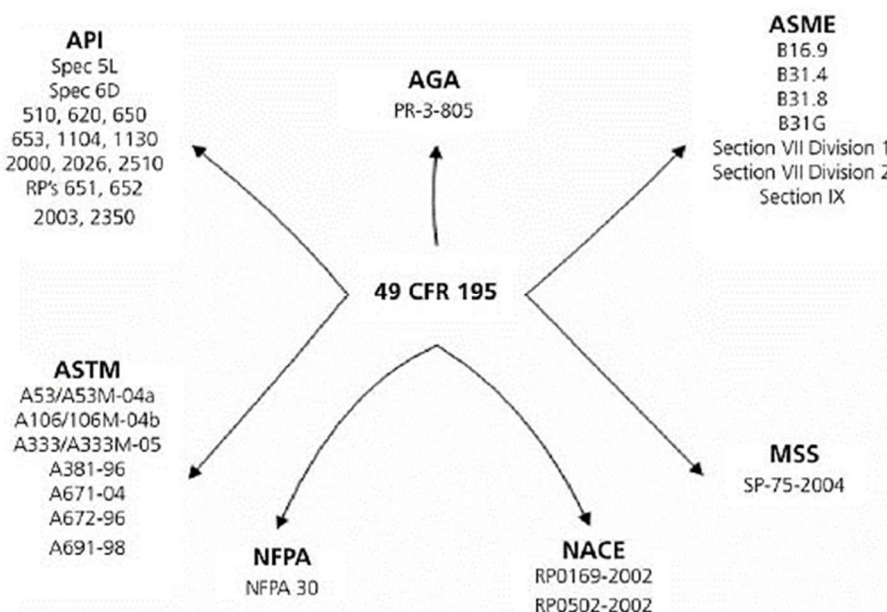


Figure 11) Prescribed standards and codes for CO₂ pipeline transportation (Global CCS Institute)

2.4. National codes and standards in Australia

In Australia, CO₂ pipelines are governed by the Australian Standards, specifically AS2885, which is the standard for liquid and gas petroleum pipelines published by the APGA (Figure 12). The Australian Standards include an appendix which focuses attention to relevant aspects for pipeline design in the case of CO₂ transport, with an emphasis on supercritical phase for carbon sequestration. It includes information regarding CO₂ properties, characteristics, safety issues and the presence of impurities. As an asphyxiant, even small releases of CO₂ could be hazardous. Gas leakages tend to collect in low-lying topographical regions, becoming difficult to be detected [18]. Visser (2008) reported that exposure to concentration of CO₂ higher than 10% may provoke health effects and above 25% leads to a significant asphyxiation hazard. The norm AS 2885.1 (2012) states that a CO₂ concentration higher than 5% can be dangerous for people.

Health risks of CO₂ pipeline transportation can be mitigated through:

- The installation of CO₂ pipelines far from populated and urban areas;
- The use of odorants for the detection of CO₂ leakages;
- The correct design of pipeline isolation valves.

The possibility of accidents for CCS pipelines can be estimated from safety data for Enhanced Oil Recovery pipelines. There are approximately 0.36 safety accidents per 1000 km per year for EOR pipeline in the US (Watt, 2010). Due to more safety issues provided, pipelines in Australia have a failure rate of 0.15 per 1000 km (The Australian Pipeliner, 2010) and no recorded injuries or fatalities. The main causes of safety accidents are relief valve failure, weld, gasket or valve failure, corrosion and outside forces (Doctor and Palmer, 2005). The presence of impurities raises additionally safety issues.



Figure 12) APGA: Australian Pipelines & Gas Association published the AS2885

2.5. Projects under proposal

There are a few projects under proposal worldwide about CO₂ pipeline transport ready to start their operation.

The CarbonNet Project [62] is exploring the feasibility of a commercial scale Carbon Capture Storage network in the Latrobe Valley, Victoria (AUS). As can be seen from Figure 13, the CCS network will transport CO₂ to a suitable storage sites in the offshore Gippsland Basin, which has more than 31 gigatons of storage capacity. During the past site characterization, a risk-based approach was adopted to minimise limitations for potential sources to be connected to the network and to minimise project costs. A geoscience guidance was provided in order to assess the CO₂ purity level, the moisture concentration limit and the effect of impurities such as H₂S and SO₂. It was introduced for safety reasons to minimise the risk of free water and to avoid the potential corrosion effects during pipeline transportation.

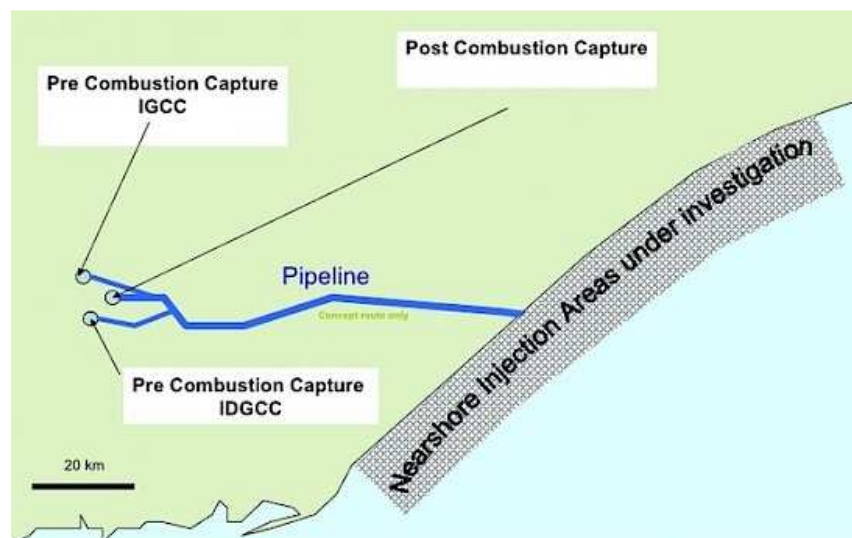


Figure 13) Latrobe Valley Project, Australian Government - Department of Resources, Energy and Tourism (2012)

The South West Hub is created by Western Australia Department of Mines and Petroleum [70]. It has the aim to coordinate the carbon capture and storage feasibility of the Leusueur Sandstone formation in the Harvey – Waroona area, as can be seen in Figure 14. In June 2011, the South West Hub became Australia's first National CCS Flagships project with a CO₂ capture capacity of 2.5 Mt/y and a possibility to grow to 5-6 Mt/y via a 109 km pipeline network. Operations could begin at around 2025. Carbon dioxide would be captured from industrial facilities and power plants and transported via pipeline to onshore injection sites for dedicated geological storage. The planning for CO₂ transportation started with the accomplishment of a detailed mapping of the proposed pipeline route from Kwinana to the Harvey region and operations could begin in 2025.

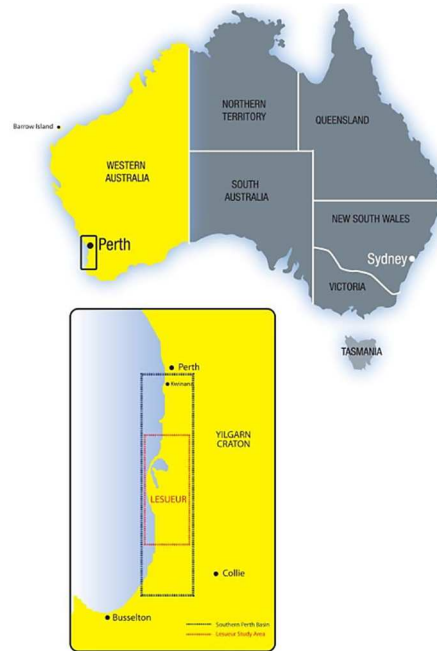


Figure 14) Location of the South West Hub project adapted from [70]

The Gorgon LNG Project located in the north-west coast of Western Australia (Figure 15) is expected to be one of the world's largest carbon capture and storage projects. Operator Chevron [71] and its partners ExxonMobil and Shell received State approvals and licences for the overall project in September 2009. The commercial-scale CCS demonstration project is shown to be able to capture and store between 3.4 and 4 Mt/y of CO₂ with an expected lifetime of 40 years. CO₂ will be captured directly from the gas field before being liquefied and transported by 7km pipeline to the injection site, the Dupuy saline aquifer. The cost is estimated to be \$2 billion in 2010, but then it increased by 46% to approximately \$3 billion. The additional cost consisting in the separation of the CO₂ from the gas was required to avoid the CO₂ causing corrosion and freezing into solid dry ice in the LNG plant.

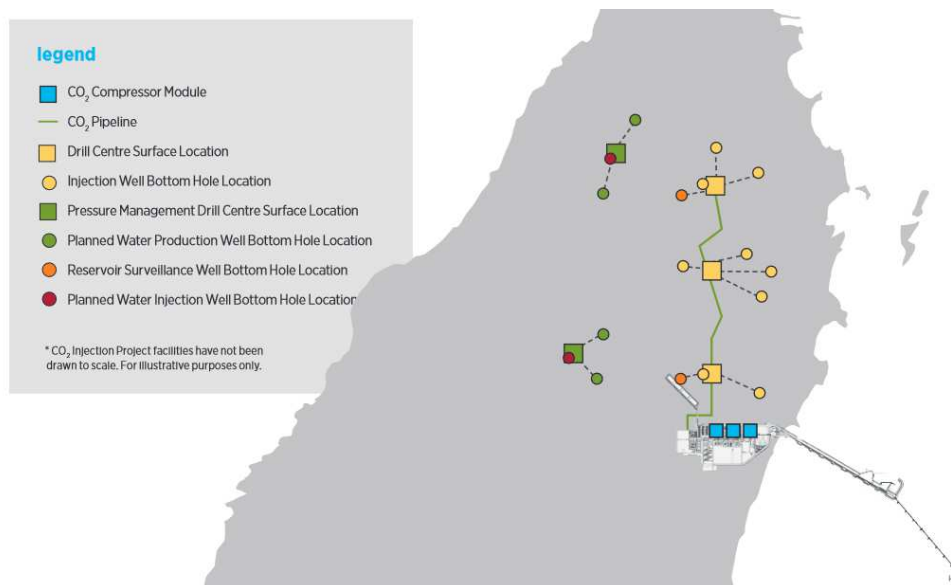


Figure 15) Location and facilities description of the Gorgon Project adapted from [71]

2.6. Pipeline transportation network

CO₂ transportation has been identified as one of the most significant challenges for a large-scale deployment of CCS (IEA, 2016). Pipelines are considered the most cost-effective and safest option to transport large amounts of CO₂ over long distances.

The Joint Research Centre [26] stated that the evolution of a CO₂ transport network will be dictated by the level of CCS deployment and the degree of coordination for its development. The simplest approach would be the construction of numerous pipelines linking individual sources, sized to meet the transport needs of individual capture facilities. This implies that pipelines will be constructed in the context of individual CCS projects and their development will be synchronous to CO₂ capture facilities. It may be an obstacle for the large-scale deployment of CCS impeding the expansion of transcontinental infrastructure and resulting in deployment delays and additional costs.

The development of integrated pipeline networks planned and constructed initially at regional or national level, but oversized to meet the transport needs of multiple and interlinked CO₂ sources, would take advantage of economies of scale and enable the connection of additional CO₂ sources with sinks during the pipeline lifetime (IEA, 2016).

Physical, environmental and social factors determine the input for the conceptual design of a pipeline. System definition, design aspects and purposes definition are required for the preliminary route and cost estimation. Physical characteristics, geotechnical considerations, optimal size and mechanical design of components have to be defined. The topography of the pipeline may include mountains, deserts, river and stream crossings, and, for offshore pipelines, the different levels of very deep or shallow basins. The local environmental data needs to be analyzed. The annual variation in temperature during operation, potentially unstable slopes, frost heave and seismic activity are crucial factors to model pipeline transportation.

A CO₂ transport chain can be analyzed from source to sink. The typical CO₂ pipeline transport system reported in Figure 16 is subdivided in:

- Low-pressure and high-pressure compression;
- Heat exchanger;
- Dehydrating process;
- Low-pressure gas phase and high-pressure dense/supercritical phase transport;
- Onshore and offshore pipelines;
- Injection in the prescribed storage site.

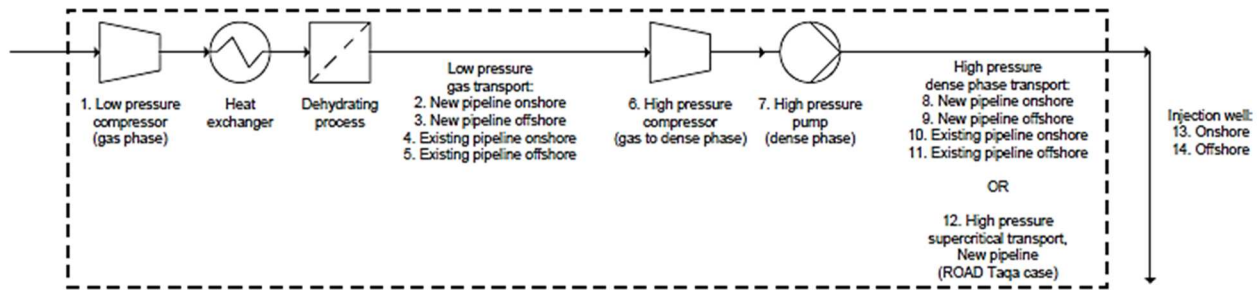


Figure 16) CO₂ transportation infrastructures adapted from Mallon et al. [6]

For the purpose of CO₂ transport in pipelines, the following design considerations were reported to be relevant by Witkowski et al. [48]:

- Pipeline route and profile;
- Pipeline flow;
- CO₂ mixture properties: viscosity and density at several temperature and pressure conditions in the preferred phase for transport (dense or supercritical);
- Maximum inlet and minimum operating pressures;
- Inlet, maximum and minimum operating temperatures;
- Pipe material;
- Pipe diameter, wall thickness and roughness;
- Depth of cover;
- Environment temperature, conductivity, specific heat, density and other properties related to heat transfer;
- Pressure losses;
- Presence of impurities and their influence on the pipeline flow.

It has been acknowledged that the design of CO₂ pipelines for Enhanced Oil Recovery is conservative with excessive investment costs. Therefore, transportation infrastructures used for natural gas cannot be employed for designing supercritical CO₂ pipelines. Re-using existing pipelines would involve additional requirements such as up-rating and changing of use requirements, integrity assessment, capacity requirements, fracture control and availability of the pipeline infrastructure. In fact, due to a significantly higher critical pressure and temperature with respect to natural gas, CO₂ pipelines are subjected to higher operating conditions. Major differences between natural gas and CO₂ operating environments, mechanical design requirements and safety issues are:

- Natural gas is typically transported at 70-100 bar (no phase change), while CO₂ is transported in supercritical phase at 150-170 bar and 313,15-333,15 K;
- Different pipeline fracture control properties;
- CO₂ is non-flammable;

- CO₂ pipelines are considered low risk facilities, but they require rigorous design and inspection;
- Natural gas systems are not usually suitable for high pressure CO₂ transmission.

Properties that make CO₂ significantly different from hydrocarbon fluids are “the decompression and dispersion characteristics and the fact that it is an asphyxiant/toxic rather than combustible” (APIA, 2009). The non-linear behaviour of supercritical CO₂ is associated with the location of the critical point in close proximity to pipeline operating conditions. This trend is further accentuated by the presence of impurities which affect significantly CO₂ transport conditions, pipeline flow assurance and design aspects. Depressurization phenomena, reduced pipeline capacity, ductile fractures, alteration of material properties and, most importantly, release and dispersion of CO₂ and toxic substances are some of the effects related to the presence of impurities.

2.7. Optimal conditions for CO₂ transportation

The physical properties of pure CO₂ have a direct effect on the development of pipeline regulations and design, property equations, operation, maintenance, routing and economic costing. CO₂ can be transported through pipelines as a gas, as a supercritical fluid or as a subcooled liquid, depending on the pressure and temperature conditions in the pipeline system. To reduce difficulties in design and operation, it is generally recommended to operate at pressures higher than 86 bar, as stated by Witkowski et al. [48]. New pipelines have been placed underground, despite the higher initial costs, for environmental, security and safety reasons and because of more stable ground temperature (Witkowski et al., 2014). As can be seen in Figure 17, transportation in dense ($T < 304,25$ K and $p > 73$ bar) or supercritical phase ($T > 304,25$ K and $p > 73$ bar) is preferred because of high density and low viscosity. It is recommended to avoid a two-phase flow due to: cavitation, vapor bubbles in liquid and reduced pipeline capacity. Gas-phase transport was reported by Witkowski et al. [48] to be disadvantageous due to the low density and the high pressure drop.

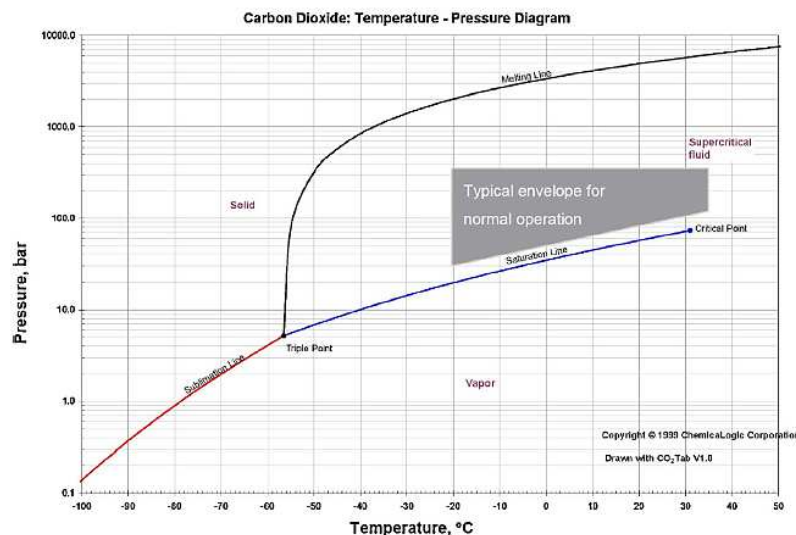


Figure 17) Phase diagram for pure CO₂ (DNV, 2010)

The physical condition which is more suitable for pipeline transportation in terms of pressure and temperature is the supercritical phase. This phase is preferable because it is relatively more stable compared to the liquid state minimizing cavitation problems in system components such as booster stations and pumps. On the other hand, transporting supercritical CO₂ will require a larger pipe size and consumes more compressor power because of lower fluid density. A significant amount of thermal insulation is also required to maintain the phase and contributes to additional cost, since critical temperature is higher than normal ground temperature. CO₂ transportation in the subcooled liquid state has some advantages over the supercritical state transport: lower compressibility and higher density. It allows smaller pipe sizes and generates lower pressure losses.

2.8. Recent Techno-Economic studies about CO₂ transportation

Knoope et al. [28] developed an economic optimization tool for CO₂ pipeline transport. This model aims to evaluate under which conditions gaseous transport is more cost effective than liquid in CO₂ pipeline transport and investigate when booster stations must be installed. The results showed that for onshore pipelines transporting liquid CO₂, the specific pressure drop was about 0.15-0.45 mbar/m, inlet pressure is set at 90-120 bar and booster stations were placed roughly every 100 km. For offshore pipelines, the installation of booster stations was excluded in the model. Consequently, for long offshore CO₂ pipelines the diameter and the inlet pressure were increased. Gaseous CO₂ transport was found to be the best cost-effective option compared to liquid CO₂ transport. Compression at the capture plant resulted to be better than compress CO₂ at the storage location resulting in savings in compression energy which balance the higher construction costs for a larger size pipeline. Nevertheless, if a pressure of 80 bar or higher is required in the storage site, transporting CO₂ as a liquid was found to be more cost-effective than transporting it as a gas. Results also showed that for onshore pipeline transporting liquid CO₂ steel grades X65 and X70 were the optimal choice. Steel grades X42 and X52 for pipeline transporting gaseous CO₂ were used.

Mallon et al. [30] presented an analysis of the overall cost for CO₂ transportation systems of the UK CCS projects in Kingsnorth (approximately 8 km onshore pipeline and 270 km offshore pipeline) and Longannet (approximately 303 km onshore pipeline and 101 km offshore pipeline). For CO₂ transportation, two alternatives were considered: transportation through pipelines and transportation by ships. They found that shipping is an actual solution only when the transported volume is small (less than 0.2 Mt/y), the distance is very long or the ramp up (increase in the production ahead of anticipated increases in product demand) requires it. The expected investment cost for the transportation infrastructure resulted to be similar to the one provided for CO₂ capture. Operational costs for compression and heating at the injection site were found to be relevant. Using existing pipeline showed to lead to a cost saving of 75% compared to building a new pipeline.

Luo et al. [29] carried out techno-economic evaluation based on steady state simulation to explore the optimal design of the CO₂ transportation pipeline network in the Humber Region (UK), as showed in Figure 18. O&M costs of CO₂ compression were found to be marginal. In the optimal network, the annual capital cost of pipelines resulted to be reduced from 69.4 to 53.6 M€ per year. A lower intercooler exit temperature resulted in lower energy and capital costs.

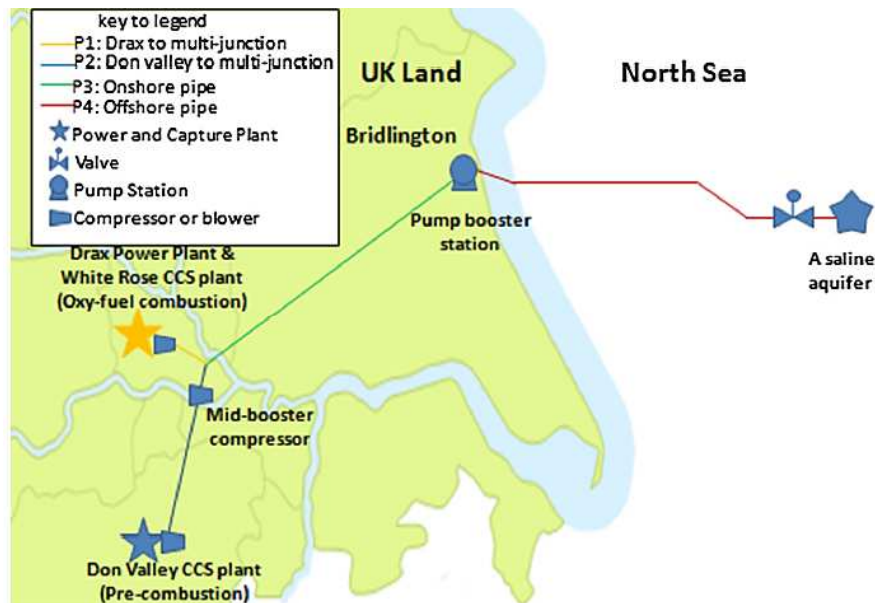


Figure 18) Pipeline route scheme [29]

Simon et al. [31] used a Multi-Criteria Decision Analysis (MCDA) method to compare onshore pipeline and shipping transport between two onshore harbors. In fact, the optimal technology cannot be selected only considering the overall project costs but also achieving a multi-criteria assessment. As can be seen in Figure 19, Seven Key Performance Indicators were considered to benchmark the two technologies. The study showed that onshore pipeline had a Net Present Value of 1.7 B€, which was only 9% less expensive than the shipping option (1.8 B€). Even if there are only small differences between the costs of the two options, pipeline transport resulted to consume much less utilities (fuel, electricity and water) to be less climate intensive than the shipping transport. Breakeven points were shown to be different: onshore pipelines require a higher initial investment (more than twice of shipping option), while shipping leads to higher operating costs.

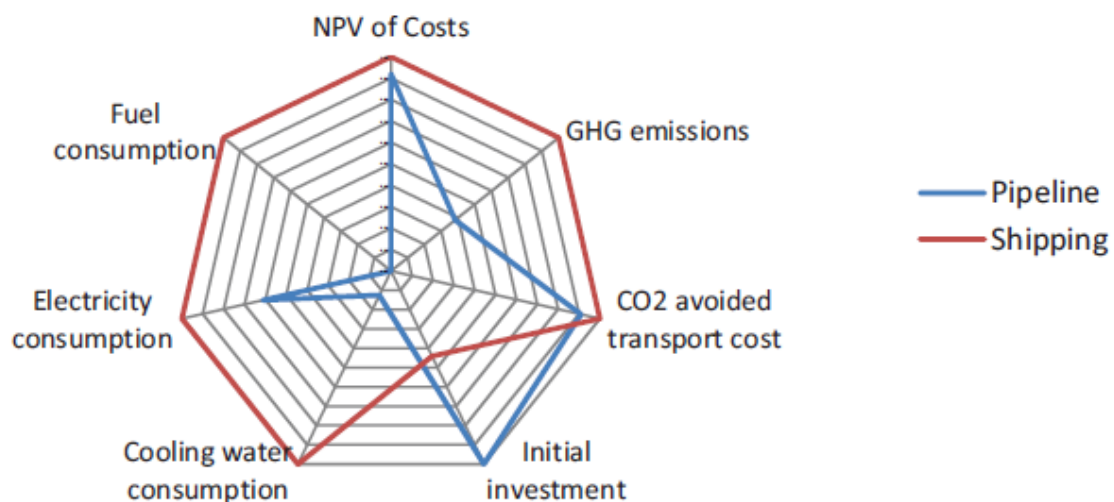


Figure 19) Multi-criteria applied to two transportation technologies for CO2 [31]

Wiley et al. [11] designed a CCS network for a set of emission sources in the south-eastern Queensland region in Australia. The optimal pipeline network obtained by minimising the present value (PV) of the total capital and operating cost of transport was compared to existing pipeline routes. The specific cost of the optimal network was found to be approximately 5% lower than a point-to-point pipeline network connecting each emission source to the same injection site. They showed that this saving was obtained due to a larger diameter provided for higher CO₂ flow rate resulting in shorter network length and lower compression energy requirements. The variation of most modelling parameters was shown in not producing significant effects on the network cost. This is because transport costs (compression and pipelines) resulted to be strongly related to the total length of the pipeline network and CO₂ flow rate. Hence, the optimal network topology was reported to be very similar to the topology with the minimum length.

In the study undertaken by Morbee et al. [26] an optimization model, named *InfraCCS*, was developed with the objective of minimizing the cost of a CO₂ pipeline transportation network in Europe for the period 2015-2050. Shipping was considered as an alternative method for transport and a comparison of the two options was performed. As can be seen in Figure 20, their results showed that the network grows steadily from 2020 until 2030 (from 2005 km to 8803 km) requiring around 9 billion euros of cumulative investment. In 2050, there is a significant step-change leading to a total investment of around 29 billion euros based on a relatively conservative scenario of CCS deployment. By 2030, 16 EU Member States resulted to be involved in cross-border CO₂ transport showing how the coordination is crucial for the development of an optimised trans-European CO₂ transport network.

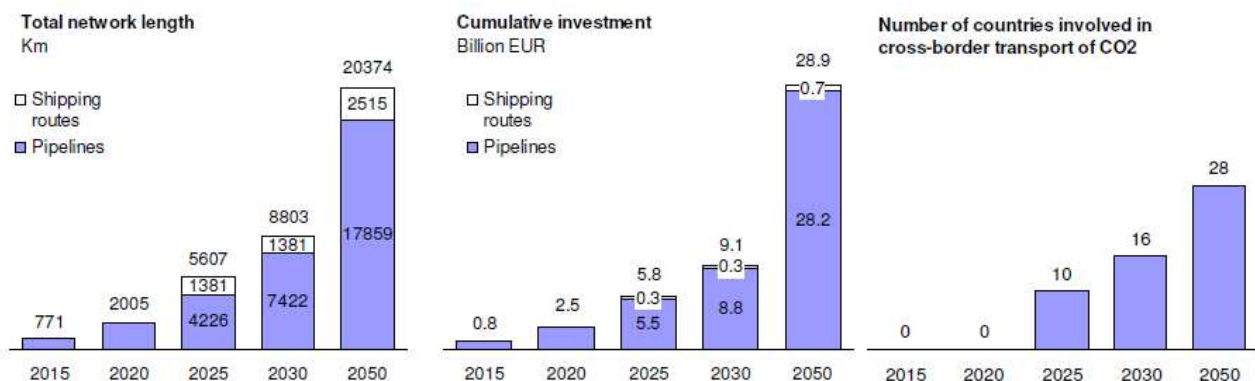


Figure 20) Network length, cumulative investment cost and number of countries involved evolution in time [26]

Kang et al. [72] developed a techno–economic model to calculate the costs of CO₂ transport in the offshore sediments of South Korea, as can be seen in Figure 21. The study considered two different transport methods: pipeline and ships. Three different CO₂ transport scenarios in South Korea were set up based on three power plants and one storage site (Ulleung Basin). The costs of pipeline transport for Scenario 1 was approximately US\$10/tCO₂. This was due to the fact that the electric power consumption for compression was showed not to be significantly affected by the amount of CO₂. They found that the costs for onshore or offshore pipelines significantly decreased as the transport rate increased. Scenario 2 resulted to have a cost reduction not as large as expected with respect to Scenario 1. This was because the cost reduction in the onshore pipeline induced by the lower transport rate (approximately 30%) was counterbalanced by an increased distance in Scenario 2 raising the carrier costs compared to Scenario 1. An additional ship route with a hub was showed to have slightly higher overall costs than an extra ship route without a hub. An extra pipeline route shown similar costs independently on the presence or not of a hub differing only in the sharing of the offshore distance. The incorporation of a hub in Scenario 3 did not result in a higher efficiency because of the relatively short distance from the hub to the storage site.



Figure 21) Locations of three CO₂ capture plants, CO₂ hub terminal, and storage site [72]

2.9. Equation of State for CO₂ modelling

In physics, an equation of state is a thermodynamic equation which describes the state of matter under a given set of physical conditions, such as pressure, volume, temperature (PVT), or internal energy. Equations of state are essential to describe the thermodynamic properties of fluids or mixtures of fluids. In order to design components or run simulation programs using carbon dioxide as a working fluid, an accurate equation of state has to be selected.

The reference equation of state (EOS) for pure CO₂ was proposed by Span and Wagner [8]. It is an empirical equation of state based on the form of a fundamental equation. It covers the fluid region from the triple point temperature (216.692 K) to 1100 K, and pressure up to 8000 bar. The Span and Wagner EOS has 42 coefficients and it was reported to completely represent all the reliable data for pure CO₂ in the homogeneous region (i.e., single phase) and in liquid-vapor region (i.e., two phases).

The equation was developed from experimental data of thermal and caloric properties of CO₂, but some terms are constituted by complex exponential which become difficult for computational calculations. A new simpler equation of state with 30 terms and more simple exponential was proposed by Kim [9], obtaining an efficacious approximation of the Span and Wagner EOS, as can be seen in Figure 20.

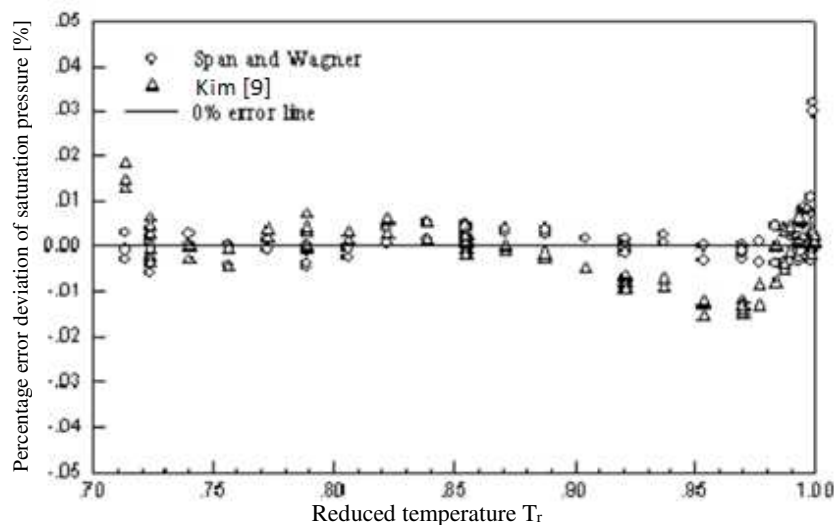


Figure 22) Deviation of saturated pressure as a function of the reduced temperature T_r , adapted from Kim [9]

Three other equations of state (EOS) have been also used for CO₂ transportation modelling:

- Redlich and Kwong equation [60] augmented by Soave [51], who proposed a novel virial equation modified by Plocker [52], known as the LKP equation of state;
- The cubic equation of state proposed by Peng and Robinson with the Boston-Mathias modifications [53], known as the PRBM equations of state;
- The Benedict, Web and Rubin equation [54] with extension by Starling [55], known as the BWRS equations of state [56].

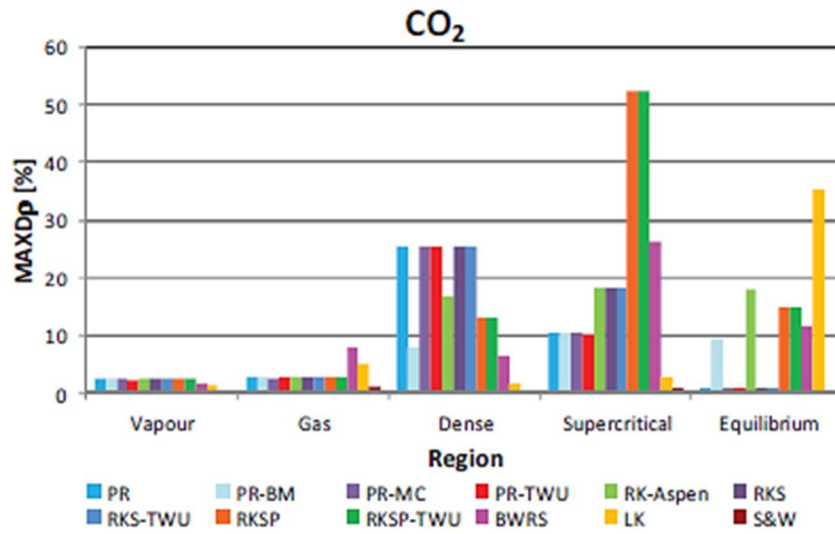


Figure 23) Maximum deviation of CO₂ density in different phase [25]

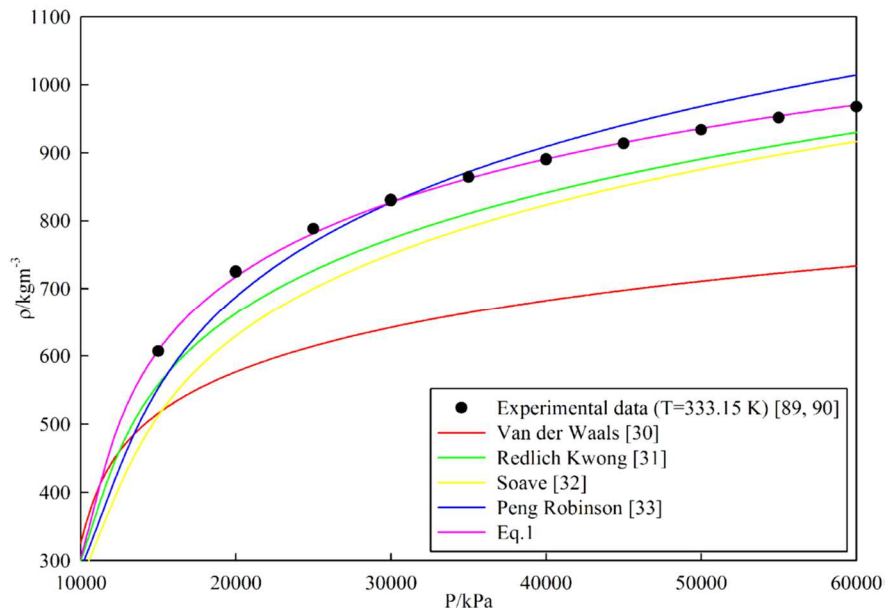


Figure 24) Density of supercritical CO₂ for different Equations of State compared to experimental data [24]

Considering pure CO₂, Figure 23 shows that the Span-Wagner equation has the lowest error in the density prediction in every region analysed. In the vapour region all the equations of state shown a similar behaviour, whereas in the liquid region the density prediction is worse. However, PR-BM equation reported by Serna [19] has a density prediction which is quite acceptable for transport.

Figure 24 shows the overview of the available calculation of carbon dioxide density with different equation of states. It can be seen that the Peng Robinson trend is very similar to experimental data and the Redlich and Kwong EOS modified by Heidaryan et al. [24] in a pressure range suitable for the transport (dense/supercritical phase).

2.10. Models for CO₂ heat transfer

Heat transfer of fluids flowing in pipelines is important to describe how the external temperature affects pressure and temperature profile. Hence, it is essential to understand the optimal way to transport carbon dioxide reducing operational costs. Due to the Joule- Thomson effect, carbon dioxide may cool rapidly. The rate of cooling depends heavily on the heat transfer characteristics of the pipeline, the flow regime and the physical properties of the surrounding. For these reasons, offshore pipelines are often partly or fully covered with gravel or clay. If the temperature at the pipeline surface falls below 0°C, dry ice can form. This must be avoided, as mentioned in 2.7..

Drescher et al. [34] analysed the heat transfer characteristics of offshore or submerged CO₂ pipelines. The contribution to the heat transfer from the surroundings and the insulation needed were calculated to analyse depressurization or crack formation involving rapid cooling. The outer heat transfer coefficient and experimental results were compared. Figure 25 describes thermoelements used in the experiment by Drescher et al. [34] to control temperature along CO₂ pipelines. The overall heat transfer coefficient for offshore pipelines was found to vary from 39.6 to 48.7 W/m²K, while the outer heat transfer coefficient was between 80 and 210 W/m²K.

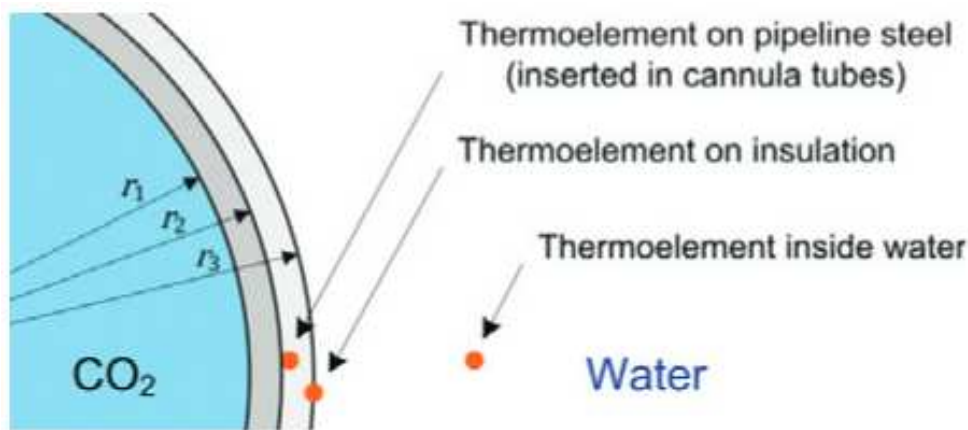


Figure 25) Temperature sensors added in CO₂ pipeline [34]

In the paper undertaken by Munkejord et al. [35], minimum temperature in the pipe wall during depressurization and magnitude of pressure oscillations during transient operation were calculated. A thermodynamic transient flow model for two-phase CO₂ transport was developed. They found that, during depressurization, the pipeline usually became colder than its environment. The outer heat-transfer coefficient was showed to be usually lower than the inner one determining heat transfer towards the surroundings.

Liljemark et al. [37] developed two models to determine pressure and flow fluctuations during pipe cooling and operation modes. The influence of the ambient temperature on heat exchange between carbon dioxide flowing in the pipe and the surroundings was calculated. The risk of two-phase flow during transient and pipe cooling was evaluated. They found that quick shut-down and load change resulted to led to the occurrence of two-phase flow creating pressure oscillations in the pipe, while cooling was found to produce a slow formation of two-phase flow. They found that an underground and insulated pipeline reduces the pressure drop and the energy losses in the system. The pipeline resulted not to need an insulation layer when advantages can be taken from cold ground conditions.

In the paper undertaken from Witkowski et al. [48] the overall heat transfer coefficient k between the ground and the carbon dioxide flux was evaluated. In order to understand the impact of the thermal insulating layer, the pipeline operational parameters (temperature, pressure, density and velocity) were calculated varying pipeline thickness and ambient temperature. Supercritical carbon dioxide density was found to change brusquely along the pipeline once the temperature reached the saturation point and a two-phase flow was obtained. Setting a lower ambient temperature, the carbon dioxide temperature was found to drop more quickly below the critical point and within a very short distance. The pressure drop was also showed to decrease significantly as the ambient temperature decreases demonstrating that low temperature is preferable for pipeline transport.

The paper undertaken by Teh et al. [66] modelled and explored the basic differences between transporting supercritical or liquid CO₂ and studied the heat exchange with the ground during liquid carbon dioxide transportation. Soil temperature, soil type, thermal conductivity of the pipe and elevation of terrain were evaluated. For areas with extremely hot weather such as countries with tropical climate, intermediate refrigeration was found to be necessary for reliquefying carbon dioxide. Transporting the same amount of carbon dioxide over the same distance at constant ambient temperature, same soil type and same buried depth, Teh et al. [66] found that using liquid CO₂ required a smaller and thinner pipe compared to supercritical phase transport. The temperature increase due to pumping was found to be less significant than the one which occurs due to compression. Cooling duty required for injecting liquid carbon dioxide was showed to be lower than injecting in supercritical phase. Hence, it was concluded that significant cost savings can be attained by transporting liquid carbon dioxide. Considering the temperature decrease along the pipe due to a lower ambient temperature of buried pipeline and a low thermal conductivity, it was concluded that

cold climate is more suitable for liquid carbon dioxide pipeline while warmer climate is more suitable for supercritical phase transport in absence of thermal insulations.

The paper proposed by Lake et al. [67] presented the first empirical data of soil temperature and soil moisture profiles in the context of a buried Carbon Capture and Storage transportation pipeline in the United Kingdom operating at higher temperature than ambient. General properties of soil that affect heat transfer was found to be soil bulk density, fraction of mineral and organic material and water content (volume fraction). These properties were showed to affect the volumetric heat capacity of a specific soil type. Thermal conductivity was found to be dependent on these properties because evaporation and condensation within soil pores affect a substantial quantity of heat transfer. A depth of 700 mm was found to have negative effects on pipeline operating temperature and on vegetation growth. Effects of higher soil temperatures resulted to have potential impacts on vegetation through redistribution and loss of available water in the soil.

The aim of the paper by Wetenhall et al. [69] was to investigate the phenomenon of heat transfer from a buried CO₂ pipeline to the surrounding soil and to identify the key parameters that influence the resultant soil temperature. They demonstrated that, unlike natural gas pipelines, carbon dioxide in the pipeline retains its heat for longer distances resulting in the potential to increase the ambient soil temperature. This was found to influence environmental factors such as crop germination and water content. Parameters which affect more the heat transfer were shown to be the inlet temperature and flow rate. Optimal pipeline design resulted to be required to control the heat transfer to the soil and the temperature drop along the pipeline. Fluid temperature was shown not to reach the soil temperature throughout the length of the pipeline. Inlet temperature, flow rate, burial depth and soil conductivity appeared to have the largest effects on temperature drop. The results concluded that the pressure drop was not significantly affected by the input parameters. A change in pipeline diameter resulted in a change in the pressure gradient along the pipeline. It was seen that changing the inlet pressure had very little effect on the outlet temperature of the fluid, however, flow rate was found to have a significant impact.

2.11. Depressurization and fracture control

Depressurization during carbon dioxide transport in pipeline is crucial to control the possible propagation of cracks. Some CO₂ sources, such as coal- or gas-fired powerplants, are fluctuating, since they operate in response to external demands. This will cause a transient flow of CO₂ in the pipeline and a pressure change which may lead to two-phase flow. Start-up, shutdown and accidents are operational modes for which the steady-state methodology could be inadequate. Decompression wave associated with these events may cause the phase change or the formation of dry-ice. The subsequent cooling might render the pipe material brittle and vulnerable to cracks with the possible formation of a running ductile fracture. An accurate prediction of depressurization and cooling are fundamental for assuring safe and reliable planned maintenance or in case of emergency shutdown of a CCS pipeline, as stated by Mahgerefteh et al. [39].

P. Aursand et al. [38] reported the modelling of the wave-propagation velocity (speed of sound) for two-phase flows. The transport of CO₂ was considered to take place at a supercritical pressure. In two- or multiphase flow, the wave-propagation speed (speed of sound) was found not to be a purely thermodynamic function, but it was also dependent on the pipeline topology. It resulted to be a function of in velocity, pressure, temperature and chemical potential. Due to the toxicity of high concentration levels of carbon dioxide, it was showed to be essential predicting the occurrence and evolution of cracks in designing a safe CCS pipeline. High-pressure pipeline design was showed to avoid the formation of cracks and to ensure the quick arrest of any ductile fracture that might form. Running ductile fractures were assessed using semi-empirical methods like the Battelle method [58] where fracture velocity was correlated to the fracture energy. As long as the fracture velocity was smaller than the decompression wave velocity, crack arrest resulted to be assured.

2.12. Leakage

Pipeline leakage process of supercritical carbon dioxide involves complex phenomena because of the high inner pressure next to the leakage point. During the leakage, carbon dioxide undergoes a significant phase change from pure supercritical phase into a supercritical-gas multiphase and an abrupt temperature drop. A layer of dry ice forms and a typical white jet flow appears outside the pipeline and develops during the depressurization process. The multiphase flow may transform into a choked one due to the throttling effect of the leakage nozzle. It is essential to study the leakage process in accidental release during carbon dioxide transport to address safety concerns, risk assessment methods, hazard prediction and new technological developments. Depressurization process and behaviour of multiphase choked flow inside the pipeline as well as the violent temperature drop near the leakage point have to be analysed.

Li et al. [47] developed a model to investigate the thermodynamic and fluid dynamic behaviour in pressurized CO₂ leakage process. Flow characteristics and heat transfer in the leakage processes were studied taking into account the variation of mass flow rate and the thermal boundary layer in the pipeline, as can be seen in Figure 26. Inner pressure, mass flow rate and Nusselt number were studied quantitatively based on experimental data. The jet flow exhibited a strong Joule-Thomson effect due to the high-pressure expansion and the air around the leakage nozzle experienced a quick temperature drop and then volatilized quickly (Figure 27).

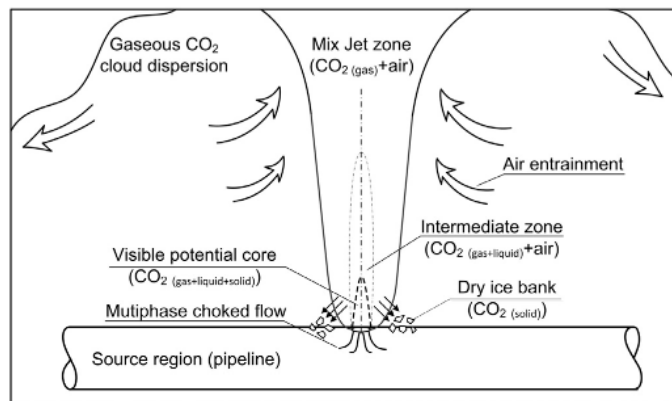


Figure 26) Diagram of the structure of the supercritical CO₂ in the pipeline [47]

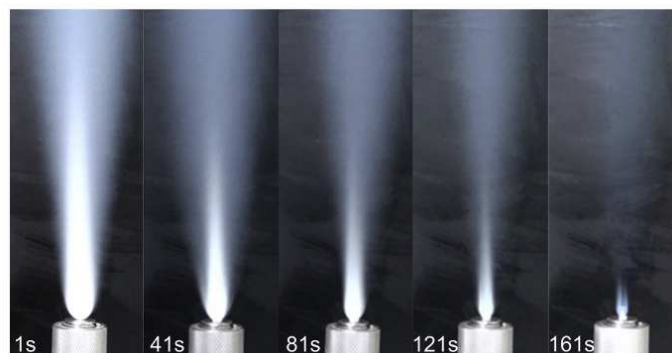


Figure 27) CO₂ jet flow during the leakage process [47]

3. Methodology

In this section, an Australian pipeline transportation network is described using data reported by the CO2CRC [10] and general assumptions are presented. The model proposed by Pellegrino et al. [12] is introduced and adapted for carbon dioxide pipeline transportation. The input parameters used for carbon dioxide are presented. Concerning the model validation, results are compared to data obtained by OLGA and a discretization scheme analysis is also performed to understand the optimal number of subintervals in which the pipeline should be divided to be more accurate. Modelled case studies with specific input data are presented.

3.1. Model Development

Natural Gas Network

The model developed by Pellegrino et al. [12] is a one-dimensional, steady state, non-isothermal, multi-component model for a natural gas network, as can be seen in the model flowchart in Figure 28. Their objective was the prediction of:

- Mass flow-rate in each branch;
- Temperature and pressure in each node;
- Natural Gas composition in each node;

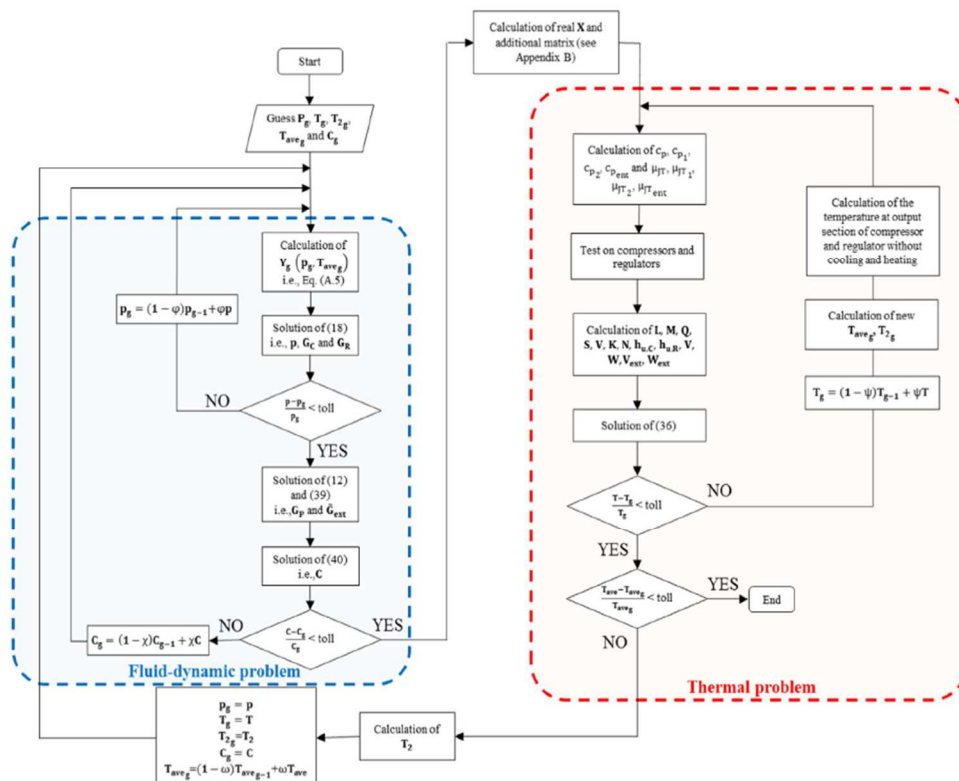


Figure 28) Algorithm flow-chart: fluid-dynamic and thermal problems [14]

Modelling the whole network was presented as a topological problem linked with fluid-dynamic and thermal ones. Momentum balance (flow equation), energy balance (energy equation) and mass balance (continuity equation) were extended to the whole network in order to get pressure and temperature predictions. This set of solving equations in differential form was applied to each branch with the chosen equation of state. Considering the gravitational and kinetic terms as negligible and exploiting a virial Equation of State [13], the thermo-fluid-dynamic problem was solved as follows.

Flow equation

$$\frac{dp}{dx} - \frac{f_d}{2D} \rho u |u| = 0$$

p is the pipeline pressure [Pa];

f_d is the Darcy friction factor calculated by the Colebrook-White equation [14];

D is the pipeline diameter [m];

u is the velocity of the flow [m/s];

Energy Equation

$$G \frac{dh}{dx} + U_L (T - T_s) = 0$$

G is the mass flow rate [kg/s];

h is the enthalpy of the flow [J/kg];

U_L is the thermal conductivity [W/mK];

T is the temperature of the flow [K];

T_s is the ground temperature [K];

Firstly, the fluid-dynamic problem was solved independently from the energy one until the convergence was reached in order to obtain p_{out} . Then, the thermal problem was solved assuming p_{out} from the previous step and obtaining T_{out} which was checked with T_{guess} iteratively until convergence was reached. A final check was performed between T_{avg_new} and T_{avg_old} .

Flow equation solution

$$p_{in}^2 - p_{out}^2 = \frac{z_{avg} R T_{avg} f_{d,avg} L}{D A^2} G^2$$

p_{in} is the pipeline inlet pressure [Pa];

p_{out} is the pipeline outlet pressure [Pa];

L is the pipeline length [m];

z_{avg} , T_{avg} , $f_{d,avg}$ are respectively the average compressibility factor, the average temperature and the average Darcy friction factor;

Rearranged in a more applicable way using the pseudo-conductance of the pipe $Y(p)$, the previous equation becomes:

$$G = Y(p)(p_{in} - p_{out})$$

$$Y(p) = A \frac{(p_{in}^2 - p_{out}^2)^{0.5}}{|p_{in}^2 - p_{out}^2|^{0.5}} \left(\frac{D}{z_{avg} R T_{avg} f_{d,avg} L} \right)^{0.5}$$

Energy equation solution

$$T_{out} = \frac{\beta}{\beta + \gamma} T_s [1 - e^{-(\beta + \gamma)L}] + T_{in} e^{-(\beta + \gamma)L}$$

$$\beta = \frac{U_L}{G \bar{c}_p}$$

$$\gamma = \bar{\mu}_{JT} \frac{f_{d,avg} z_{avg} R G |G|}{2 D p_{avg} A^2}$$

$\bar{c}_p = c_p(T_{avg})$ is the average molar constant pressure specific heat $\left[\frac{J}{molK} \right]$;

$\bar{\mu}_{JT} = \mu_{JT}(T_{avg}, p_{avg})$ is the average Joule-Thomson coefficient $\left[\frac{K}{Pa} \right]$;

p_{avg} is the average pressure [Pa];

A is the pipeline area [m²];

Then, once determined T_{out} , they calculated the average temperature T_{avg} :

$$T_{avg} = \frac{1}{L} \int_0^L T dx = \frac{1}{L} \left[\frac{\beta}{\beta + \gamma} T_s L + \left(\frac{T_{in}}{\beta + \gamma} - \frac{T_s}{(\beta + \gamma)^2} \right) (1 - e^{-(\beta + \gamma)L}) \right]$$

The thermo-fluid-dynamic problem was then extended to the whole network (topological problem) expressing it in matrix form. The Incidence Matrix was introduced in order to describe source or sink nodes and to identify exchanged flows with the environment.

Adapting the model for CO₂ transportation

The model proposed by Pellegrino et al. [12] was adapted to carbon dioxide property calculation suitable for the transportation in pipelines. According to Lüdtke [57], carbon dioxide transport in supercritical state occurs at higher pressure ranges. Hence, the cubic equation of state formulated by Peng and Robinson (**PR**) was used for modelling the carbon dioxide transport. The PR equation was chosen as it has one of the lowest maximum variation of density in the supercritical region and it better approximates experimental data than Span and Wagner EOS.

The Peng and Robinson equation of state as reported by Serna [19] was used in this thesis and as follows:

$$p = \frac{RT}{V_m - b} - \frac{a\alpha}{V_m^2 + 2bV_m - b^2}$$

$$a = \frac{0.457235R^2T_c^2}{p_c}$$

$$b = \frac{0.077796RT_c}{p_c}$$

$$\alpha = (1 + \kappa(1 - T_r^{0.5}))^2$$

$$\kappa = 0.37464 + 1.54226\omega - 0.26992\omega^2$$

In polynomial form:

$$A = \frac{a\alpha p}{R^2 T^2}$$

$$B = \frac{bp}{RT}$$

$$Z^3 - (1 - B)Z^2 + (A - 2B - 3B^2)Z - (AB - B^2 - B^3) = 0$$

Where ω is the *acentric factor*, R is the *universal gas constant* and Z is the *compressibility factor*. It was calculated, as suggested by Serna [19], as a Matlab function of CO₂ pressure and temperature. The compressibility factor was obtained as the real positive root of the previous equation.

CO₂ stream flowing in the pipeline exchanges heat with the environment. Soil temperature for onshore pipelines and sea water temperature for offshore pipelines have been assumed.

The average yearly soil temperature at 20 cm from the ground in New South Wales reported by the Department of Primary Industries (NSW Government) [75] was used for onshore transportation.

The average sea water temperatures in Victoria, Queensland, New South Wales and Western Australia reported in the Global Sea Temperature website [76] were used for offshore transportation (Table 2).

$$T_{soil,20cm,NSW}^{avg} = 292,65 \text{ K}$$

Table 2) Average sea water temperature (Global Sea Temperature)

State	Sea Water Temperature [K]
Victoria	289,2
South Queensland	297,4
North Queensland	299,3
North NSW	296,1
South NSW	293,8
Western Australia	294,2

The thermal conductivity was needed for the calculation of heat transfer from the pipe to the surroundings. The overall heat transfer coefficient assumed by Pellegrino et al. [12] was used for onshore pipelines. The overall heat transfer coefficient proposed by Drescher et al. [34] was used for offshore pipelines.

$$h_{onshore} = 3.69 \left[\frac{W}{m^2 K} \right]$$

$$h_{offshore} = 39.6 \left[\frac{W}{m^2 K} \right]$$

Viscosity μ , density ρ , compressibility z and isobaric heat capacity c_p were calculated for different values of pressure and temperature along the pipeline length, as proposed by Fimbres et al. [11], using a function to predict CO₂ main properties based on parameters reported in Table 3.

Table 3) Carbon Dioxide critical properties used by Fimbres et al. [11] for property calculations

Parameter		Value
M	Molar Mass (g/mol)	44,0095
P _c	Critical Pressure (bar)	73,8
T _c	Critical Temperature (K)	304,2
V _c	Critical Volume (m ³ /mol)	0,000094
Z _c	Critical Compressibility (-)	0,274
w	Acentricity Factor (-)	0,224
visc	Dynamic Viscosity at 300 K (cP)	0,015
C _{p0}	Isobaric Heat Capacity at standard condition (kJ/kgK)	0,8412

The Joule-Thomson effect expresses the real-gas deviation from ideal-gas behaviour and it is fundamental for a correct modelling. In order to accurately predict the Joule–Thomson coefficient expressed in K/MPa at different phase states, a 25-parameter Joule-Thomson coefficient improved equation proposed by Wang et al. [77] was used in this report. The constant parameters, presented in Table 4, depend on the CO₂ phase and the proposed prediction can accurately describe the drastic change near the critical point. The value obtained is compared to the Joule-Thomson coefficient from the NIST presented in Figure 29.

Table 4) Constant parameters for supercritical and liquid phase for the Joule-Thomson coefficient calculation [77]

Parameter	Supercritical	Liquid
a1	0,000320416	-0,97691
a2	-0,000500541	-0,17001
a3	-1,240038034	2,588231
a4	1,602043851	-3,58062
b01	26,9938414	-1,04241
b02	31,85673253	-1,10319
b03	-4,924875039	-1,61615
b04	-27,30412073	3,007577
b05	-1,398898202	0,865499
b06	-26,35582147	4,178501
b07	-1,547471619	43,88879
b11	1,614587686	0,091823
b12	-0,687932605	-1,40486
b13	7,202133882	2,351797
b14	1,943701324	1,398443
b15	4,656579412	5,916127
b16	-3,790346436	0,491014
b17	-15,32574224	3,485393
b21	4,657393579	-2,04372
b22	-1,750785386	0,765129
b23	7,711345498	-1,50194
b24	5,195716844	1,31922
b25	5,809280334	2,837301
b26	-7,830618934	0,109432
b27	2,217206517	-0,78721

$$\eta = \frac{\left(\frac{p}{p_c}\right)^{a_1} - \left(\frac{2}{p_c}\right)^{a_2}}{\left(\frac{40}{p_c}\right)^{a_3} - \left(\frac{2}{p_c}\right)^{a_4}}$$

$$\eta_1 = \frac{\left(\frac{16}{p_c}\right)^{a_1} - \left(\frac{2}{p_c}\right)^{a_2}}{\left(\frac{40}{p_c}\right)^{a_3} - \left(\frac{2}{p_c}\right)^{a_4}}$$

$$\eta_2 = \frac{\left(\frac{30}{p_c}\right)^{a_1} - \left(\frac{2}{p_c}\right)^{a_2}}{\left(\frac{40}{p_c}\right)^{a_3} - \left(\frac{2}{p_c}\right)^{a_4}}$$

Where $\frac{2}{p_c}$ was set at 0.27, $\frac{16}{p_c}$ was set as 2.17, $\frac{30}{p_c}$ was set as 4.06 and $\frac{40}{p_c}$ was set at 5.42.

$$\mu_{JT-(0)} = b_{01} + b_{02}T_r^{b_{03}} + b_{04}T_r^{b_{05}} + b_{06}T_r^{b_{07}}$$

$$\mu_{JT-(1)} = b_{11} + b_{12}T_r^{b_{13}} + b_{14}T_r^{b_{15}} + b_{16}T_r^{b_{17}}$$

$$\mu_{JT-(2)} = b_{21} + b_{22}T_r^{b_{23}} + b_{24}T_r^{b_{25}} + b_{26}T_r^{b_{27}}$$

$$\mu_{JT} = \left(\frac{(\eta - \eta_1)(\eta - \eta_2)(1 - (\eta - \eta_1))}{\eta_1\eta_2} \mu_{JT-(0)} + \frac{\eta(\eta - \eta_2)(\eta - 1)}{\eta_1(\eta_1 - \eta_2)(\eta_1 - 1)} \mu_{JT-(1)} \right. \\ \left. + \frac{\eta(\eta - \eta_1)(\eta - 1)}{\eta_2(\eta_2 - \eta_1)(\eta_2 - 1)} \mu_{JT-(2)} + \frac{\eta(\eta - \eta_1)(\eta - \eta_2)}{(\eta_1 - 1)(\eta_2 - 1)} \right)$$

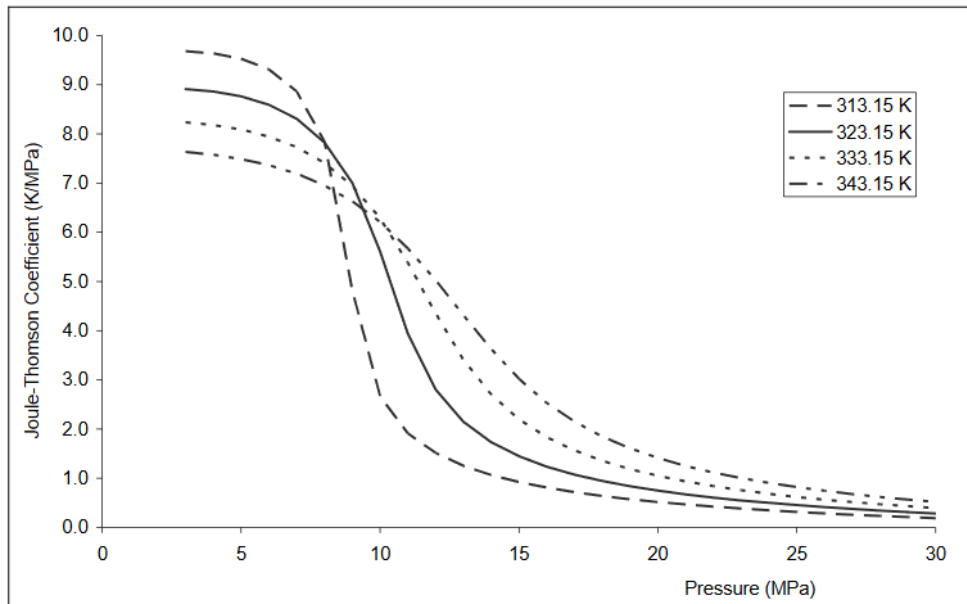


Figure 29) Joule-Thomson coefficient for CO₂ as a function of pressure and temperature (NIST Webbook)

Pipeline flow velocity (v) and Reynold number (Re) were calculated as follows:

$$v = \frac{G}{\rho \left(\frac{\pi D^2}{4} \right)}$$

$$Re = \frac{\rho v D}{\mu}$$

The Fanning friction factor for carbon dioxide is calculated from the Colebrook-White equation:

$$\begin{cases} f = \frac{64}{Re} & Re < 2300 \\ f = 0.06539 \exp \left(- \left(\frac{Re - 3516}{1248} \right)^2 \right) & 2300 \leq Re \leq 3400 \\ \frac{1}{2\sqrt{f}} = -2.0 \log \left(\frac{\varepsilon}{3.7 D} - \frac{5.02}{Re} \log \left[\frac{\varepsilon}{3.7 D} - \frac{5.02}{Re} \log \left(\frac{\varepsilon}{3.7 D} + \frac{13}{Re} \right) \right] \right) & 3400 < Re < 2 \times 10^6 \end{cases}$$

The Darcy friction factor is obtained from the Fanning value as follows:

$$f_d = 4 f$$

Where ε is the roughness ($\varepsilon=45.72 \mu\text{m}$) for a carbon steel pipe (McCoy and Rubin, 2008).

Model Validation

Results obtained from the developed model have been compared with results obtained by *OLGA* using the same input data for modelling pipelines. The relative error for outlet pressure and temperature with respect to their results was analysed to comprehend the quality of the results from the developed model.

Three pipelines (Table 5) were analysed setting the inlet temperature at 298,15 or 323,15 K and estimating the differences between the two models.

In Table 6 and 7, results for outlet pressure and temperature values calculated by the two models have been reported as a model validation.

Table 5) Input data for the three pipelines analysed by OLGA

Pipeline	Flow-rate (Mt/y)	Nominal pipeline outer diameter (mm)	Total distance (km)	Ambient Temperature (K)	Pipeline inlet pressure (bar)	Roughness (μm)	Overall heat transfer coefficient ($\text{W/m}^2\text{K}$)
1	1	250	37	290,76	102	45,72	3,96
2	18	1200	1312	292,65	149	45,72	3,96
3	12,9	1350	574	292,65	149	45,72	3,96

Table 6) Comparison with OLGA: inlet temperature equal to 298,15 K

Pipeline	Pipeline outlet pressure present work (bar)	Pipeline outlet pressure OLGA (bar)	Pipeline outlet temperature present work (K)	Pipeline outlet temperature OLGA (K)	Pressure relative error (%)	Temperature relative error (%)
1	96,7	97	292,74	292,45	-0,3	0,10
2	132,5	133	292,59	292,65	-0,4	-0,02
3	146,9	146	292,64	292,65	0,6	-0,003

Table 7) Comparison with OLGA: inlet temperature equal to 323,15 K

Pipeline	Pipeline outlet pressure present work (bar)	Pipeline outlet pressure OLGA (bar)	Pipeline outlet temperature present work (K)	Pipeline outlet temperature OLGA (K)	Pressure relative error (%)	Temperature relative error (%)
1	94,8	94	305,45	306,15	0,9	-0,23
2	132,2	132,5	292,59	292,65	-0,2	-0,02
3	146,9	146	292,64	292,65	0,6	-0,003

As can be seen from Table 8 and 9, the relative error with respect to the results from *OLGA* for pipeline outlet pressure is always well below the 1%, while it is negligible for the outlet temperature.

Optimal discretization scheme analysis

In this section, the optimal number of intervals in which the pipeline may be subdivided has been calculated. The pipeline presented in Table 8 was subdivided in 10, 50, 100 or 200 intervals to calculate the computational time to reach the convergence and the relative error for temperature and pressure in each node with respect to the best case (200 intervals).

Table 8) Input data for the discretization scheme analysis

Parameters	Value
Roughness [μm]	45,72
Heat Transfer Coefficient [$\text{W/m}^2\text{K}$]	3,69
External Temperature [K]	292,65
Diameter [mm]	600
Flow-rate [Mt/y]	5
Pipeline length [km]	1000
Pipeline Inlet Pressure [bar]	150
Pipeline Inlet Temperature [K]	323,15

Figure 30 presents results for the computational time needed to reach the convergence with the specified number of intervals. Figure 31 and 32 report results for the temperature and pressure relative error with respect to a 200-node discretization.

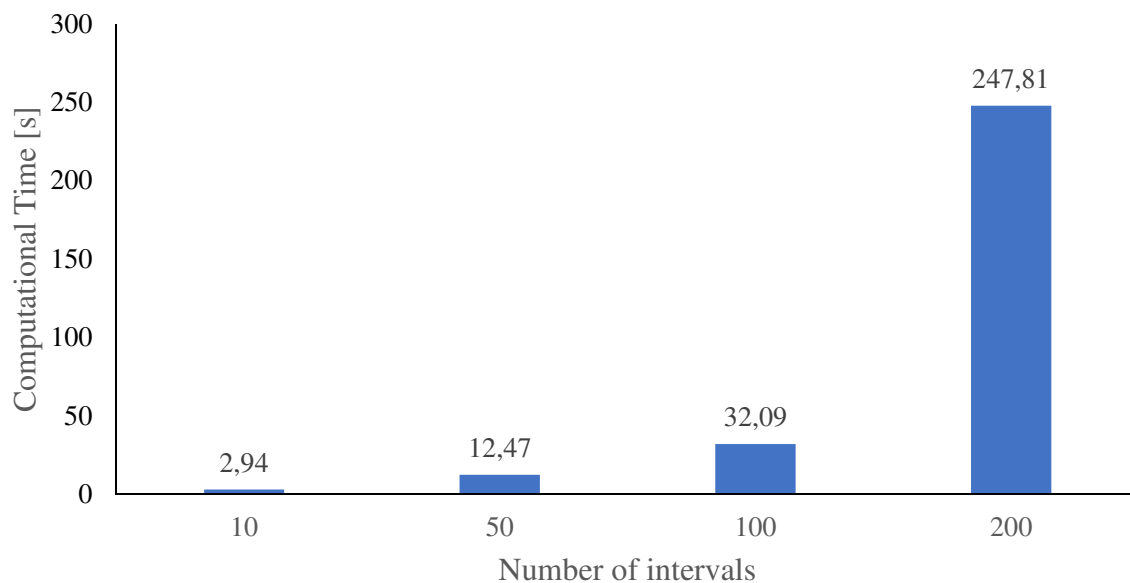


Figure 30) Computational time to reach the convergence

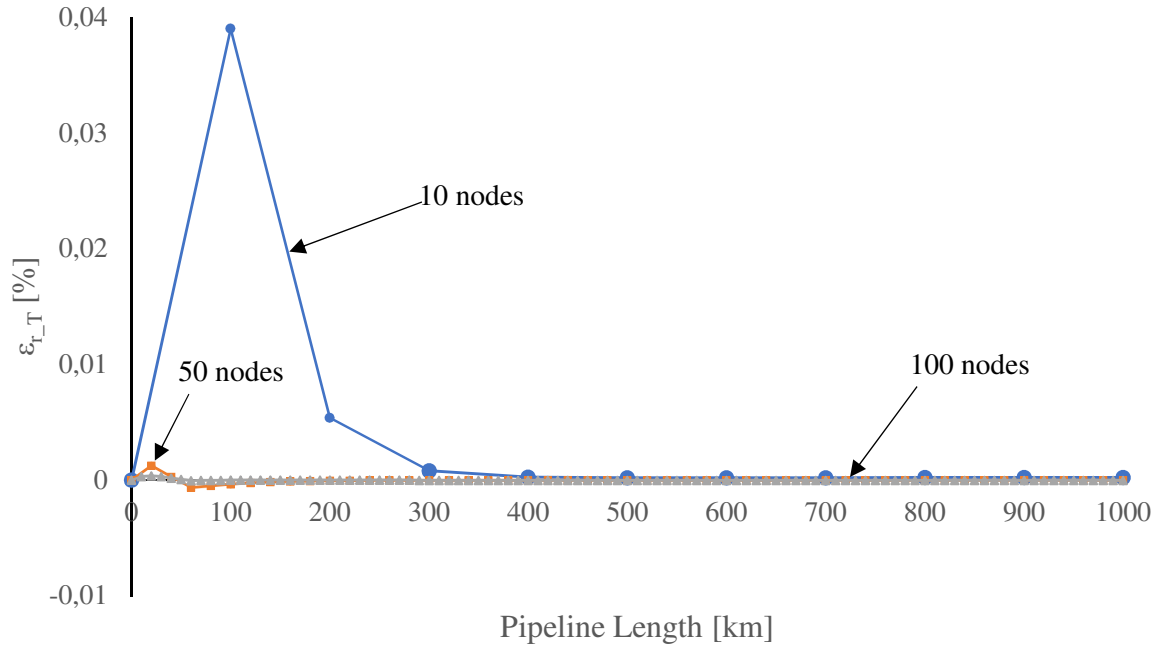


Figure 31) Temperature Relative Error with respect to 200-node discretization

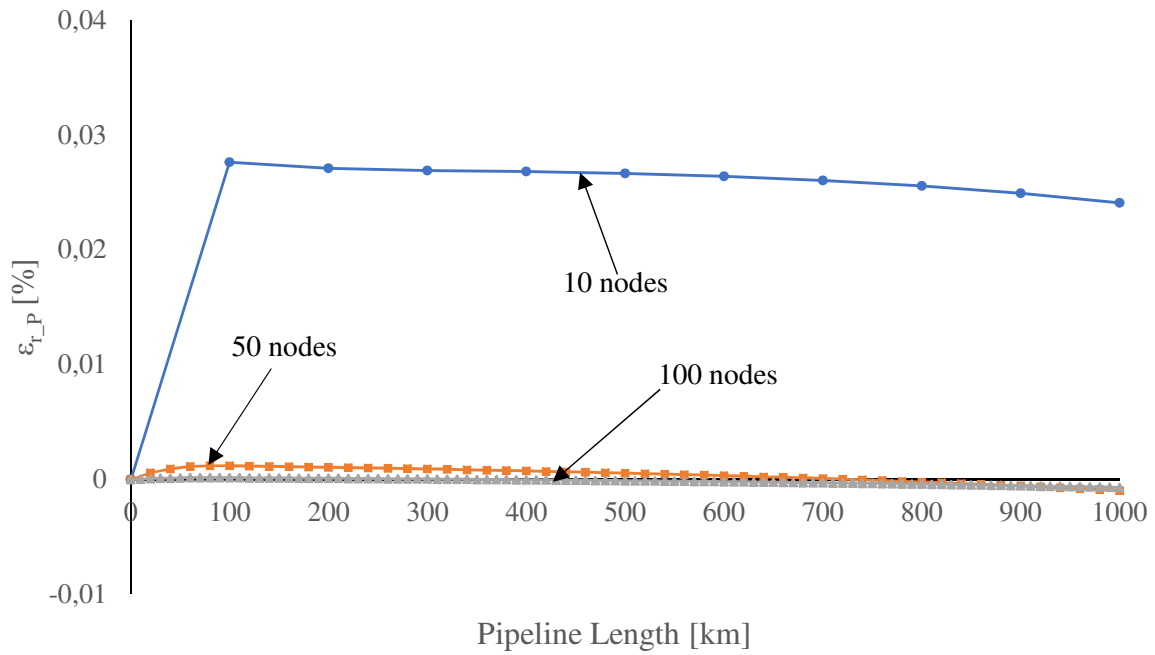


Figure 32) Pressure Relative Error with respect to 200-node discretization

The computational time is showed to increase exponentially passing from 100 to 200 subintervals showing that the maximum tolerable number of nodes is almost reached by the model.

Results highlight that the best compromise concerning accuracy (relative error) and computational time is the division of the pipeline in 50 nodes. This discretization scheme has a negligible relative error for pressure and temperature variation along the pipe and a reasonable computational time to reach the model convergence.

3.2. Case studies

In this section, all the case studies undertaken with the proposed adapted model are presented. Pipeline outlet pressure and temperature are calculated for each case study assuming an inlet temperature of 298,15 or 323,15 K.

Australian Network

An Australian transportation point-to-point system for pure CO₂ was built using data reported by the CO2CRC [10]. The network provides the connection of single main sources with single main sinks tailored to meet the end-user and pipeline transportation necessities.

The major assumptions used by Fimbres et al. [11] to model the pipeline network were:

- Flow rates of CO₂ are fixed for the duration of the project (steady-state);
- Pure CO₂ is produced after capture;
- CO₂ is compressed to the pressure required for transport through the pipeline network;
- The total amount of CO₂ injected at each storage location is equal to flow rate for a given pipeline;
- The effects of topography are ignored;

For the purposes of modelling the topology of the network connecting emission sources and injection sites (sinks), CCS transport facilities are defined in Figure 33 by making use of two component types: nodes and links.

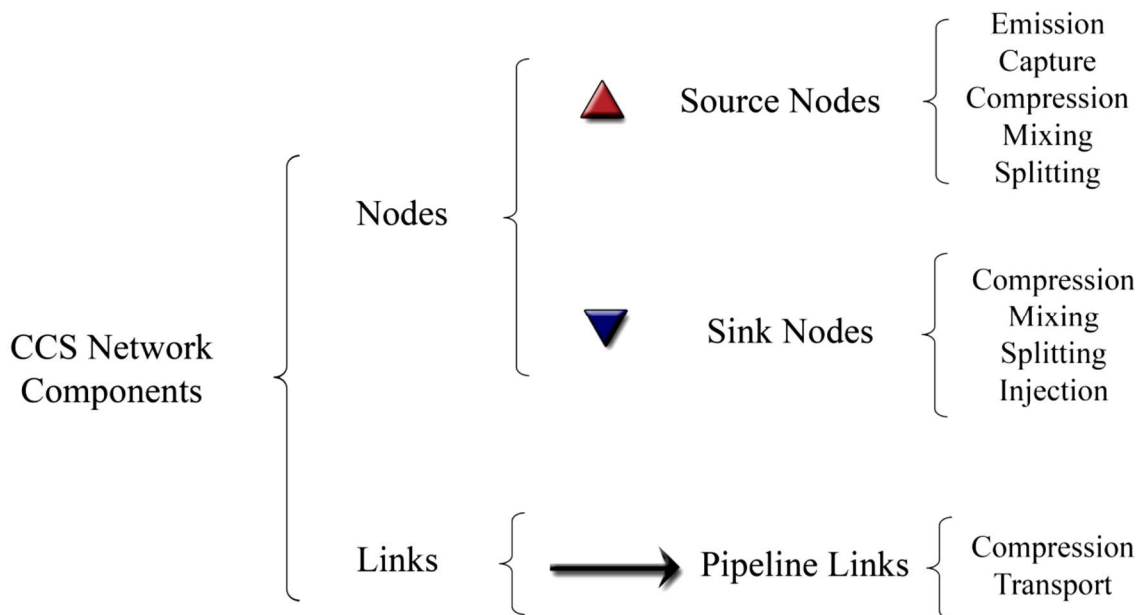


Figure 33) Network component types and the operations permitted for each component [11]

Nodes are points with a specified location where one or more operations may take place. There are two types of nodes – source nodes and sink nodes. In source nodes, only capture is permitted and only injection is permitted in sink nodes. Each node has an emission rate associated with it, which could be positive (at source nodes) or negative (at active sink nodes).

Links are the physical connections between two nodes and allow a flow between nodes. They represent pipelines in the CCS network and may include booster stations. At this stage of model development, the number of parallel pipelines (pipeline loops) and the pipeline diameter are constant throughout the length of the link.

In this section, pipelines are designed as described by the Cooperative Research Centre for Greenhouse Gas Technologies [10] using X70 steel and a 1500 lb flange rating (rated to 255 bar upper working pressure) following Australian Standard AS2885. The pipeline thickness was determined by Fimbres et al. [11] using the standard equation with a weld joint factor of 1, a corrosion tolerance of 1 mm and a design factor of 0.72 typical for gas pipelines in rural areas. The nominal pipeline diameter was calculated as a function of flow-rate and distance as it increases with both to compensate frictional pressure losses.

Source hubs and storage sites from the analysed Australian network are presented in Table 9 and located in the map in Figure 34 and 35. In Table 10, the main parameters needed for modelling each CO₂ pipeline are introduced.

Table 9) Source hubs and storage sites for case study [10]

Source hubs	Storage sites
Latrobe Valley, Victoria	Gippsland (nearshore, intermediate and basin centre)
East Victoria	Surat (shallow, mid-depth and deep)
South Qld (East Surat)	Eromanga (shallow, mid-depth and deep)
North NSW (Hunter Valley–Newcastle)	Darling (Pondie Range average core and average mini-DST)
South NSW (NSW West–Lithgow)	Cooper (shallow, mid-depth and deep)
Southwest WA (Collie)	North Perth Offshore (shallow, mid-depth and deep)
Kwinana WA	Lesueur Sandstone (shallow, mid-depth and deep)

Sources & Sinks - East

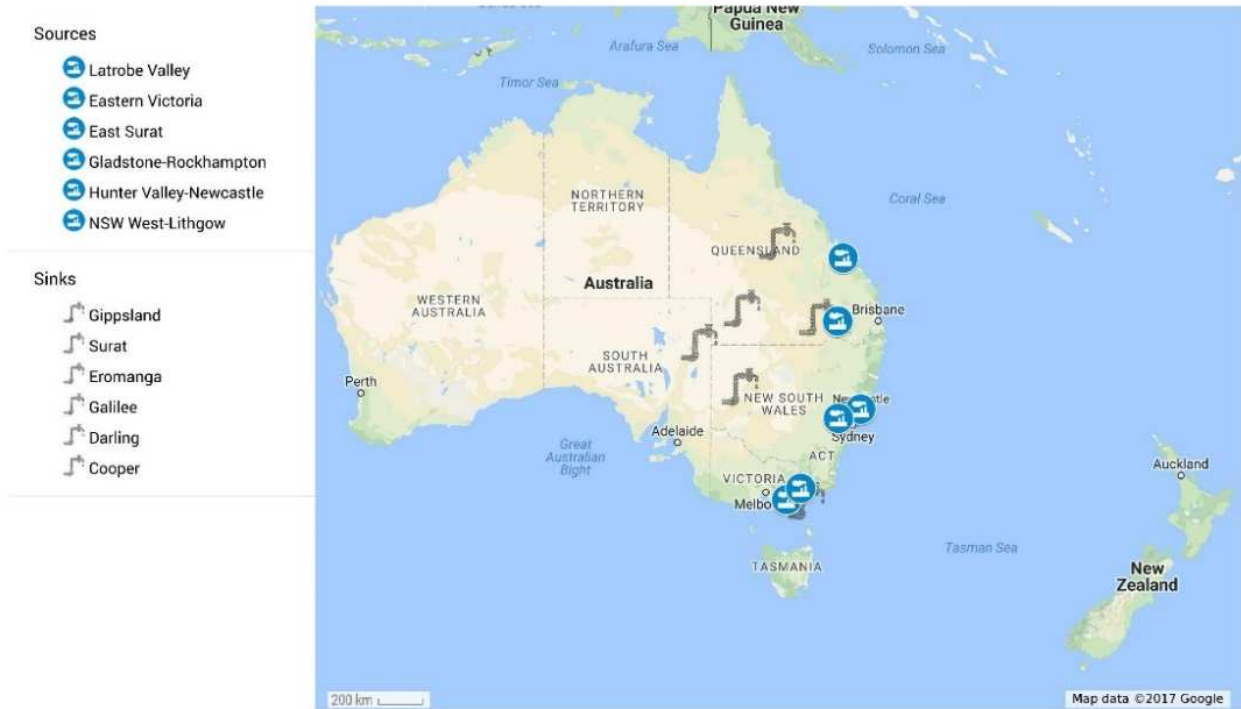


Figure 34) Sources and Sinks - Eastern Australia

Sources & Sinks - West

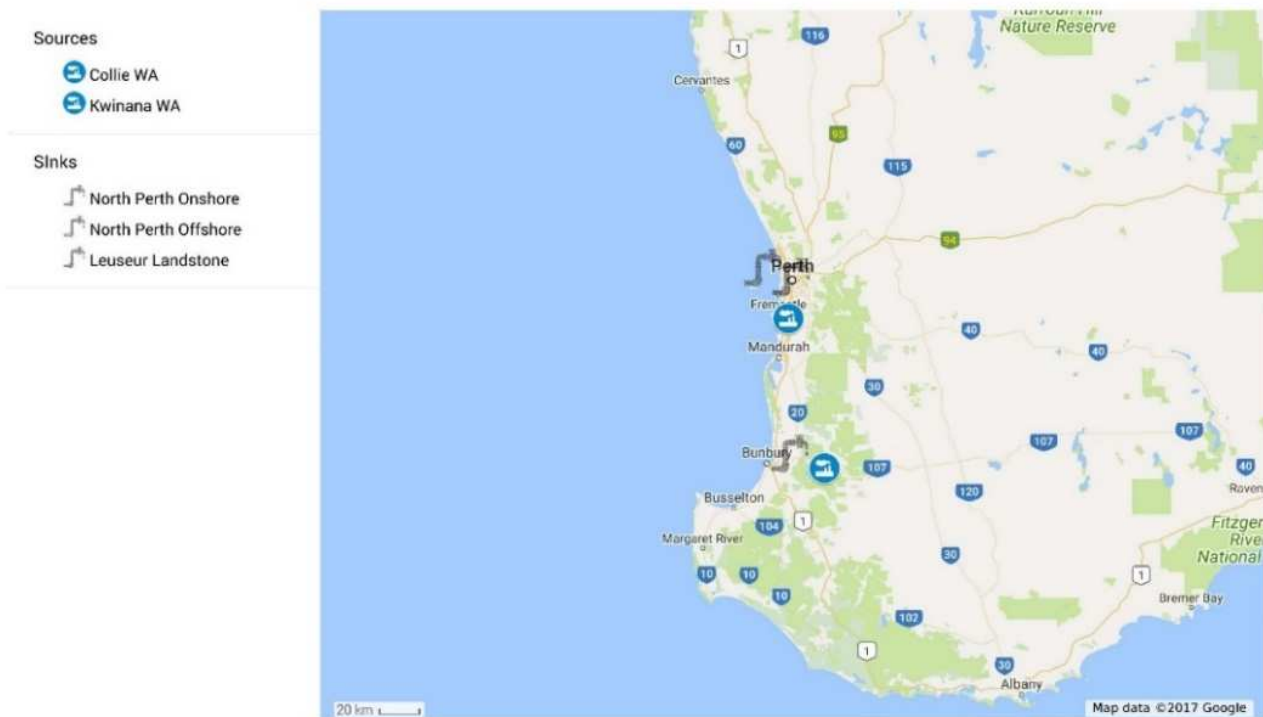


Figure 35) Sources and Sinks - Western Australia

Table 10) Pipeline database for the Australian network [10]

Source hub	Storage basin	Flow-rate (Mt/y)	Onshore distance (km)	Offshore distance (km)	Total distance (km)	Pipeline inlet pressure (bar)	Pipeline wall thickness (mm)	Nominal Pipeline diameter (mm)	T _{soil} (K)	T _{water} (K)
Latrobe Valley, Victoria	Gippsland (nearshore)	1	85	20	105	116	7,3	250	292,65	289,15
East Victoria	Gippsland (nearshore)	1	17	20	37	92	6,4	250	292,65	289,15
South Qld (East Surat)	Surat (shallow)	4	130	0	130	145	10,4	400	292,65	297,15
South Qld (East Surat)	Eromanga (shallow)	18	1312	0	1312	149	29,3	1200	292,65	297,15
North Qld (Gladstone–Rockhampton)	Galilee (mid)	16,1	618	0	618	146	24,6	1000	292,65	299,15
North Qld (Gladstone–Rockhampton)	Eromanga (shallow)	16,1	1020	0	1020	146	27	1100	292,65	299,15
North NSW (Hunter Valley–Newcastle)	Surat (shallow)	33,5	813	0	813	143	32,9	1350	292,65	296,15
South NSW (NSW West–Lithgow)	Gippsland (nearshore)	12,9	930	20	950	144	23,4	950	292,65	294,15
North NSW (Hunter Valley–Newcastle)	Darling (DST)	33,5	915	0	915	149	32,9	1350	292,65	296,15
South NSW (NSW West–Lithgow)	Darling (core)	12,9	574	0	574	149	32,9	1350	292,65	294,15
Southwest WA (Collie)	North Perth Offshore (shallow)	8,4	635	100	735	142	19,9	800	292,65	294,15
Southwest WA (Collie)	Lesueur Sandstone (shallow)	8,4	80	0	80	145	16,3	650	292,65	294,15
Kwinana WA	Lesueur Sandstone (shallow)	8,4	100	0	100	148	15,2	600	292,65	294,15

Understanding pipeline pressure and temperature profile

An example of pressure and temperature profile along the Latrobe Valley-to-Gippsland pipeline is presented to better understand the effects of the inlet temperature on the carbon dioxide transportation along the pipe. The pipeline inlet pressure was set at 116 bar as reported by the Cooperative Research Centre for Greenhouse Gas Technologies (2015). A comparison of the two cases is reported to highlight the differences in terms of pressure and temperature drop and to understand the possible consequences on the cost of the pipeline.

In Table 11, it is reported the datasheet of the input parameters used to model the pipeline. The external temperature was set equal to the average soil temperature for the onshore length and equal to the average sea water temperature in Victoria for the offshore one.

Table 11) Input Data: Latrobe Valley to Gippsland

Parameters	Value
Roughness [μm]	45,72
Heat Transfer Coefficient onshore [$\text{W}/\text{m}^2\text{K}$]	3,69
Heat Transfer Coefficient offshore [$\text{W}/\text{m}^2\text{K}$]	39,6
Soil Temperature [K]	292,65
Sea Water Temperature [K]	289,15
Diameter [mm]	250
Flow-rate [Mt/y]	1
Onshore pipeline length [km]	85
Offshore pipeline length [km]	25
Pipeline Inlet Pressure [bar]	116

Network evaluation

Latrobe Valley and South New South Wales to Gippsland Basin

A possible network connection between two sources (Latrobe Valley and South New South Wales) and one sink (Gippsland), as reported in Figure 36, was modelled. The top-hole pressure (trunk C outlet pressure) was set 100 bar as stated by the CO2CRC [10]. Every trunk was firstly modelled as a separate pipeline. Then, the model was adapted for the whole network calculation to determine pressure and temperature variation fixing the outlet pressure at the storage site (APPENDIX B).

A gradient of pressure in the opposite direction of the flow may develop backward from the Junction if the pressure in the two pipelines had different values. This pressure wave destabilizes carbon dioxide flowing in the pipeline generating more turbulences and it has to be avoided in order

to control the possible propagation of fractures. Hence, the same pressure at the Junction for trunk A and B was set to achieve a more effective transport of the carbon dioxide.

In order to allow a lower inlet pressure in A and B and to get the same outlet pressure (100 bar) for the injection, a booster station at the Junction was provided. In fact, due to higher mass flow-rate obtained as a sum of the flows linked in the Junction, a bigger pressure drop is predictable in the last trunk. A higher inlet pressure for trunk A and B could be an alternative to the booster station in the Junction to get the same value for the top-hole pressure. Both cases were analysed to understand the technical and economical differences to have or not a pumping stage at the Junction.

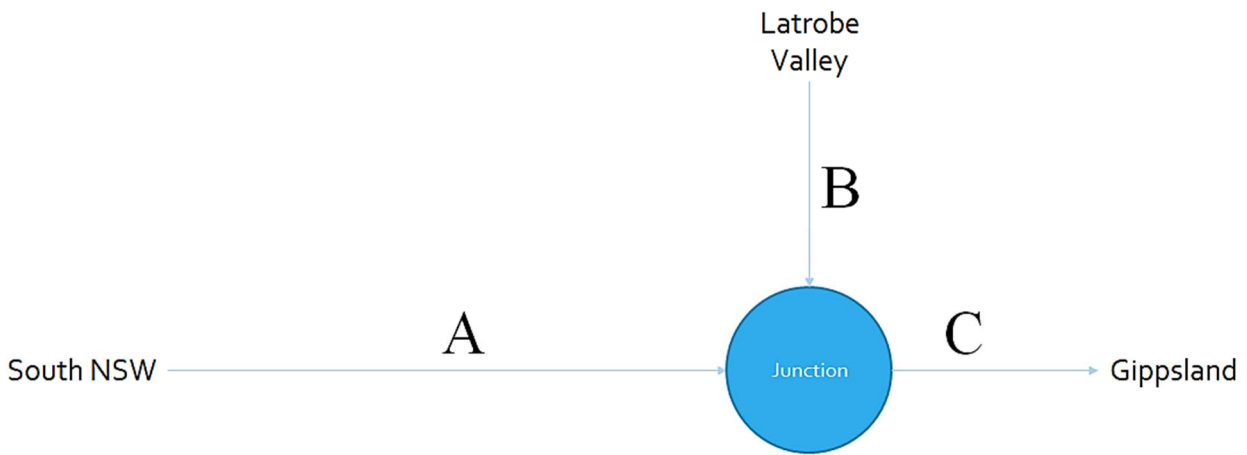


Figure 36) Pipeline scheme: Latrobe Valley & South NSW to Gippsland

The temperature at the Junction ($T_{C,in}$) was calculated as a weighted average temperature balanced on mass flow-rate and heat capacity of the two pipelines joining together as reported in the equation below:

$$T_{C,in} = \frac{T_{A,out} G_{A,out} Cp_{A,out} + T_{B,out} G_{B,out} Cp_{B,out}}{G_{A,out} Cp_{A,out} + G_{B,out} Cp_{B,out}}$$

$T_{A,out}$, $G_{A,out}$, $Cp_{A,out}$ are the outlet temperature, mass flow-rate and isobaric heat capacity of the trunk A (Latrobe Valley to the Junction);

$T_{B,out}$, $G_{B,out}$, $Cp_{B,out}$ are the outlet temperature, mass flow-rate and isobaric heat capacity of the trunk B (South New South Wales to the Junction);

General parameters for modelling the described network are introduced in Table 12 and 13. Soil temperature was set at 294,65 K, while the sea water temperature for the offshore length in the trunk C was equal to 289,15 K. The outlet pressure for A and B before being pumped up at the Junction was set at 80 bar.

Table 12) Input data in case of booster at the Junction

Input	A	B	C
Diameter [mm]	950	650	850
Flow-rate [Mt/y]	12,9	18,3	31,2
Pipeline length onshore [km]	930	60	60
Pipeline length offshore [km]	n/a	n/a	20
Pipeline Inlet Pressure [bar]	102	90	118
Pipeline Inlet Temperature [K]	298,15	298,15	294,05

Table 13) Input data in case of absence of booster at the Junction

Input	A	B	C
Diameter [mm]	950	650	850
Flow-rate [Mt/y]	12,9	18,3	31,2
Pipeline length onshore [km]	930	60	60
Pipeline length offshore [km]	n/a	n/a	20
Pipeline Inlet Pressure [bar]	139	137	118
Pipeline Inlet Temperature [K]	298,15	298,15	294,45

In Figure 37 and 38, the transport infrastructure is reported to highlight the pressure drop generated by compressor, pump, pipeline trunk and booster station towards to storage site.

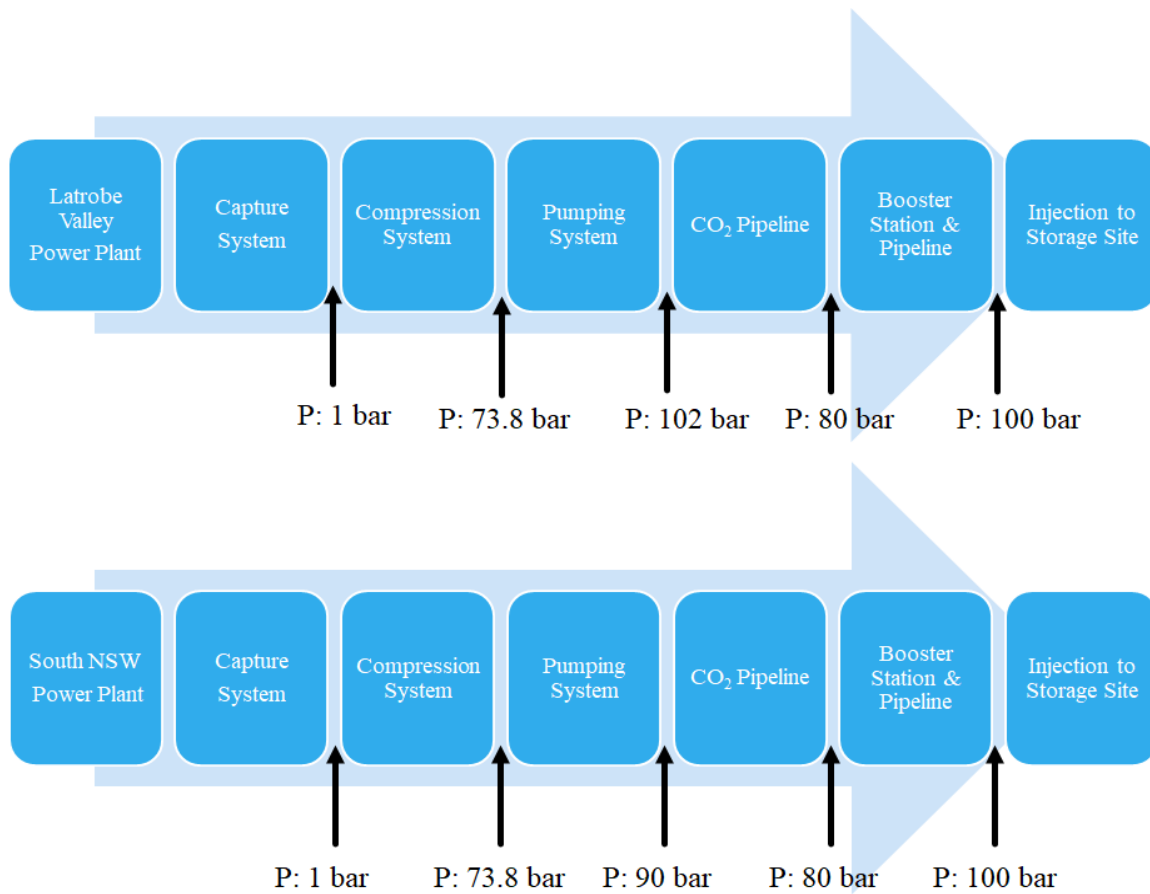


Figure 37) Transport infrastructure with booster station at the Junction

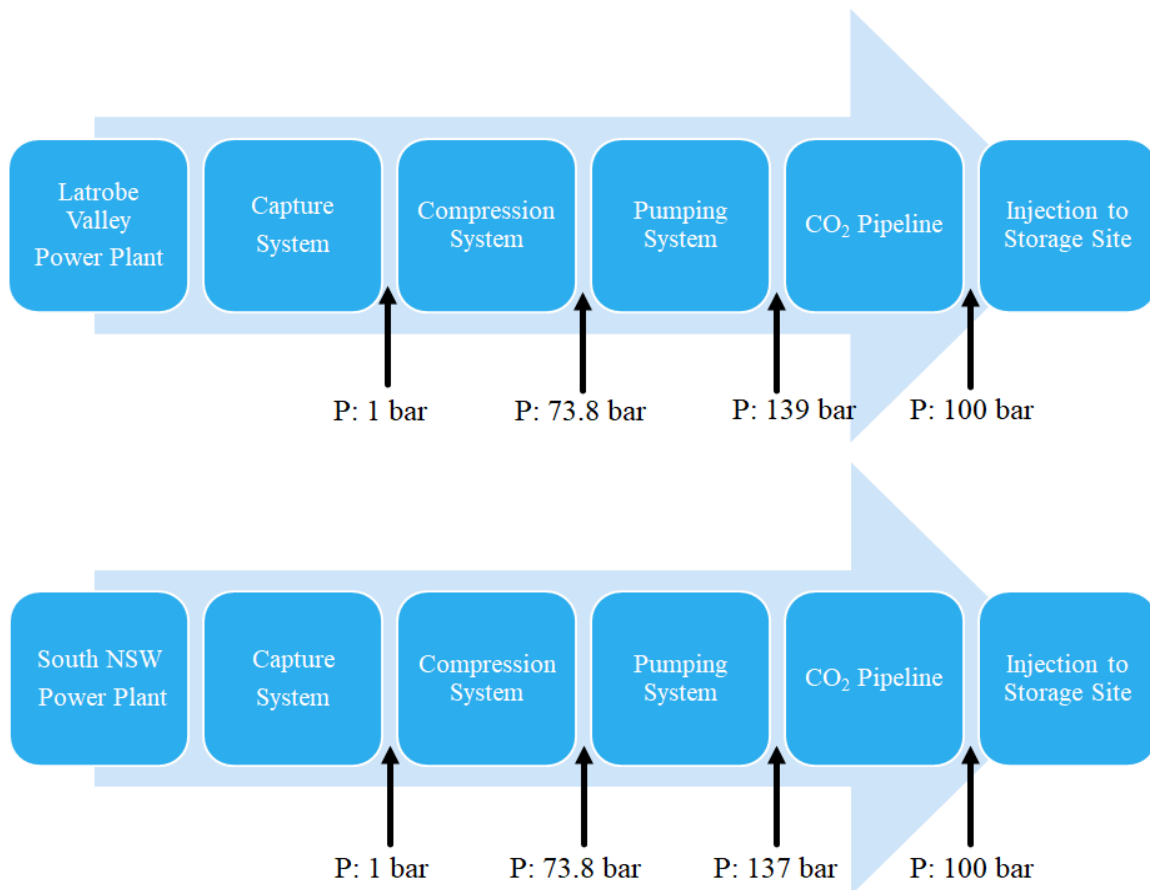


Figure 38) Transport infrastructure without booster station at the Junction

South-Eastern Queensland to the Surat Basin

The model was also used to calculate pressure and temperature in a CCS hub network for a set of emission sources in the south-eastern Queensland region in Australia, as reported by Fimbres et al. [11]. All emission sources were assumed to commence deployment of CCS concurrently and all pipelines and injection facilities were assumed to begin operating at the same time.

The emission sources consist of flue gases from several pulverised black coal, NGCC power plants and petroleum refineries, as reported in Table 14. Figure 39 shows the location and connection of the emission and injection sites considered. The storage sink is located in the Surat basin (approximately 250 km far from the emission sources). The top-hole pressure for the shallow storage site was fixed at 92 bar.

Table 14) Carbon dioxide emission sources described by Fimbres et al. [11]

Emission source	Source type
Bulwer Island & Lytton, Brisbane	Petroleum refineries
Condamine	Natural gas power plant
Darling Downs	Natural gas power plant
Kogan Creek	Black coal power plant
Millmerran	Black coal power plant
New CCGT	Natural gas power plant
Swanbank E	Natural gas power plant
Tarong North	Black coal power plant

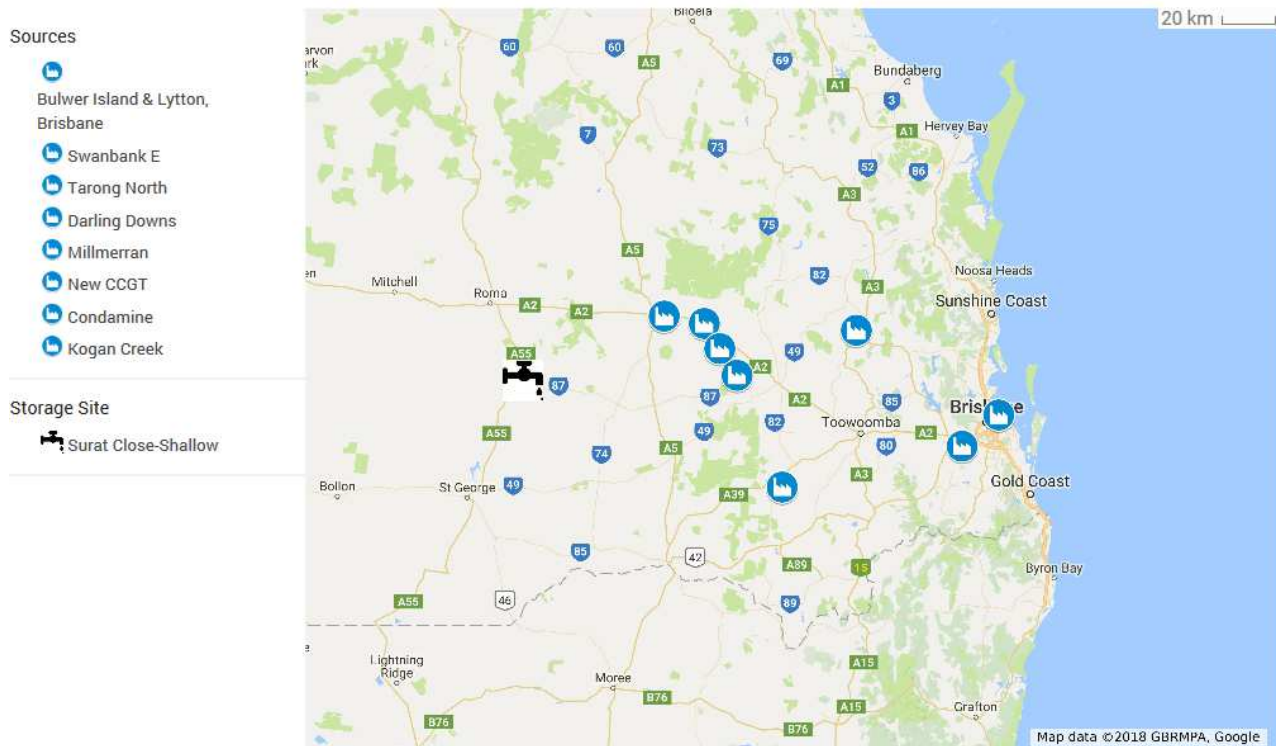


Figure 39) Location of sources and sinks of the hub network described by the CO2CRC [10]

In the first set of the analysis, the diameter for pipeline connecting the emission sources was set at 450 mm; while the value for the last trunk from “New CCGT” to the storage site was set at 850 mm considering the higher amount of carbon dioxide transported. In the second set of analysis, the value of the pipeline diameter was then estimated based on data from Table 15 for each trunk [10]. The pressure and temperature were calculated to understand the differences in having a fixed value of the nominal outer diameter or the optimal one calculated for the specific flow rate of transported carbon dioxide. A summary of the data used for the hub network analysis is shown in Table 16.

Table 15) Data and equation coefficients for pipeline diameter as a function of distance and flow-rate for steel grade X70 [10]

Nominal diameter (mm)		CO ₂ flow-rate (Mt/y)									
		1	3	5	10	15	20	25	30	35	40
Pipeline length (km)	17	150	250	300	400	450	500	550	600	650	700
	50	200	300	400	500	550	650	700	750	800	850
	100	200	350	450	550	650	750	800	850	900	950
	200	250	400	500	650	750	850	900	1,000	1,050	1,100
	400	300	450	550	750	850	950	1,050	1,100	1,200	1,250
	600	300	500	600	800	900	1,050	1,150	1,200	1,300	1,350
	800	350	550	650	850	1,000	1,100	1,200	1,300	1,350	1,450
	1,000	350	550	650	850	1,000	1,150	1,250	1,350	1,400	1,500
	1,200	400	550	700	900	1,050	1,200	1,300	1,400	1,450	n/a
	1,400	400	600	700	950	1,100	1,200	1,350	1,450	1,500	n/a
a		79.3	141	187	233	255	296	315	344	380	406
b		0.2194	0.197	0.184	0.192	0.201	0.197	0.200	0.198	0.190	0.189
R²		0.976	0.994	0.990	0.996	0.997	0.996	0.999	0.998	0.999	0.999

Table 16) Input data used for modelling the Hub Network described by Fimbres et al. [11]

Pipeline	Inlet Node	Outlet Node	Flow rate [Mt/y]	Diameter [mm]	Pipeline Length [km]	Estimated Diameter [mm]
1	Bulwer Island & Lytton, Brisbane (A)	Swanbank E (B)	1.5	450	35	250
2	Swanbank E (B)	Tarong North (C)	2.5	450	132	350
3	Tarong North (C)	Darling Downs (D)	4.9	450	107	450
4	Millmerran (E)	Darling Downs (D)	4.6	450	100	450
5	Darling Downs (D)	New CCGT (F)	11.1	450	23	450
6	Condamine (H)	Kogan Creek (G)	0.3	450	55	150
7	Kogan Creek (G)	New CCGT (F)	4.4	450	22	300
8	New CCGT (F)	Surat (I)	17.1	850	257	850

Effects on pressure due to variable flow-rates: Tarong North and Millmerran to the Surat Basin

An analysis to understand the effect on the inlet pressure with variable flowrates was carried out using two sources from the South-Eastern Queensland Hub Network (Tarong North and Millmerran). Figure 40 shows the two sources connected to the storage site (Surat). The top-hole pressure was fixed to 92 bar. The analysis considers annual profile of the power plants for the year 2010 as shown in Figures 41 and 42. The figures show the daily variation in the amount of CO₂ captured for Tarong North and Millmerran.

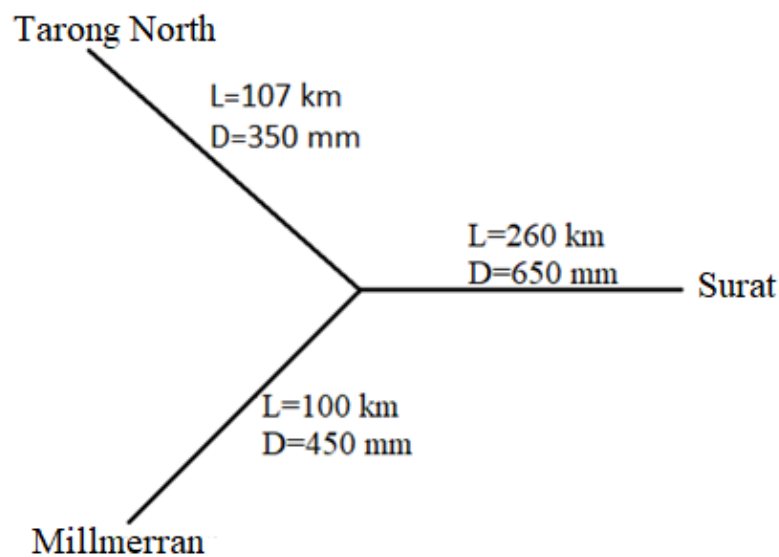


Figure 40) Tarong North & Millmerran to Surat

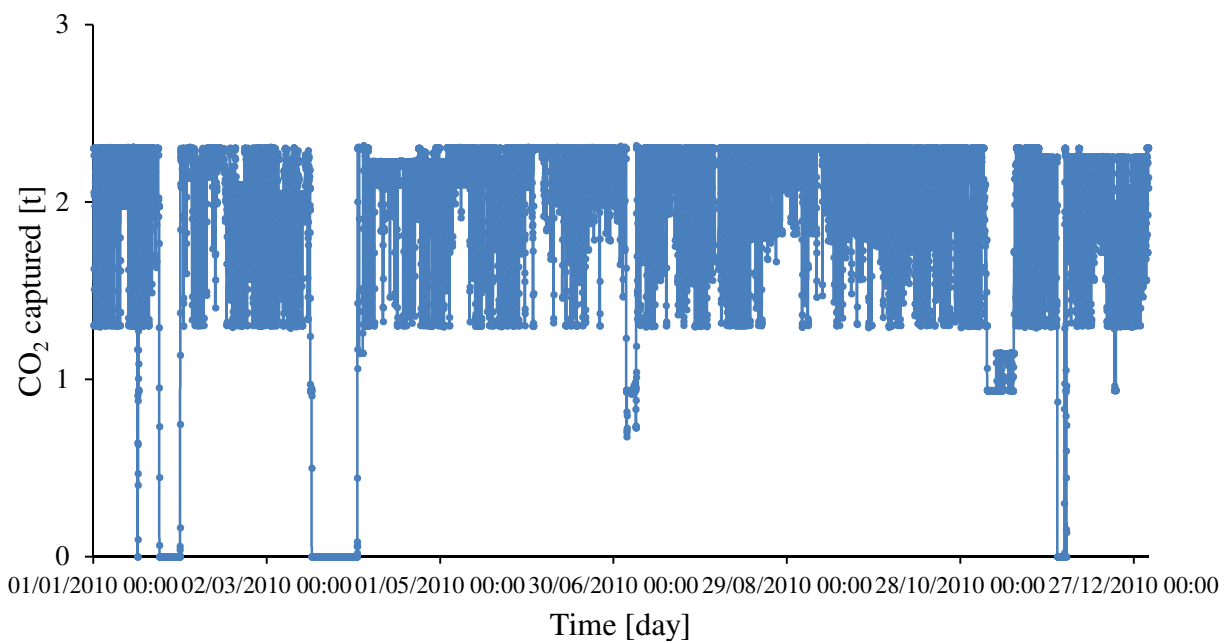


Figure 41) Tarong North CO₂ captured yearly profile (2010)

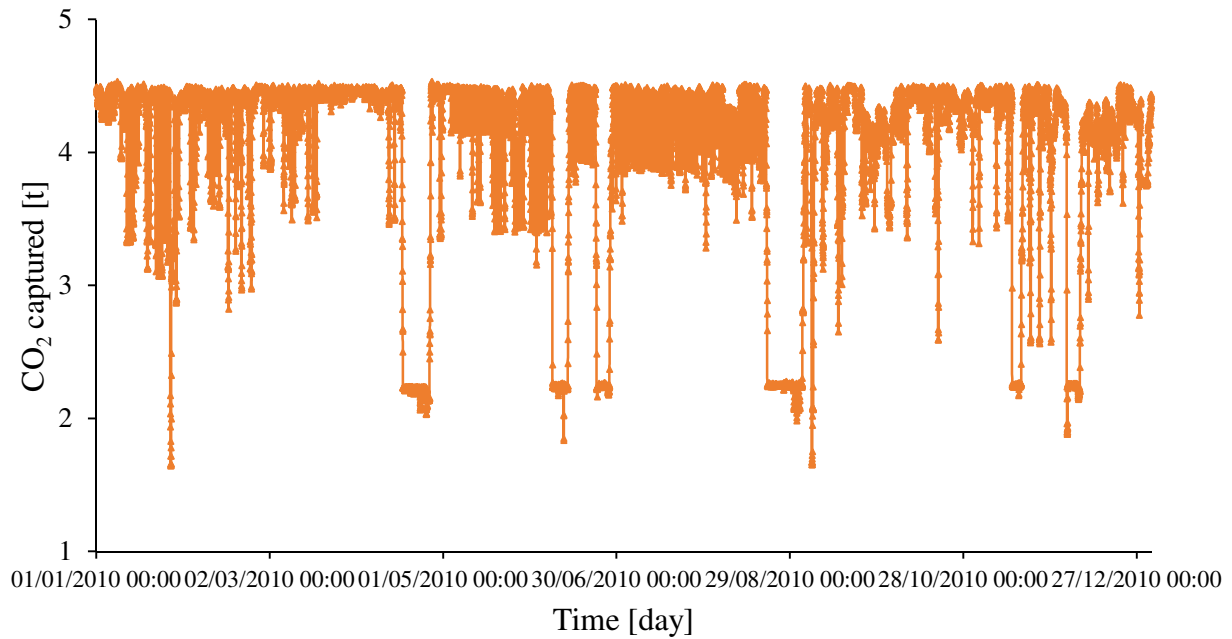


Figure 42) Millmerran CO₂ captured yearly profile (2010)

Sensitivity Analysis

A sensitivity analysis on the results has been accomplished to comprehend the effects on the carbon dioxide transportation in terms of pressure and temperature variation through the length of the following parameters:

1. Diameter, flow rate and pipeline length;
2. Inlet pressure;
3. Inlet Temperature;
4. Overall Heat Transfer Coefficient;
5. Ambient temperature.

In table 17 the main input parameters used for this analysis are introduced.

Table 17) Input data for the sensitivity analysis

Parameters	Value
Soil Temperature [K]	292,65
Sea Water Temperature [K]	294,15
Diameter [mm]	650
Flow-rate [Mt/y]	5
Onshore pipeline length [km]	900
Offshore pipeline length [km]	100
Pipeline Inlet Pressure [bar]	150
Pipeline Inlet Temperature [K]	298,15

3.3. Economic assumptions

Cost calculation of compressors, pumps and boosters in the previously described network cases has been performed as reported in the cost model proposed by McCollum et al. [78]. Costs are expressed in year 2017 A\$m and have been scaled using the CEPCI.

The Chemical Engineering Plant Cost Index (CEPCI) was 468.2 in 2005 and 556.8 in 2015. Hence, C_{comp} , C_{pump} and $C_{booster}$ have been scaled in A\$m in 2017.

$$CEPCI_{2017} = 558.3$$

$$(1 \text{ US\$})_{2005} = (1.312077 \text{ A\$})_{2005}$$

$$Cost_{2017} = Cost_{2005} * \frac{CEPCI_{2017}}{CEPCI_{2005}}$$

Compression and pumping cost estimation

Pressure from the capture system was assumed to be 1 bar. Carbon dioxide is then compressed to the critical pressure of 73.8 bar by the compressor and to the selected value of inlet pressure for each pipeline via a pump. The compressor was assumed to have five stages with a compression ratio of 2.36.

C_{comp} (US\$) is the capital cost of the compressor, G (kg/s) is the CO₂ mass flow-rate through the compressor train, $P_{cut-off}$ (MPa) is the target pressure for the compressor (critical value) and $P_{initial}$ (MPa) is the pressure after the capture system.

$$C_{comp} = G \left[(0.13 \times 10^6)(G)^{-0.71} + (1.40 \times 10^6)(G)^{-0.60} \ln \left(\frac{P_{cut-off}}{P_{initial}} \right) \right]$$

C_{pump} (US\$) is the capital cost of the pump, W_p pumping power requirement (kW) for boosting the pressure from $P_{cut-off}$ (73.8 bar) to P_{final} (pipeline inlet pressure) expressed in MPa, G is the mass flow rate (t/day), $\rho = 630 \text{ kg/m}^3$, $\eta_p = 0.75$.

$$W_p = \left(\frac{1000 * 10}{24 * 36} \right) \left[\frac{G(P_{final} - P_{cut-off})}{\rho \eta_p} \right]$$

$$C_{pump} = (1.11 \times 10^6) \frac{W_p}{1000} + 0.07 \times 10^6$$

$C_{booster}$ (US\$) is the capital cost of the booster station, W_p pumping power requirement (kW) for boosting the pressure from $P_{cut-off}$ (pressure at the Junction) to P_{final} (required value after the booster station) expressed in MPa.

$$C_{booster} = (7.82 \times 10^6) \frac{W_p}{1000} + 0.46 \times 10^6$$

Pipeline cost estimation

The unit pipeline cost $C_{u,onshore}$, expressed in [A\$/m²], was extracted from data reported by the CO2CRC in the Australian Power Generation Technology Report [10]. Then, it was multiplied for the proper values of length [km] and diameter [mm] of each trunk to find the pipeline cost $C_{onshore}$ [A\$m] and scaled to 2017 with the CEPCI. The cost for the offshore trunk $C_{offshore}$, expressed in [A\$m], was obtained multiplying the pipeline cost for a factor equal to 2 considering the additional installation costs.

Table 18 presents the unit pipeline cost [\$/m²] for different diameter values.

Table 18) Unit pipeline cost $C_{u,onshore}$ estimated from data reported by the CO2CRC [10]

Diameter [mm]	$C_{u,onshore}$ 2015 [A\$/m²]	$C_{u,onshore}$ 2017 [A\$/m²]
150	2,00	2,01
200	2,00	2,01
250	2,00	2,01
300	2,00	2,01
350	2,00	2,01
400	2,10	2,11
450	2,20	2,21
550	2,25	2,26
600	2,30	2,31
650	2,40	2,41
700	2,50	2,51
750	2,55	2,56
800	2,67	2,68
850	2,75	2,76
900	2,82	2,83
950	2,88	2,89
1000	2,95	2,96

4. Results

In this section, results for outlet pressure and temperature obtained from the developed model are reported. A sensitivity analysis is performed on the results to identify the key parameters that affect the carbon dioxide transport. Pressure and temperature profiles are examined to understand the best solution in terms of initial pressure and temperature, insulation, cost and other pipe characteristics.

4.1. Australian Network Results

In this section, results obtained by the developed model for pipeline pressure and temperature of the described Australian Network are reported.

Table 19 shows the outlet pipeline pressures and temperatures for the different Australia Case Studies when the external soil temperatures are 298,15 and 323,15 K.

As can be seen from the results, the outlet temperature reaches the ambient value almost in all pipelines analysed apart from those which are very short, as in the case of these last two pipelines where the source hub and the storage site are very close. The heat transfer in submerged pipelines (offshore) is also shown to be much higher (about 10 times more) than those for buried ones (onshore). This arises because of convection in water compared with soil. In fact, the resulting convective motion in offshore pipelines is a state characterized by a high degree of mixing which depends on the hydrodynamic regime. Water flowing around the pipeline creates a greater degree of mixing, and, consequently, the heat exchange coefficient is higher. Due to the higher heat transfer in the offshore trunk, the second pipeline analysed (East Victoria to Gippsland) reaches the sea water temperature despite being short (less than 40 km). In some cases, the outlet temperature goes below the ambient value due to the high Joule-Thomson effect which occurs through the pipeline length during the carbon dioxide depressurization. It is recorded due to the steady state characteristic of the model even if it is noticeable that, through the transient transport of carbon dioxide in the pipeline, the fluid temperature fluctuates until it reaches a stable value with respect to the surroundings.

The outlet pressure is related to the flow-rate, length and diameter. In fact, the combination of these three parameters affects carbon dioxide property calculations and the transport along the pipeline. This effect is particularly noticeable in the South NSW-to-Darling pipeline where despite having high length and flow rate, the pressure drop is very low due to the large diameter. Turbulences inside the pipeline are limited and, consequently, the friction factor is lower.

The results show that the pressure drop is higher when the pipeline inlet temperature was set 323,15 K compared to 298,15 K. This is because the carbon dioxide is in supercritical state with high density and low viscosity.

The results suggest that operating at lower temperature has more advantages as it reduces the pressure drop along the pipeline. Hence, the level of turbulence of carbon dioxide flowing inside the pipeline and, as a consequence, the friction factor is lower resulting in an overall lower pressure drop.

However, if the outlet temperature from the carbon dioxide transport compressor is high, subsequent cooling would be required adding additional costs. As can be seen from Figure 43, the transportation infrastructure is affected by the chosen values at the inlet node for temperature and pressure and the other input parameters in order to minimize losses and cost.

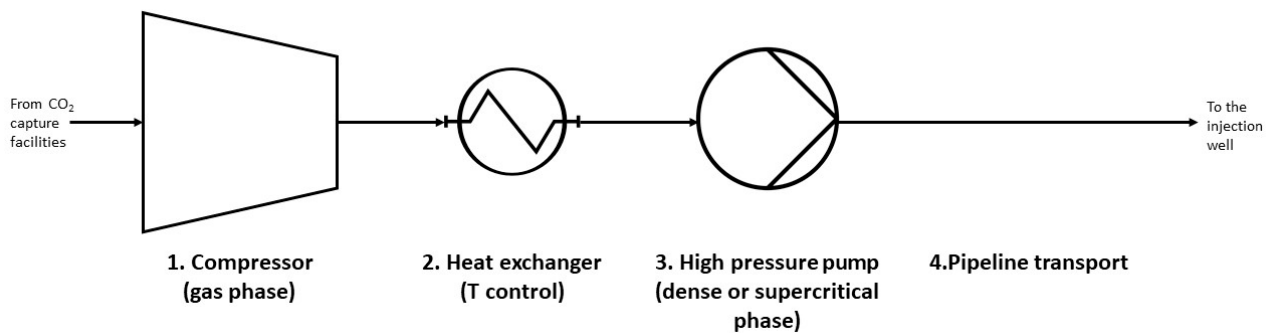


Figure 43) CO₂ transportation infrastructure adapted from Mallon et al. [6]

Table 19) Results for outlet temperature and pressure with inlet temperature at 298,15 K and 323,15 K

Source hub	Storage basin	Pipeline inlet pressure (bar)	T _{in} =298,15 K				T _{in} =323,15 K			
			Pipeline outlet pressure (bar)	ΔP (bar)	Pipeline outlet temperature (K)	ΔT (K)	Pipeline outlet pressure (bar)	ΔP (bar)	Pipeline outlet temperature (K)	ΔT (K)
Latrobe Valley, Victoria	Gippsland	116	101,5	14,5	289,13	9,02	99,80	16,20	289,13	34,02
East Victoria	Gippsland	102	96,8	5,2	289,13	9,02	95,50	6,50	289,17	33,98
South Qld	Surat	145	121,10	23,9	292,85	5,30	118,10	26,90	297,11	26,04
South Qld	Eromanga	149	132,5	16,5	292,59	5,56	132,2	16,80	292,59	30,56
North Qld	Galilee	146	130,1	15,9	292,54	5,61	129,4	16,60	292,61	30,54
North Qld	Eromanga	146	129,9	16,1	292,58	5,57	129,5	16,50	292,58	30,57
North NSW	Surat	143	123,8	19,2	292,49	5,66	122,7	20,30	292,69	30,46
South NSW	Gippsland	144	123,4	20,6	293,96	4,19	122,80	21,20	293,96	29,19
North NSW	Darling	149	127,5	21,5	292,48	5,67	126,50	22,50	292,58	30,57
South NSW	Darling	149	146,9	2,1	292,64	5,51	146,9	2,10	292,64	30,51
Southwest WA	North Perth	142	125,4	16,6	294,14	4,01	124,9	17,10	294,14	29,01
Southwest WA	Lesueur Sandstone	145	132,6	12,4	294,65	3,50	130,2	14,80	307,41	15,74
Kwinana	Lesueur Sandstone	148	138,1	9,9	294,14	4,01	136,50	11,50	303,99	19,16

4.2. Temperature and pressure profile along the pipeline

Figure 44 shows the temperature and pressure profile along the pipeline for the Latrobe Valley to Gippsland case study (85 km onshore and 20 km offshore).

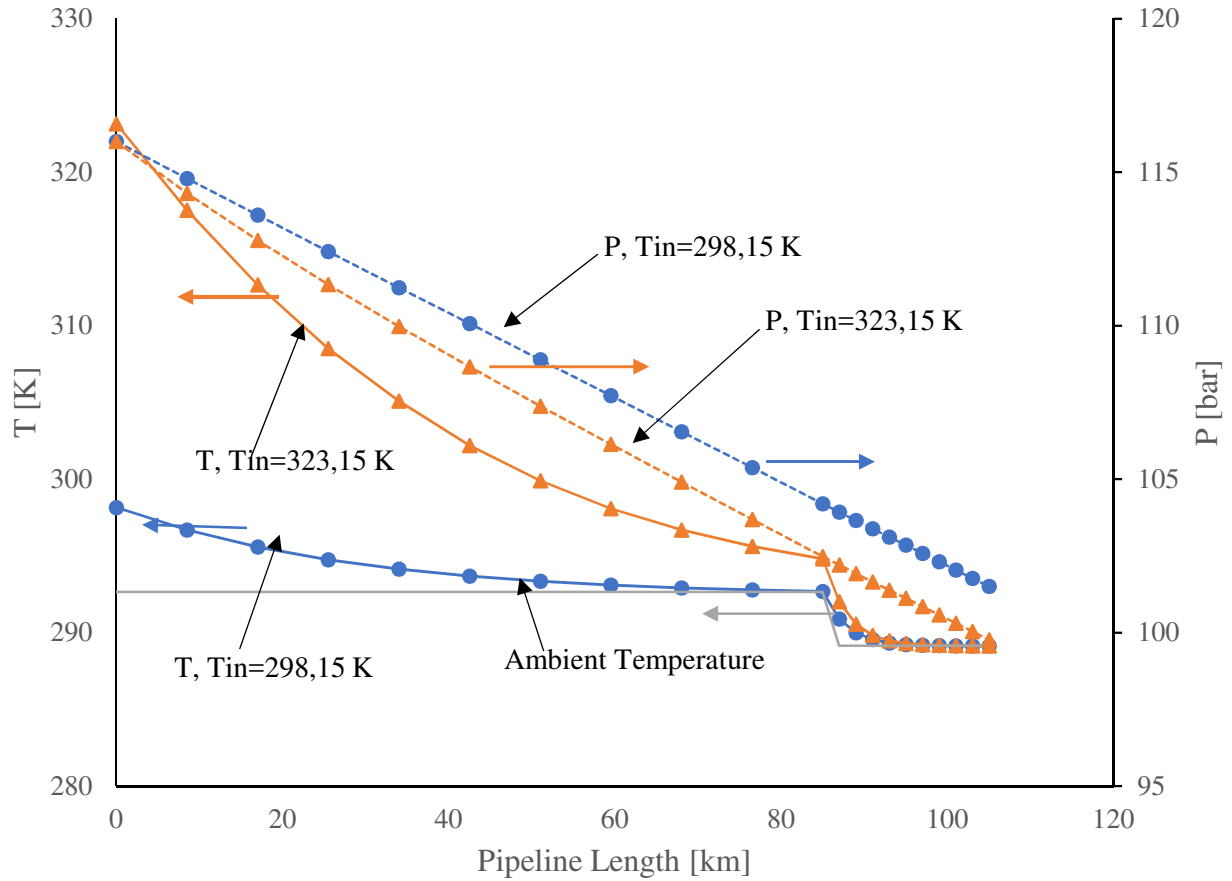


Figure 44) Latrobe Valley to Gippsland: Temperature and Pressure variation along the pipeline

Setting the pipeline inlet temperature at 323,15 K, the results show that the fluid temperature does not reach the ambient value in the onshore trunk (almost 3 K above the soil temperature) even if it experiences a rapid temperature drop due to the higher difference with respect to the surroundings. While with an inlet temperature of 298,15 K, the carbon dioxide temperature undergoes a slower decrease along the pipeline length, but it reaches the soil value after almost 60 km.

A faster drop in the fluid temperature is achieved in the offshore trunk independently of the inlet temperature. The sea water temperature value is reached after a very short distance (almost 8 km) due to the higher heat transfer coefficient for offshore transportation.

As demonstrated by the Bernoulli's principle, the pressure drop and temperature relationship is:

$$\frac{v^2}{2} + gz + \frac{p}{\rho} = \text{constant}$$

Where

v is the fluid flow velocity

g is the acceleration due to gravity

z is the elevation

p is the pressure of the fluid

ρ is the density of the fluid

Having a lower inlet temperature results in a lower velocity of the carbon dioxide particles being transported in the pipeline due to less turbulences. As a consequence of the Bernoulli's principle, a decrease in the fluid velocity due to the lower temperature results in a decrease in the pressure drop.

Figure 44 also shows that the pressure profile along the pipeline is linear regardless of the profile of the temperature. The results also show that there is a bigger slope in the onshore trunk when the temperature difference between the fluid and the environment is higher. In the offshore trunk, pressure has a slight decrease (approximately 2 bar over 20 km) due to the fact that the temperature is practically constant for both inlet temperatures.

Extending the above analysis for a longer pipe length, Figure 45 shows the pressure profile along two 300 km pipelines (onshore and offshore). The results here show that the outlet pressure goes below the critical value (73,8 bar) after approximately 300 km for onshore pipeline. However, for the offshore case to reach the critical pressure, the length is slightly longer at 320 km. This arises due to the high heat transfer which determines a bigger temperature drop at the pipeline inlet and, consequently, a more constant temperature for the rest of the pipe. For this reason, it is advisable to have a recompression station along the onshore trunk in case of a required bigger length or top-hole pressure to avoid the transport in gas phase.

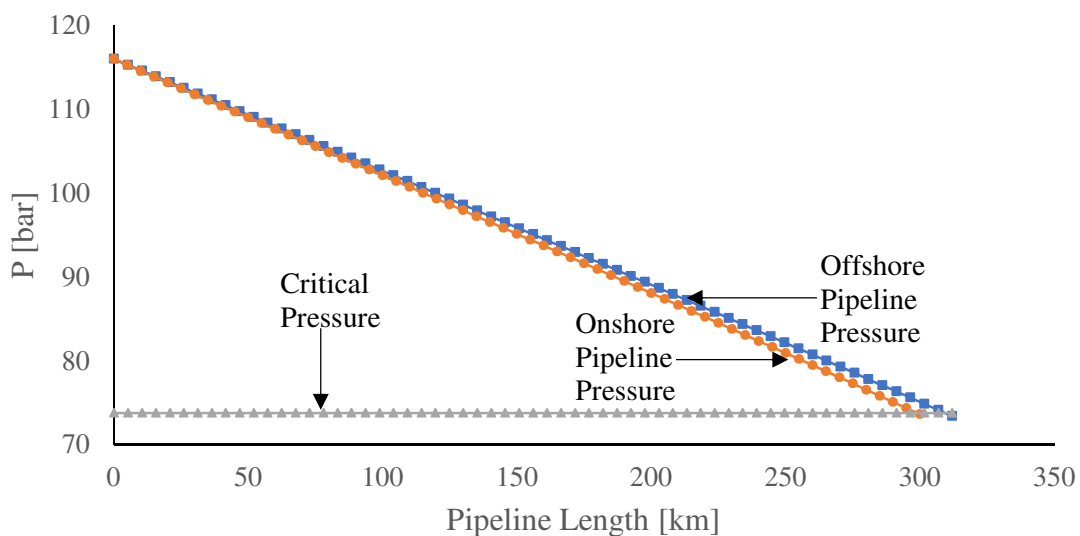


Figure 45) Pressure drop over the length using the input parameters of the Latrobe Valley to Gippsland pipeline

4.3. Latrobe Valley and South New South Wales to Gippsland Basin

Figures 46 and 47 shows the pressure and temperature profiles along the pipelines for two sources (Latrobe Valley and South New South Wales) to a single sink (Gippsland). Figure 46 shows the profiles for the three trunklines with a booster station at the Junction, while Figure 47 shows them without. Every trunk was modelled as a separated pipeline.

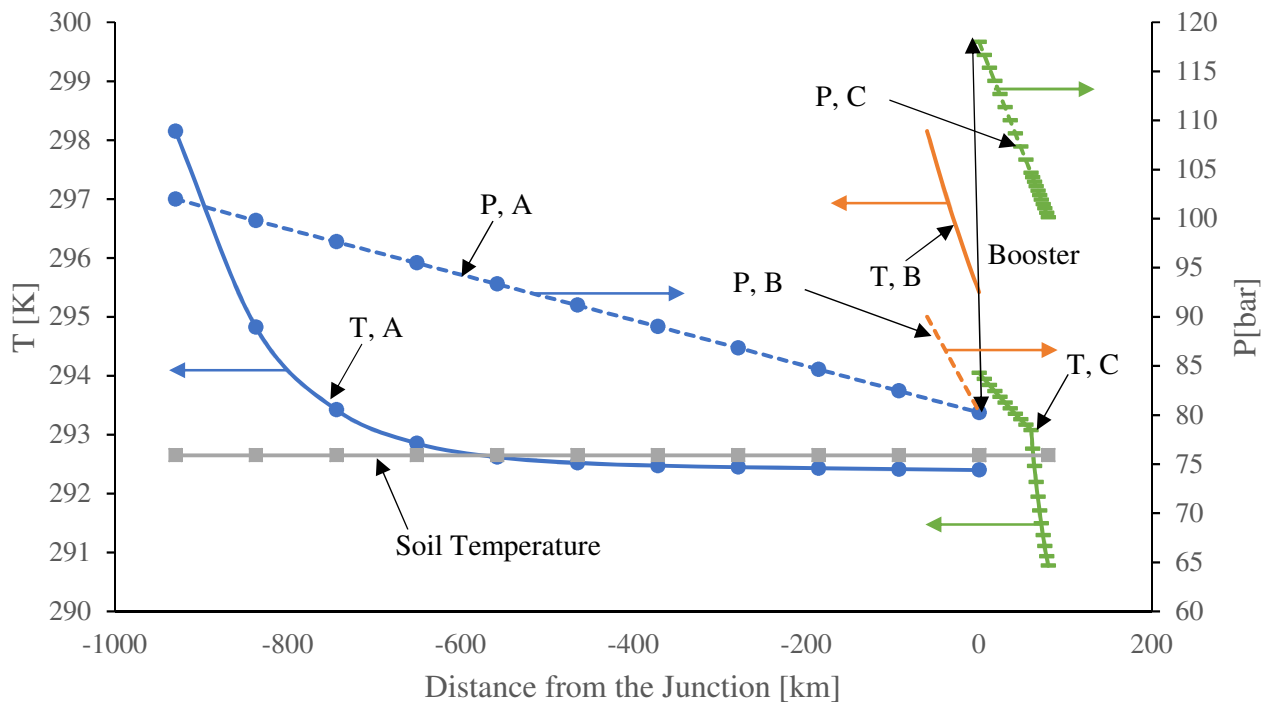


Figure 46) Pressure and temperature profiles in trunk A, B and C with booster station at the Junction

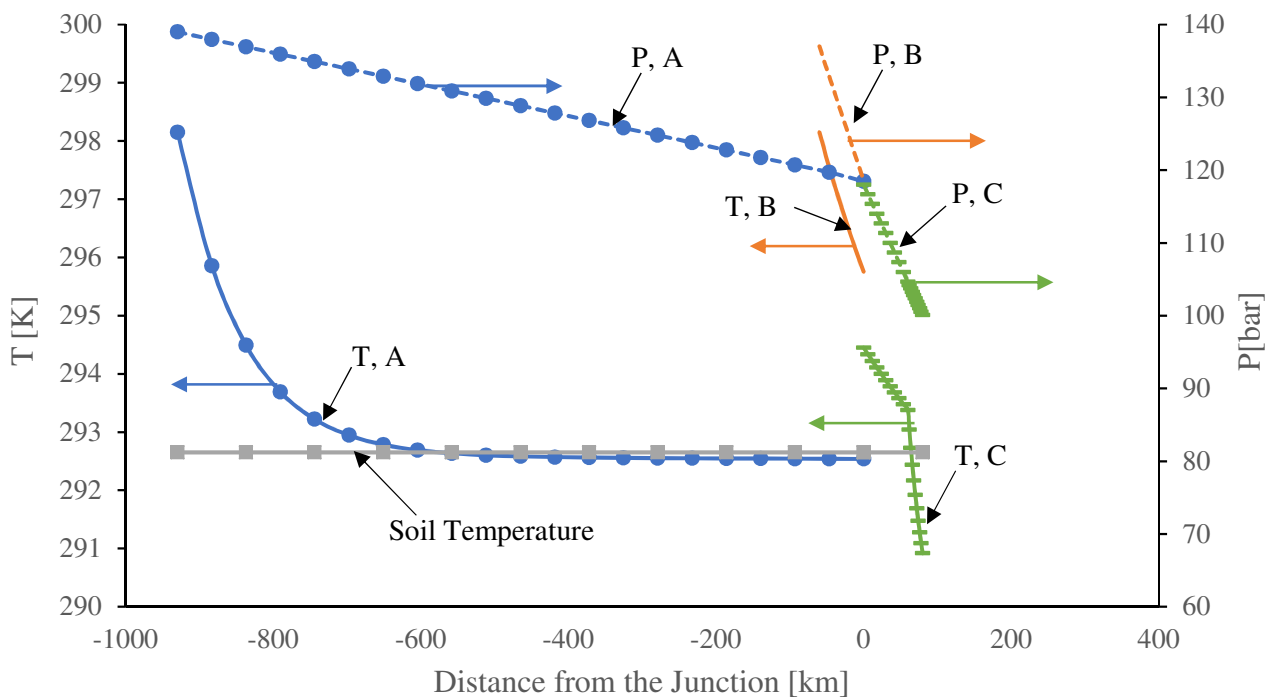


Figure 47) Pressure and temperature profiles in trunk A, B and C without booster station at the Junction

The results from Figures 46 and 47 show that the inlet pressure at point A (South NSW) and point B (Latrobe Valley) is larger for Trunks A and B when no booster is used at the Junction by about 36 and 52% respectively compared to when a booster is used at the Junction. This is to overcome the absence of the booster station and achieve the same value for the fixed top-hole pressure of 100 bar. Figure 46 shows that the carbon dioxide needs to be pumped up to 118 bar before flowing in the trunk C towards the storage site, as the outlet pressure at the Junction for Trunks A and B are fixed at 80 bar.

The results show that the pressure drop per unit of length along Trunk A ($\approx 0,023$ bar/km) is relatively small. This is due to the large diameter of 950 mm and the relatively small flow-rate of 12,9 Mt/y resulting in a low friction factor along the pipe. In contrast, the pressure drop per unit of length along Trunk B is higher ($\approx 0,17$ bar/km) because of the smaller size of the pipe (650 mm) and the larger flow-rate (18,3 Mt/y).

Figures 46 and 47 show that Trunk A reaches the ambient temperature after about 350 km and remains almost constant, whilst the temperature of the trunk B is always above the ambient one (295,42 K in the first case and 295,76 K in the second one). This is because of the small length of the pipeline. In the trunk C there is a rapid temperature decrease in the offshore length because of the higher heat transfer and lower ambient temperature of the sea water. The inlet temperature of the trunk C differs just of 0,4 K in the two cases.

Without the booster at the Junction, the inlet pressure of the trunk B has almost the same value of the trunk A because of the higher level of turbulence related to the small size of the pipe. This means that, in the second case, a bigger pump will be required in order to assure the selected values of pressure to avoid problems at the Junction.

Technically, the use of a regulation station is considered to be a safer option because it allows better control of the transport, in particular to rectify possible inequalities generated along the pipeline, such as variable ambient temperature and impurities.

In Tables 20, 21 and 22 results for the pumping duty (kW) required by pumps and booster station and the corresponding capital cost (A\$m) of the various components are presented.

In Figures 43 and 44, components cost as a percentage (%) of the final cost of the transport infrastructure are reported.

Table 20) Pumping duty (kW) calculated with $\rho=630 \text{ kg/m}^3$ and $\eta_p=0,75$

Pump	Flow rate (t/day)	P_{cut-off} (MPa)	P_{final} (bar)	W_p (kW)
Trunk A no booster	35320,41	73,8	139	5641
Trunk B no booster	50105,69	73,8	137	7757
Total without booster				13398
Trunk A with booster	35320,41	73,8	102	2440
Trunk B with booster	50105,69	73,8	90	1988
Booster Station (80 to 118 bar)	85426,10	8	118	7952
Total with booster				12380

Table 21) Pipeline capital cost (A\$m)

	Trunk A	Trunk B	Trunk C	Total
Diameter [mm]	950	650	850	
Onshore Length [km]	930	60	60	
Offshore Length [km]	0	0	20	
Unit pipeline cost [A\$/m ²] 2017	2,89	2,41	2,76	
Onshore Pipeline CAPEX [A\$m] (2017)	2553	94	141	2788
Offshore Pipeline CAPEX [A\$m] (2017)	0	0	94	
Total CAPEX [A\$m] (2017)	2553	94	235	2882

Table 22) Compressors, pumps and booster cost calculation (A\$m)

Compressor	Component Cost (A\$m) 2017
Trunk A	105,57
Trunk B	121,37
Pump	
Trunk A no booster	9,91
Trunk B no booster	13,58
Total pump cost without booster	23,49
Trunk A with booster	4,35
Trunk B with booster	3,56
Booster at the Junction	
Booster Station (80 to 118 bar)	98,01
Total pump cost with booster	105,92

The results show that the pumping duty (kW) of Trunk B is approximately 37% higher when the booster station is not provided. In contrast, when the booster station is used at the Junction, the pumping duty (kW) and, as a consequence, pumping costs are higher for Trunk A by approximately 22%. This is because in this case the inlet pressure for Trunk A (102 bar) is higher than the value for Trunk B (90 bar).

Compression cost is slightly higher for Trunk B because of the higher amount of carbon dioxide flowing in the pipeline.

The results also show that the booster cost is about 10 times higher than pumping costs because of the additional expenses provided.

Trunk A is showed to be the most expensive pipeline because of the higher length (930 km) and diameter (950 mm) compared to the other two Trunks. The cost for the offshore length in Trunk C is showed to be very similar to the cost of Trunk B despite the lower length (20 km compared to 60 km of Trunk B) considering the additional costs of submerged pipelines. The results also show that approximately 88% of pipeline cost is for Trunk A.

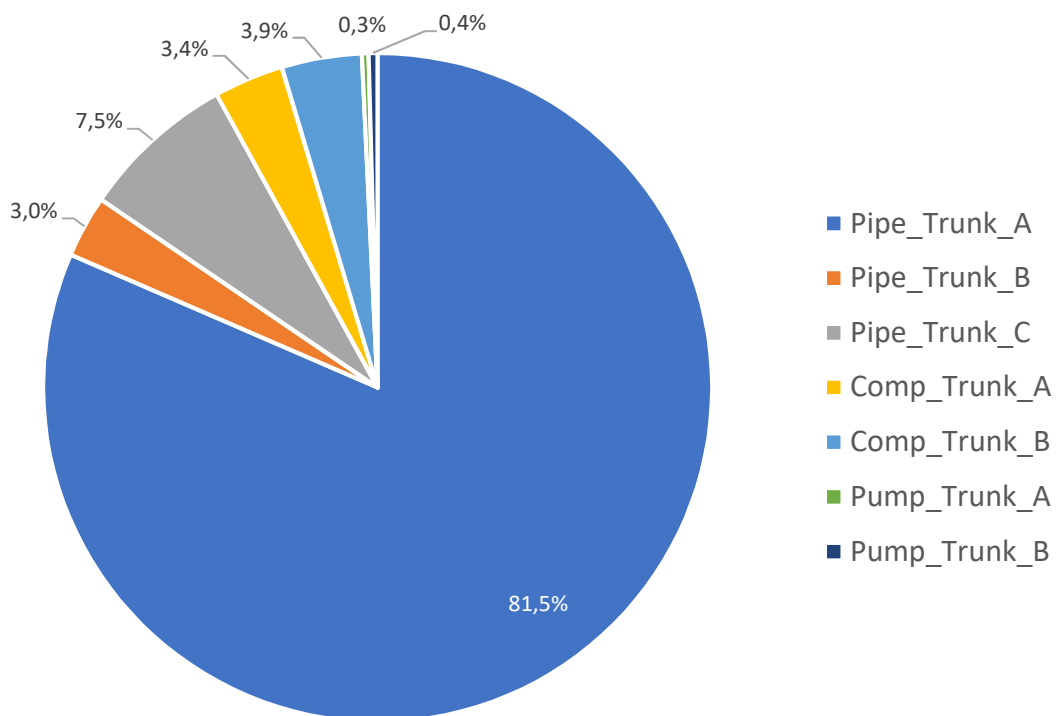


Figure 48) Component contribute (%) to the transport infrastructure cost without Booster Station

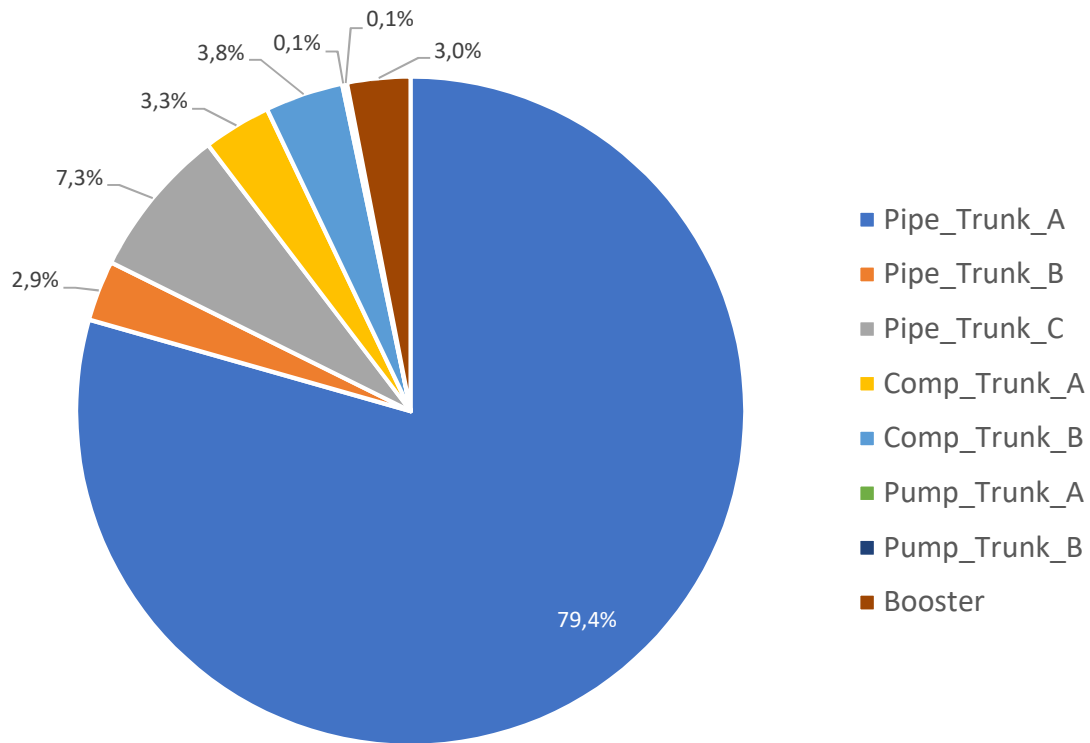


Figure 49) Component contribute (%) to the transport infrastructure cost with Booster Station

Figure 48 shows that when the booster station is not provided at the Junction, about 81,5% of the total transport costs is represented by the Trunk A pipeline and it slightly decreases to 79,4% when the booster is used at the Junction.

The results show that the pumps contribute is negligible (approximately 0,1% of the total transport cost) in both cases (with or without booster at the Junction).

Trunk B and C are showed to represent about 3 and 7 % of the final cost respectively. The compressor cost for each trunk is showed to be approximately the 3%.

4.4. South-Eastern Queensland to the Surat Basin

In this section, results for the South-Eastern Queensland network are presented (Figure 50). In Table 23, temperature and pressure values are reported assuming that each pipeline is fixed at a diameter of 450 mm for pipelines 1-7 (that are those which connect emission sources) and 850 mm for pipeline 8 (the final trunk). The analysis is also repeated but with variable diameters for each pipeline (see Table 16). The case study was modelled as a whole network setting the top-hole pressure at 92 bar without booster stations.

In Figures 51 and 52, the pressure profile for both cases is presented highlighting the pressure variation along the network length towards the storage site for each trunk.

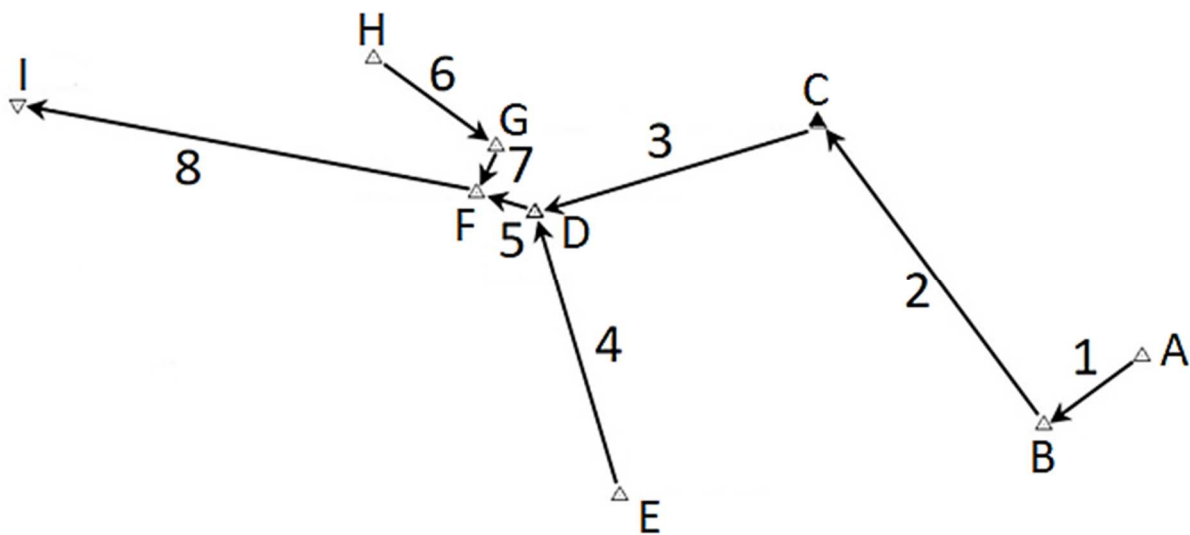


Figure 50) Description of the modelled pipeline network as reported by Fimbres et al. [11]

The results show that, generally, the pressure with the estimated diameter value is higher by 8% on average than fixing the diameter at 450 mm. This is to take into account the higher level of turbulence generated by a decreased size in some of the pipelines. In particular, pipelines 1, 2 and 3 shows a significant difference in pressure because of the different diameters. When the pipelines are reduced, there is to an increase of the pressure of approximately 15%. Pipeline 6 is the most affected because of the small flow rate and the inlet pressure increases by about 25% when the diameter changes from 450 to 150 mm.

The results show that there is less significant variation in temperature between the two cases. Pipeline 1 shows a lower temperature drop of approximately 1 K when using 450 mm diameter compared to when the diameter is estimated at 250 mm. This is because a larger diameter increases the expansion of carbon dioxide and, as a consequence, results in a higher decrease in temperature.

Table 23) Pressure and temperature results for the Hub Network with a fixed diameter or the optimal diameter for each pipeline

Pipeline	Inlet Node	Outlet Node	Fixed Diameter (450 mm cases 1-7, 850 mm case 8)				Estimated Diameter				
			Inlet Pressure [bar]	Outlet Pressure [bar]	Inlet Temperature [K]	Outlet Temperature [K]	Inlet Pressure [bar]	Outlet Pressure [bar]	Inlet Temperature [K]	Outlet Temperature [K]	Diameter [mm]
1	Bulwer Island & Lytton	Swanbank	148,2	147,7	298,15	293,66	171,1	161,0	298,15	294,47	250
2	Swanbank	Tarong North	147,7	142,6	293,66	292,62	161,0	142,5	294,47	292,51	350
3	Tarong North	Darling Downs	142,6	126,8	292,62	292,27	142,5	126,8	292,51	292,25	450
4	Millmerran	Darling Downs	140,1	126,8	298,15	293,51	140,1	126,8	298,15	293,51	450
5	Darling Downs	New CCGT	126,4	109,9	292,89	292,15	126,8	110,0	292,88	292,14	450
6	Condamine	Kogan Creek	112,7	112,6	298,15	292,65	140,3	130,9	298,15	292,62	150
7	Kogan Creek	New CCGT	112,6	109,9	292,65	292,51	130,9	110,0	292,62	291,77	300
8	New CCGT	Surat close-shallow	109,93	92	292,33	292,01	109,89	92	291,95	291,96	850

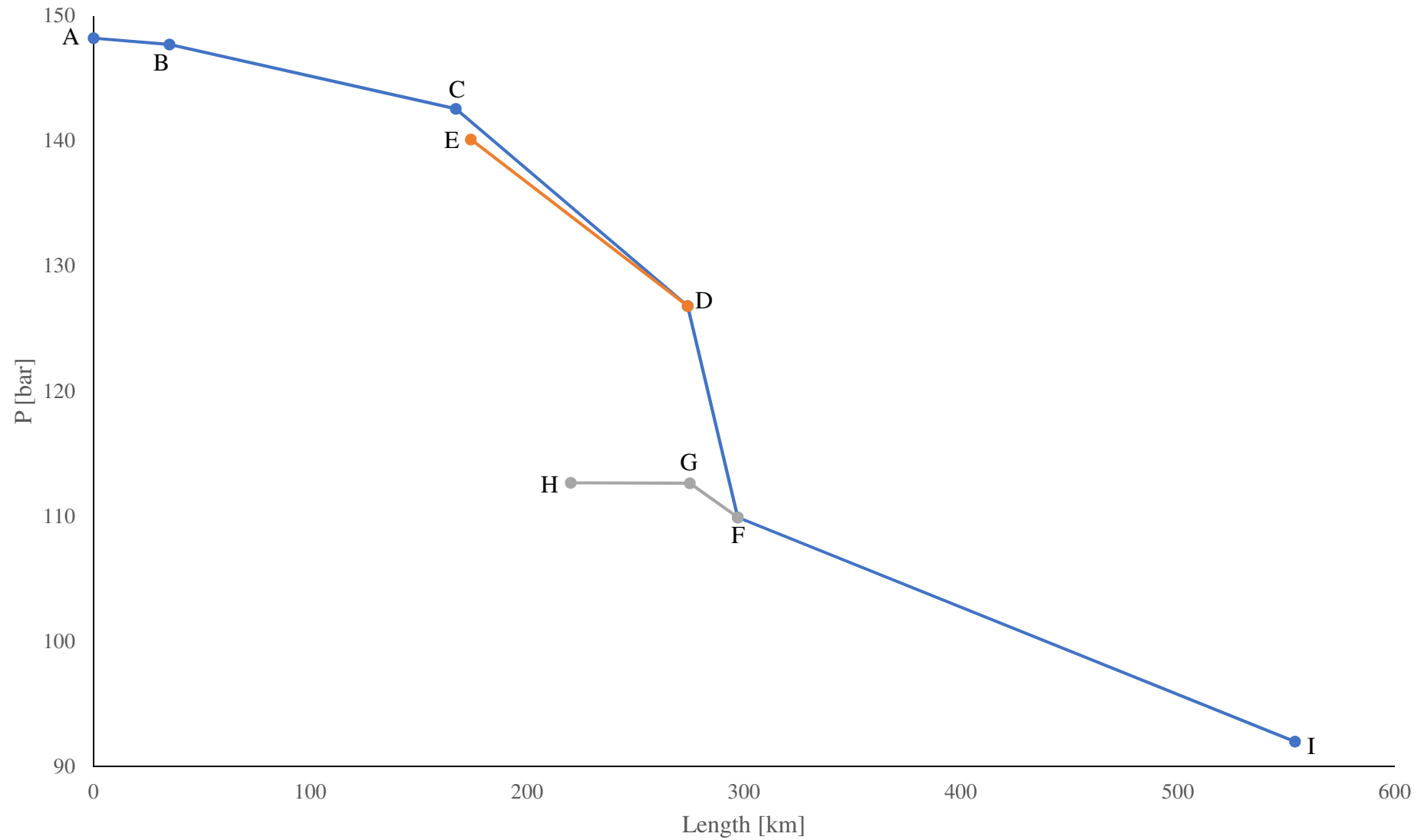


Figure 51) Pressure profile in the modelled Hub Network with a fixed value of diameter (450 mm for pipelines 1-7 and 850 mm for pipeline 8)

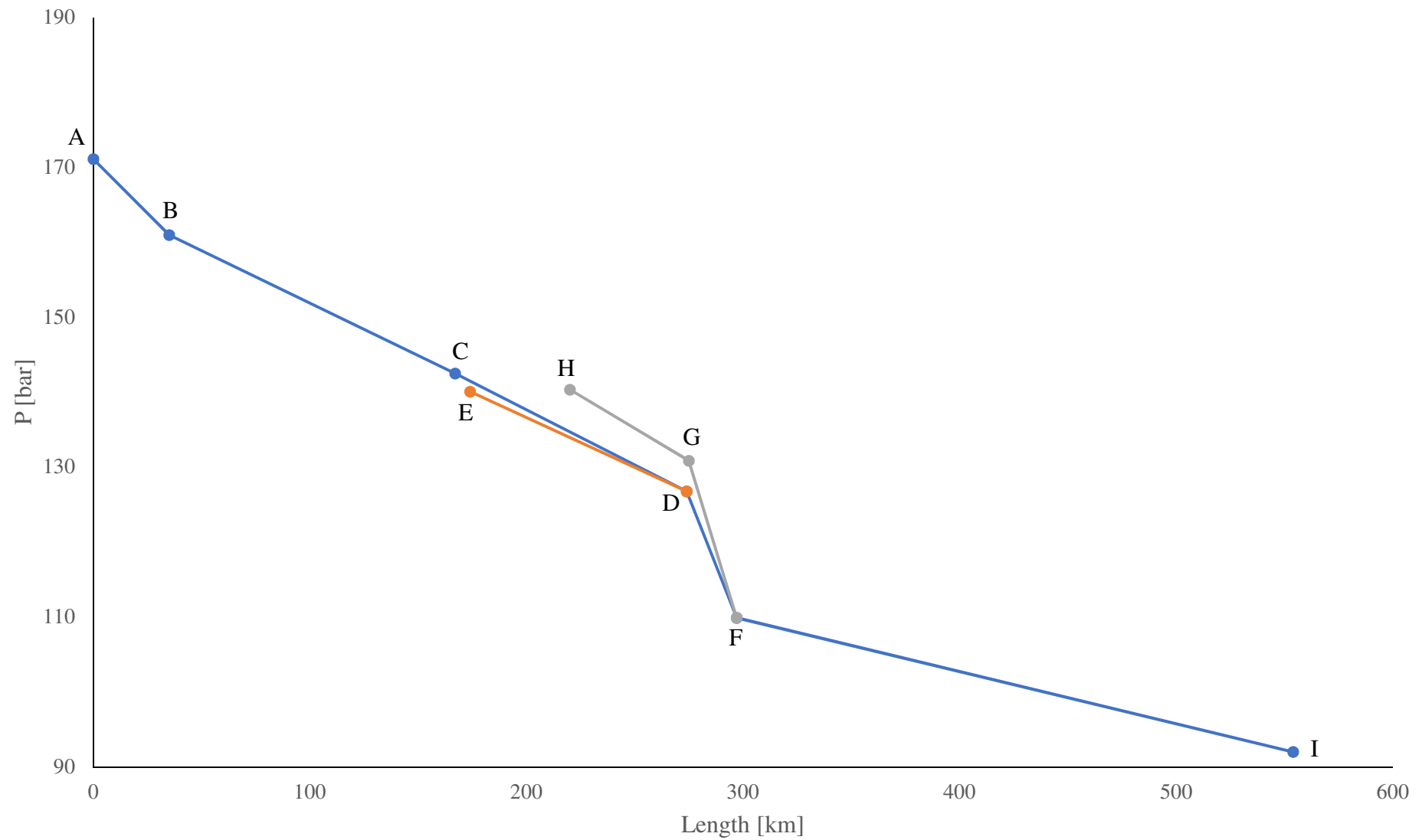


Figure 52) Pressure profile in the modelled Hub Network with the estimated value of diameter by CO2CRC [10]

The cost calculation for every component of the transport infrastructure (compressors, pumps and pipelines) is reported in Tables 24, 25 and 26. The component breakdown of the total cost is presented in Figures 53 and 54 for the network configuration with a fixed diameter value (450 mm for trunk 1 to 7 and 850 mm for trunk 8 and for the estimated diameters respectively.

Table 24) Compressor cost calculation [A\$m] 2017 with $P_{initial}=0,1$ MPa and $P_{cut-off}=7,38$ MPa

Compressor	Flow-rate (kg/s)	C_{comp} (A\$m) 2017
Bulwer Island & Lytton, Brisbane	47,535	45
Condamine	9,507	24
Darling Downs	50,704	46
Kogan Creek	129,929	67
Millmerran	145,774	70
New CCGT	50,704	46
Swanbank E	31,69	38
Tarong North	76,056	54

Table 25) Pumping Duty (kw) and pump cost calculation [A\$m] 2017 with $P_{cut-off}=7,38$ MPa, $\rho=630$ kg/m³ and $\eta_p=0,75$

Pump (Fixed Diameter)	Flow-rate (t/day)	P_{final} (MPa)	W_p (kW)	C_{pump} (A\$m) 2017
Bulwer Island & Lytton, Brisbane	4107	14,821	748,59	1,41
Condamine	821	11,268	78,23	0,25
Darling Downs	4381	12,677	568,42	1,10
Kogan Creek	11226	13,086	1569,05	2,83
Millmerran	12595	14,008	2044,85	3,66
New CCGT	4381	10,993	387,71	0,78
Swanbank E	2738	14,77	495,64	0,97
Tarong North	6571	14,256	1106,80	2,03
Pump (Estimated diameter)	Flow-rate (t/day)	P_{final} (MPa)	W_p (kW)	C_{pump} (A\$m) 2017
Bulwer Island & Lytton, Brisbane	4107	17,109	978,77	1,81
Condamine	821	14,035	133,90	0,34
Darling Downs	4381	12,677	568,42	1,10
Kogan Creek	11226	13,086	1569,05	2,83
Millmerran	12595	14,008	2044,85	3,66
New CCGT	4381	10,989	387,28	0,78
Swanbank E	2738	16,098	584,71	1,12
Tarong North	6571	14,251	1105,99	2,03

Table 26) Pipeline cost calculation [A\$m] 2017 for the Hub Network with fixed or estimated diameter value

Pipeline	Unit cost [A\$/m ²]	Diameter [mm]	Pipeline Length [km]	Cost [A\$m] 2017
Fixed Diameter Value				
1	2,21	450	35	35
2	2,21	450	132	131
3	2,21	450	107	106
4	2,21	450	100	99
5	2,21	450	23	23
6	2,21	450	55	55
7	2,21	450	22	22
8	2,76	850	257	603
Estimated Diameter Value				
1	2,01	250	35	18
2	2,01	350	132	93
3	2,21	450	107	106
4	2,21	450	100	99
5	2,21	450	23	23
6	2,01	150	55	17
7	2,01	300	22	13
8	2,76	850	257	603

The results show that the compressor cost is very similar in pipelines 4 and 5 (67 and 70 A\$m respectively) and in pipelines 1, 3 and 6 (45 and 46 A\$m). This is because of the same amount of carbon dioxide flows in these trunks. The compressor cost of pipeline 2 is the lowest due to the lowest flow-rate.

Pumping duty (kW) is showed to differ in the two cases just for pipelines 1, 2 and 7 of approximately 30% on average. This is because the smaller diameter value (250, 350 and 300 mm instead of 450 mm) leads to an increase of the inlet pressure and, as a consequence, a higher pumping duty. Hence, the pumping cost for these three pipelines in the case of estimated diameter value is higher of approximately 30 %.

Table 26 shows that in the case of fixed diameter value (450 mm for trunk 1 to 7 and 850 mm for trunk 8) the cost of pipelines 1, 2, 6 and 7 is higher of approximately 50% on average due to the higher diameter (250, 350, 150 and 300 mm in the second case). This leads to a total cost saving in the case of estimated diameter value (see Table 16) of approximately 100 A\$m considering the smaller size of some pipelines even if the pumping cost is reported to be higher.

Figures 53 and 54 show that pipeline 8 (the last trunk) has a percentage contribute of approximately 40% in both cases due to the higher diameter and length. Pipelines 1,2 and 7 are showed to have a variation of about 57% on average. Pipeline 6 results to have the biggest variation

as its value goes from 3,7% with fixed diameter value (450 mm) to 1,2% with estimated diameter value (150 mm). The other contributes result not significantly vary if the pipeline diameter is fixed (250, 350, 150 and 300 mm in the second case) or estimated (see Table 16).

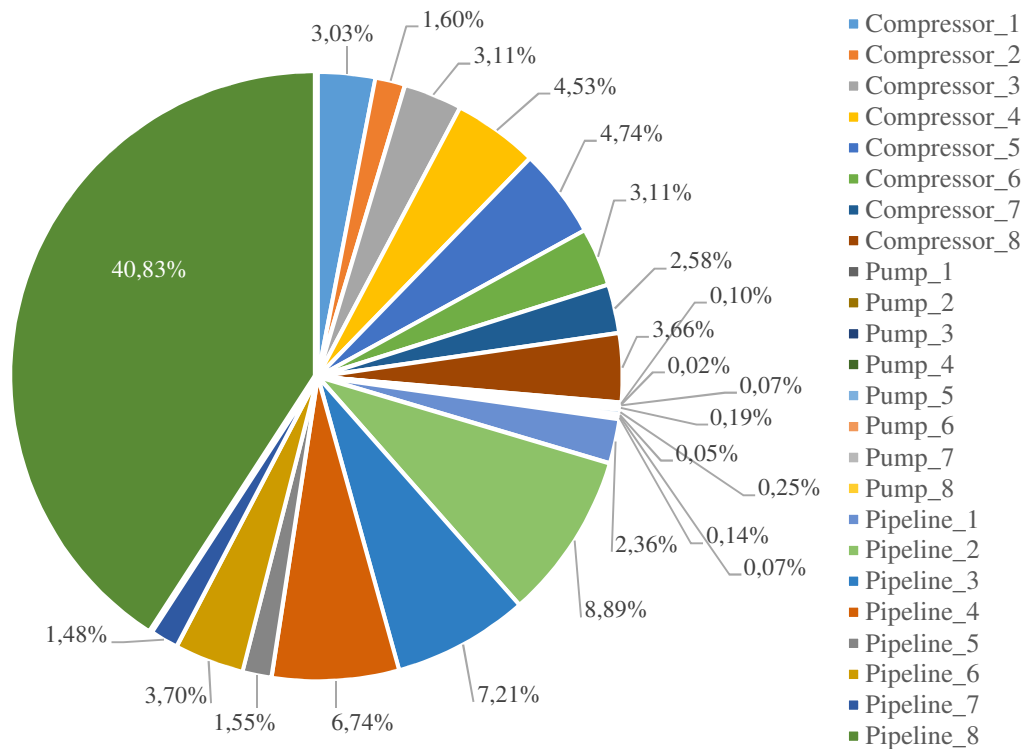


Figure 53) Component contribute (%) to the total infrastructure cost [A\$m] 2017 with a fixed diameter value (450 mm for trunk 1 to 7 and 850 mm for trunk 8)

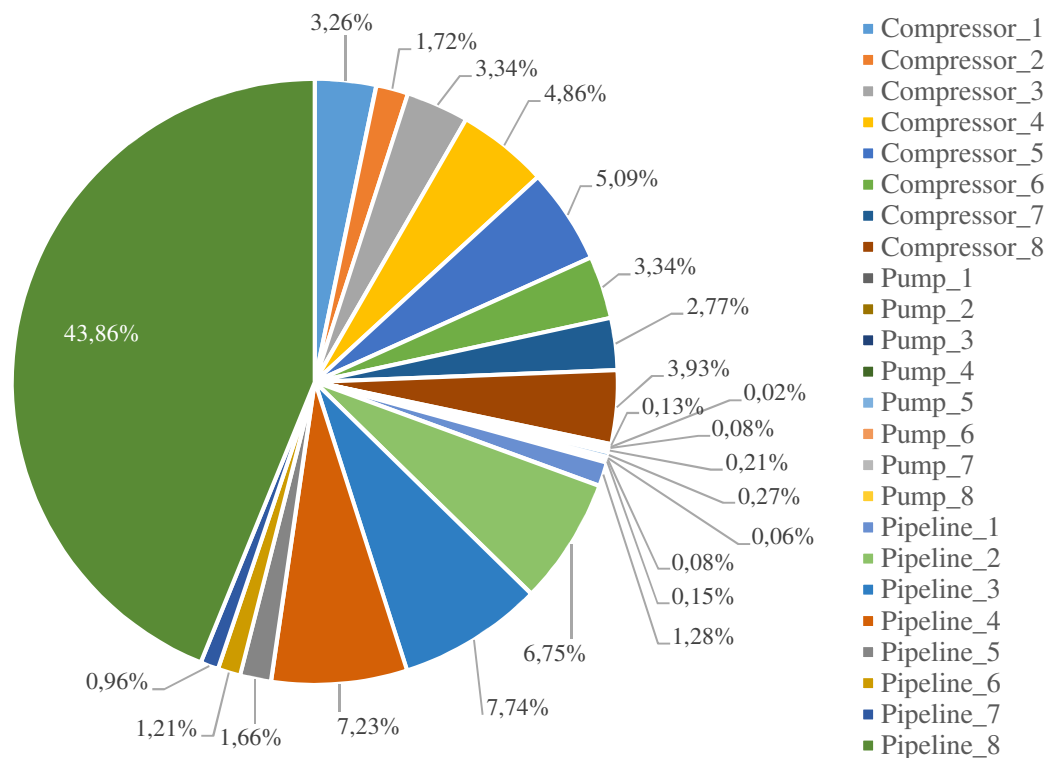


Figure 54) Component contribute (%) to the total infrastructure cost [A\$m] 2017 with an estimated diameter value by the CO2CRC [10]

4.5. Effects on pressure due to variable flow-rates: Tarong North and Millmerran to the Surat Basin

In this section, the effect on pipeline inlet pressure of variable flow-rates of CO₂ captured in two power plants (Tarong North and Millmerran) connected to the storage site in the Surat Basin is presented.

Figure 55 shows the yearly profiles of CO₂ captured for both power plants in 2010 (30-minute steps).

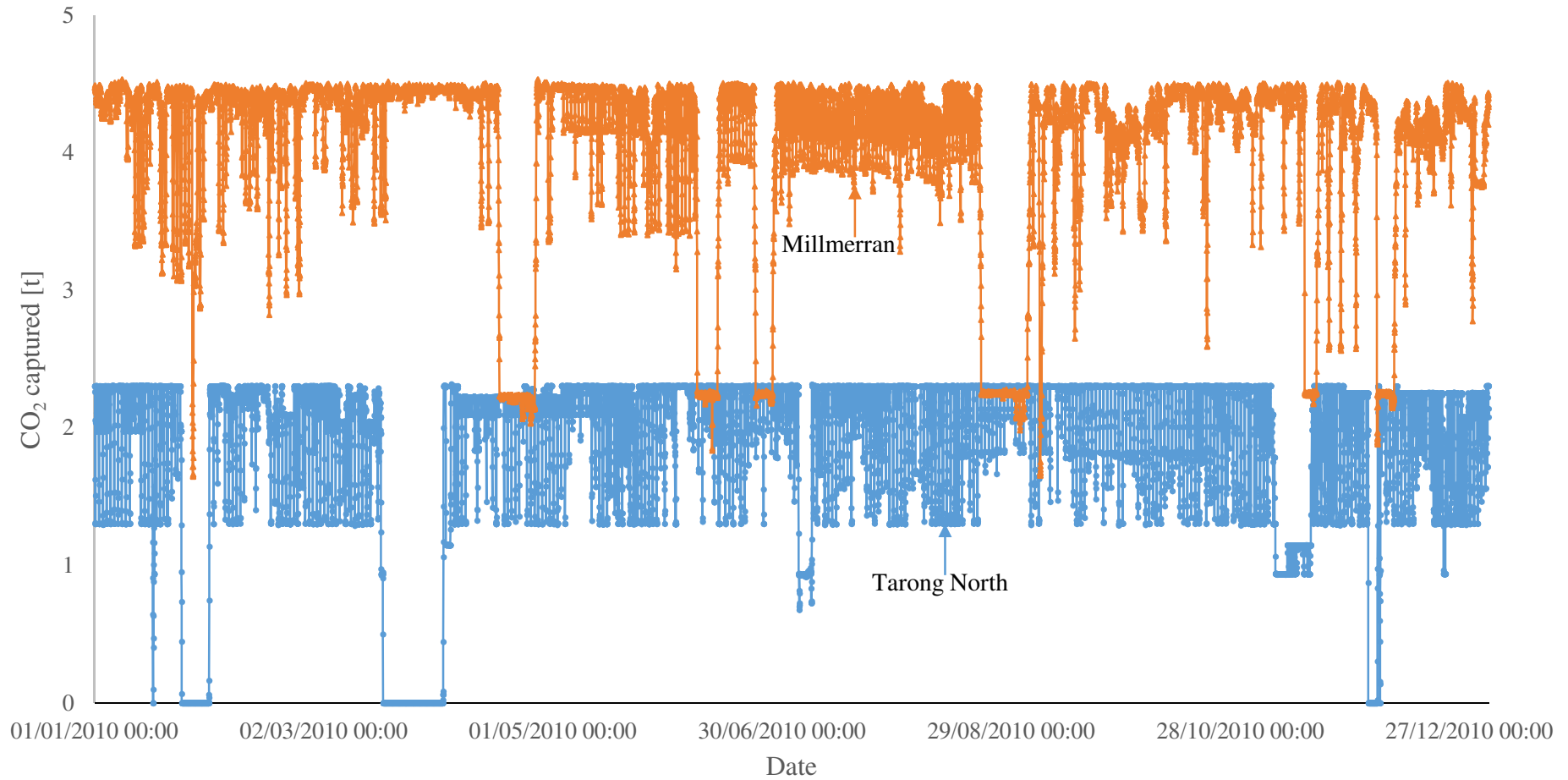


Figure 55) Yearly flow-rate profiles in 2010 for Tarong North and Millmerran

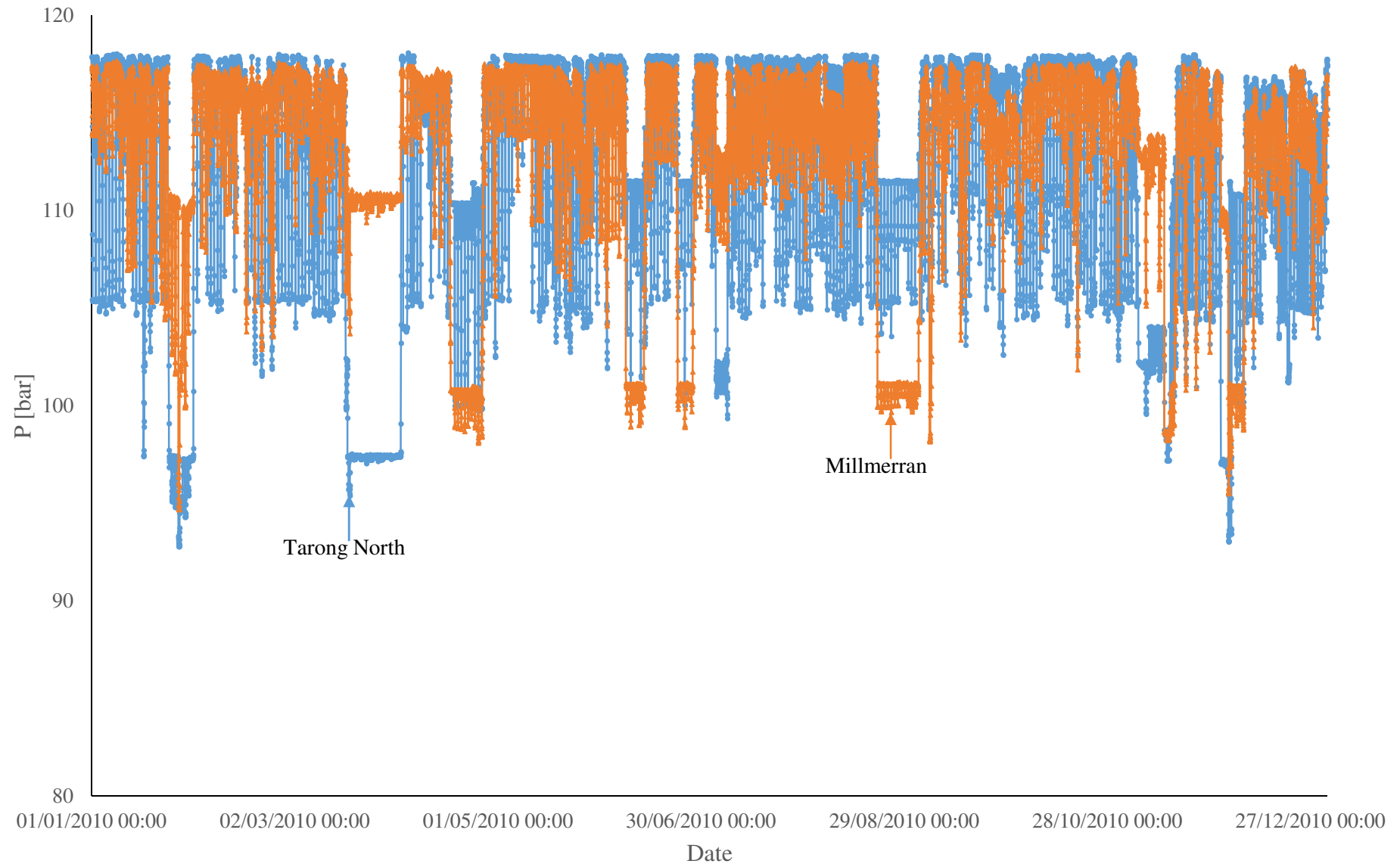


Figure 56) Yearly inlet pressure profiles for Tarong North and Millmerran depending on the flow-rate of the two power plants

Figure 56 shows that the inlet pressure for the two power plants has to adapt to the variations with the flow-rates and to ensure a top-hole pressure of 92 bar in the storage site (Surat). The pressure for Tarong North is usually higher than for Millmerran due to the longer pipeline length and smaller diameter. Tarong North was also shut down 4 times in 2010, while Millmerran only decreased its production without being shut down. This leads to a fast decrease in the fluid pressure in Tarong North that implies a fast reaction of the pumps in order to achieve a safe and effective transport.

For approximately 75% of the year, the inlet pressure of the two power plants is showed to be almost constant with a variation of about 10 bar (between 117 and 107 bar approximately). This variation in flow-rate and pressure corresponds to the changing power demand for peak and off-peak periods in the two power plants.

The two power plants also showed to have approximately 8 significant decreases in the inlet pressure value during the year (that is when the inlet pressure goes below 100 bar). These corresponded to times when the flow-rate was very low, as it was zero in Tarong North and less than 3 tons for Millmerran.

Table 27 shows the inlet pressure in Tarong and Millmerran calculated with the mean value of the yearly flow-rate profile in order to obtain a top-hole pressure of 92 bar in the storage site.

Table 27) Inlet pressure [bar] in Tarong North and Millmerran calculated with the yearly average flow-rate [Mt/y]

	Yearly average Flow-rate [Mt/y]	Inlet Pressure [bar]
Tarong North	1,916	111,04
Millmerran	4,033	112,20

As can be seen from Figure 56, the inlet pressures showed in Table 27 are a good approximation of the average values for the two power plants during the year (being comprised between 107 and 117 bar). In contrast, Figure 56 shows that the inlet pressure is higher than the value obtained with the yearly average flow-rate for about 12'000 times (30-minute steps considered during the year) over 17'500 in Tarong North and Millmerran (approximately 75%).

4.6. Sensitivity analysis

In this section, results for the sensitivity analysis are reported to understand how and which parameters affect the transport of carbon dioxide.

Effects of diameter, flow-rate and length

The aim of this section is to comprehend the effects on the outlet pressure of diameter, flow-rate and pipeline length with respect to the inlet value.

Figures 57, 58 and 59 present the effect of diameter, flow-rate and length on the outlet pressure. The inlet pressure of 150 is also presented to show a comparison and the resultant pressure drop for each of the cases.

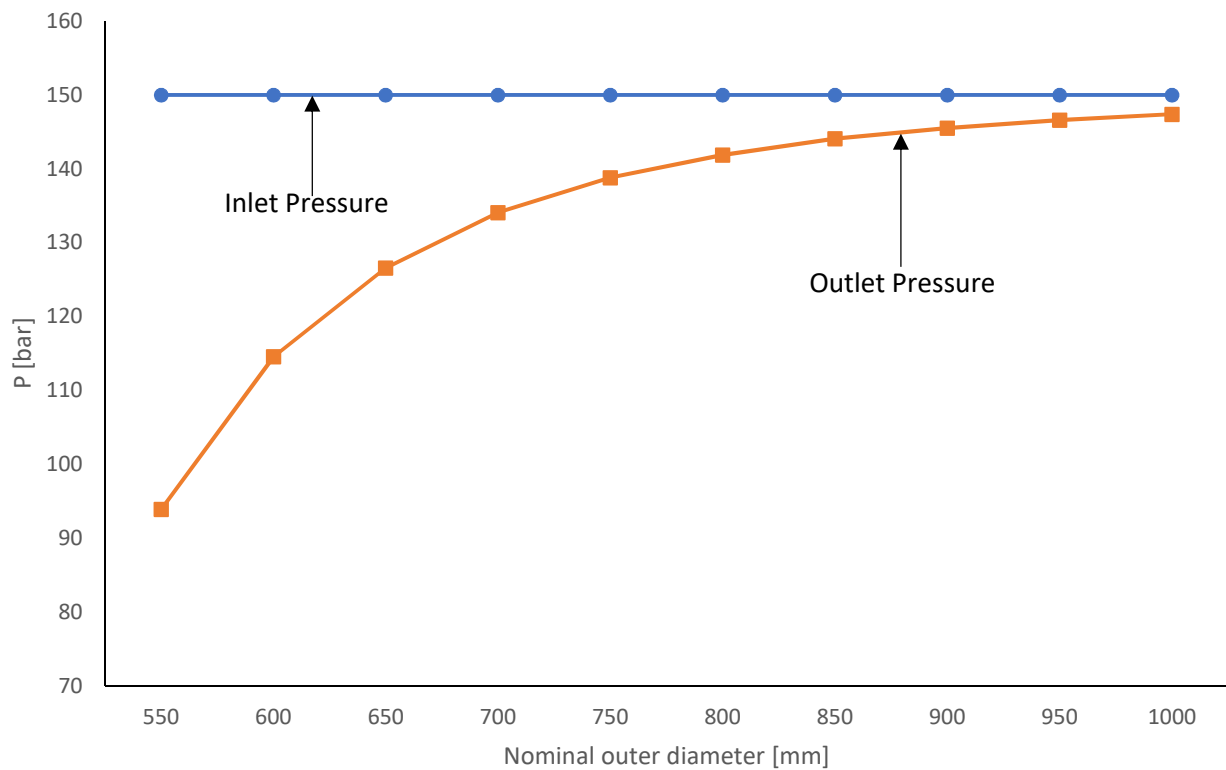


Figure 57) Effects of nominal outer diameter on the outlet pressure in a 1000 km pipeline with a flow rate of 5 Mt/y

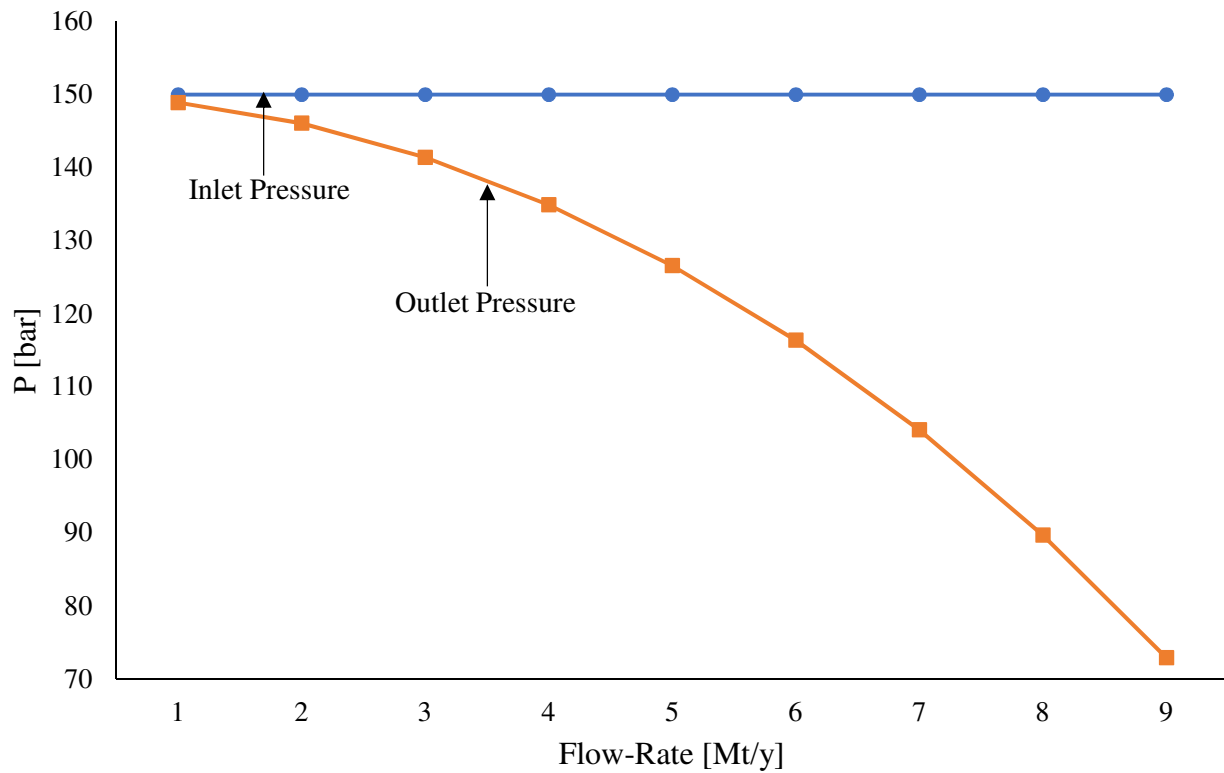


Figure 58) Effects of flow-rate on the outlet pressure in a 1000 km pipeline with a diameter of 650 mm

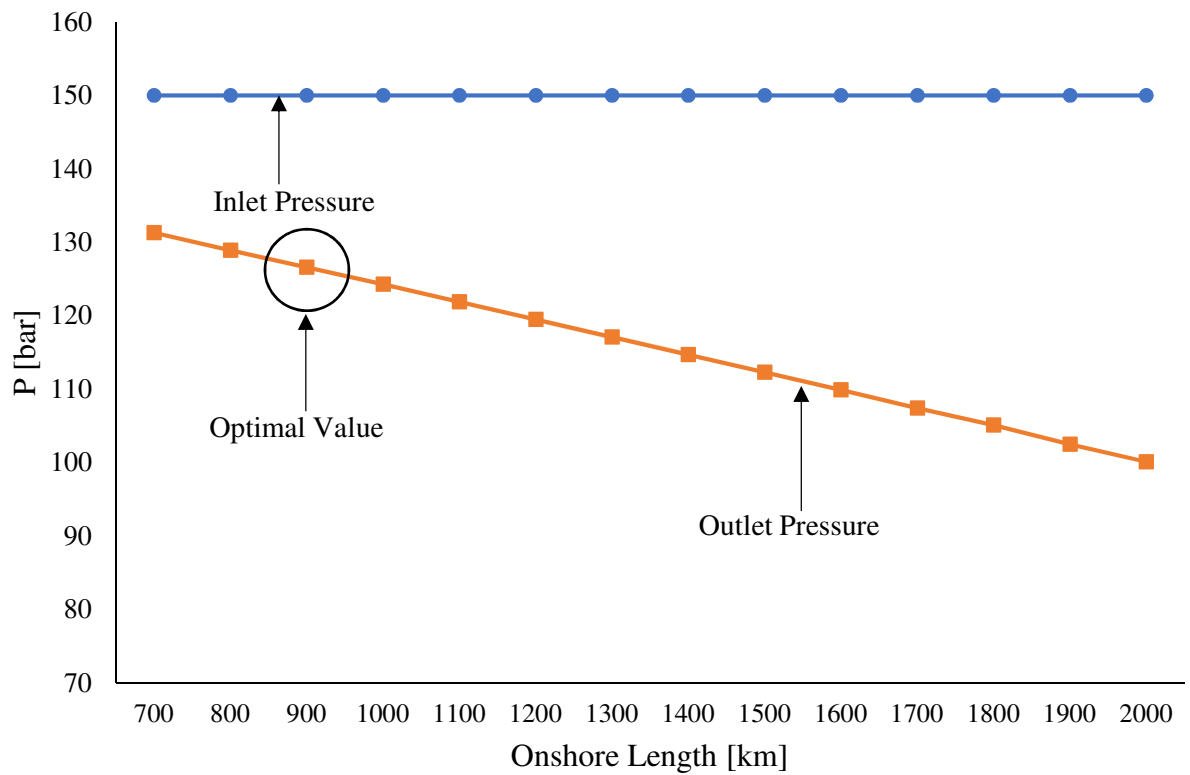


Figure 59) Effects of onshore pipeline length on the outlet pressure with a diameter of 650 mm and flow-rate of 5 Mt/y

The results highlight a strong relationship between the nominal outer diameter and the outlet pressure. Increasing the diameter of about 30 % from the determined value of 650 mm is showed to determine a very low pressure drop along the pipeline because of a lower friction factor and velocity of the carbon dioxide during the transport.

A small decrease in the diameter size leads to an important increase in the friction factor and, consequently, a bigger pressure drop. Hence, the diameter of the pipeline has to be kept as small as possible for economic reasons, but the turbulence level of carbon dioxide flowing in the pipe has a critical influence on the design selected. If the diameter is too small, carbon dioxide may undergo a phase changing creating cavitation problems increasing the probability for the propagation of ductile fractures and leakage. Therefore, the nominal outer diameter must be calculated balancing cost and technical factors in order to achieve a safe pressure drop along the pipeline.

The results related to the influence of the flow-rate on the outlet pressure show that an increase of approximately 60% (from 5 to 8 Mt/y) determines a very high increase in the pressure drop. The outlet pressure decreases from 127 to 90 bar outlining a higher turbulence level which increases the friction factor along the pipeline. If the flow-rate increases to 9 Mt/y, the results show that carbon dioxide undergoes the phase change along the pipeline with an outlet pressure below the critical value (73,8 bar).

Hence, if an emission source is likely to increase its carbon dioxide flow-rate in future, the higher pressure drop generated due to this higher amount must be considered to avoid the transition to the gas phase along the pipeline. For this reason, carbon dioxide pipelines are usually oversized to avoid the line packing of the link if the mass flow rate has to be increased.

The pipeline length is showed to be the less significant parameter of the three. Hence, doubling the length increases the pressure drop by approximately 24%. The variation in the length is found not to create as a high turbulence level in the pipe compared to the diameter and flow-rate. This is due to the fact that the friction factor is relatively constant with a change in the pipeline length.

In conclusion, a slightly oversized pipeline (100 mm higher than the estimated diameter value) may be the best solution for the transport of carbon dioxide. Hence, it is a good compromise between the higher pipeline cost and the lower pressure drop (for example 10 bar instead of 20 in 1000 km transporting 5 Mt/y) which determines a lower acceptable inlet pressure. As a consequence, the transport would be safer, with a lower level of turbulence and friction factor, and a lower risk of propagation of ductile fractures due to the highly pressurized carbon dioxide inside the pipeline.

Effects of inlet pressure, inlet temperature and heat transfer coefficient

The aim of this sensitivity analysis is to calculate the pressure drop along the length of the pipe with variations in the inlet pressure (130 and 150 bar) and temperature (298,15 and 323,15 K). The analysis considers both calculation isothermally and non-isothermally behaviour. Different Overall Heat Transfer Coefficients (3,69 and 0,1 W/m²K) are also investigated to represent insulated pipelines.

In Figures 60 and 61, pressure drop results have been reported modelling the transported carbon dioxide isothermally or non-isothermally setting the Overall Heat Transfer Coefficient equal at 3,69 W/m²K respectively.

Figure 62 and 63 report the same calculations for an Overall Heat Transfer Coefficient equal to 0,1 W/m²K to replicate an insulated pipeline.

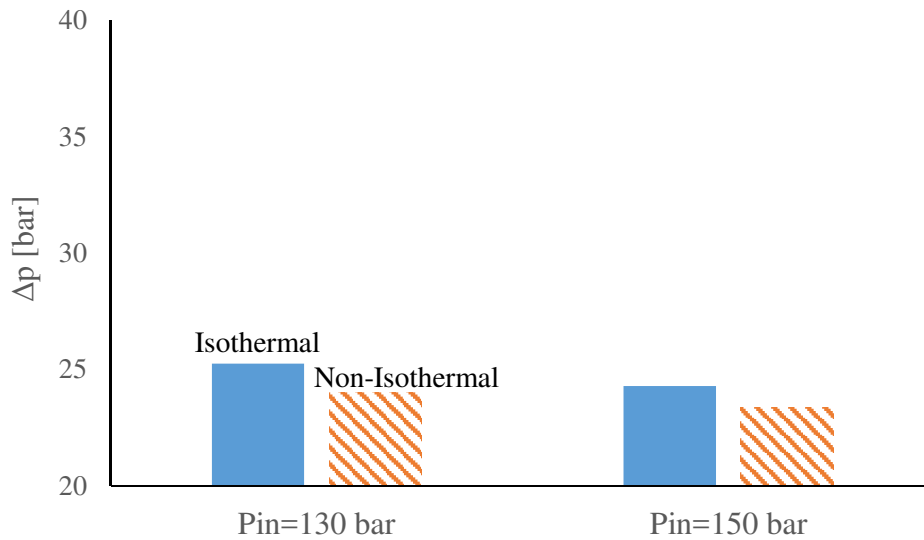


Figure 60) Pressure drop with inlet temperature equal to 298,15 K and $U_{onshore}=3.69$ W/m²K

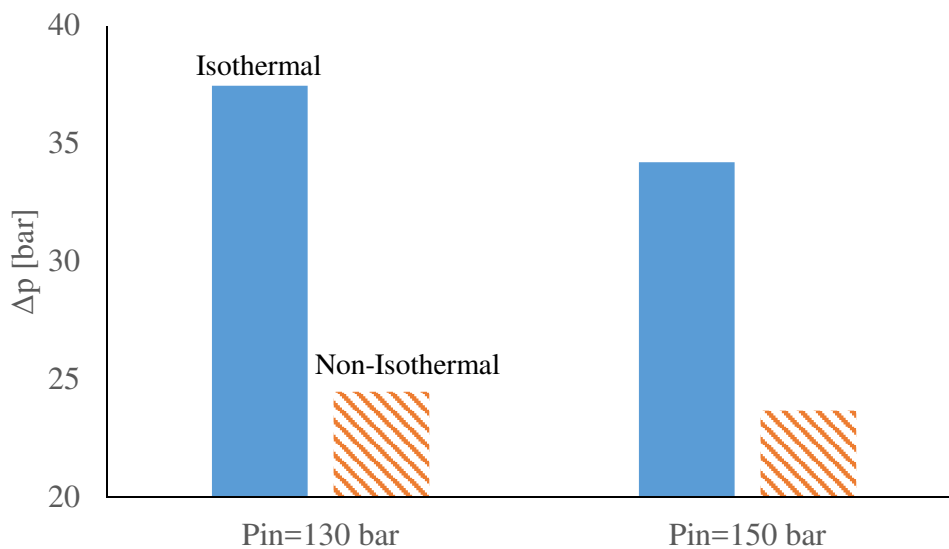


Figure 61) Pressure drop with inlet temperature equal to 323,15 K and $U_{onshore}=3.69$ W/m²K

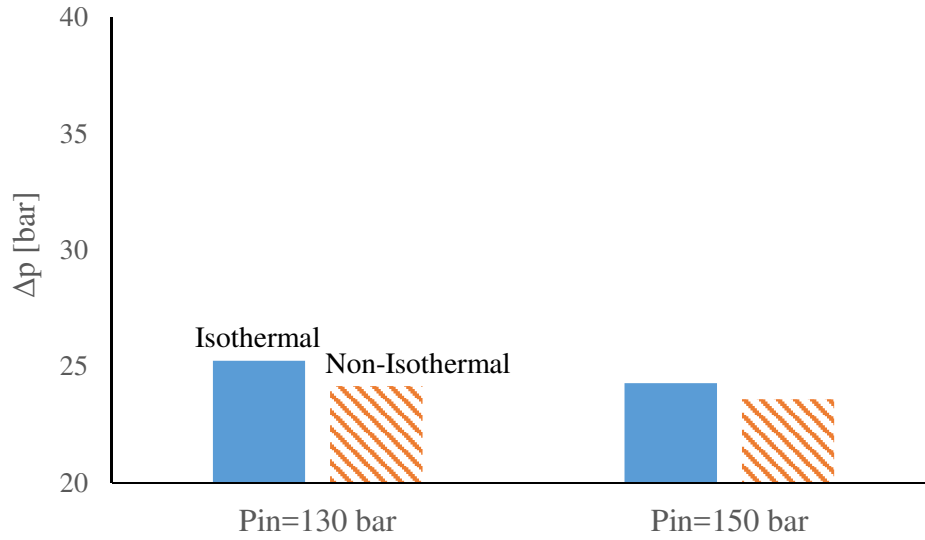


Figure 62) Pressure drop with inlet temperature equal to 298,15 K and $U_{onshore}=0.1 \text{ W/m}^2\text{K}$

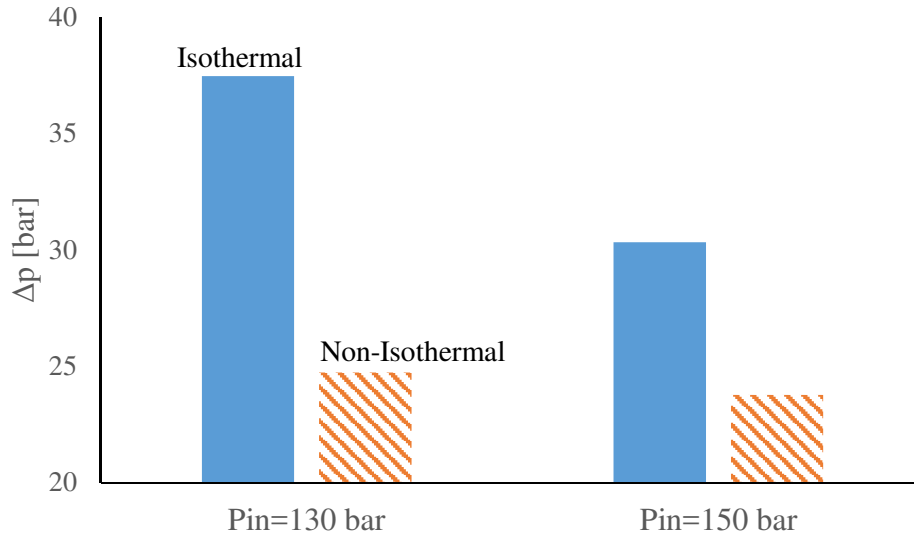


Figure 63) Pressure drop with inlet temperature equal to 323,15 K and $U_{onshore}=0.1 \text{ W/m}^2\text{K}$

The results show that modelling carbon dioxide transportation isothermally may lead to an overestimation of the pressure drop along the pipeline. Hence, independently of the inlet temperature, pressure and Overall Heat Transfer Coefficient, the pressure drop calculated assuming the isothermal fluid behaviour resulted in a higher value by approximately 5% on average. This is because the fluid temperature during the non-isothermal calculation decreases below the inlet value (external soil temperature of 292,65 K) and, as a consequence, the friction factor is lower than for the isothermal fluid behaviour.

The results show that this difference is particularly marked when the inlet temperature is high (323,15 K compared to 298,15 K). This is because at higher temperatures, the level of turbulence

is higher due to the higher fluid temperature, as stated by the Bernoulli's Principle, leading to a higher friction factor and Joule-Thomson coefficient.

The results also show that an inlet pressure of 130 bar leads to a slightly higher pressure drop of approximately 3% on average independently of the inlet temperature.

Figures 64 and 65 presents the above data showing pressure drop obtained with an Overall Heat Transfer Coefficient of 3,69 and 0,1 W/m²K, with the two pressures and temperatures for the non-isothermal case. The results show that the Overall Heat Transfer Coefficient has minimal effect on the pressure drop. This highlights that a possible insulated pipeline does not lead to an increase in the pressure drop along the length and, consequently, does not need a higher inlet pressure to avoid the phase changing.

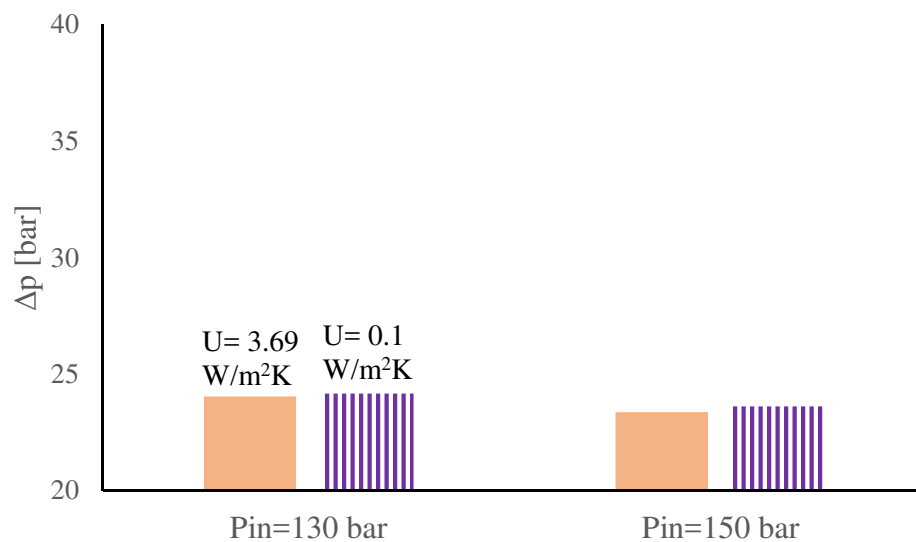


Figure 64) Pressure drop with inlet temperature equal to 298,15 K with different values of $U_{onshore}$

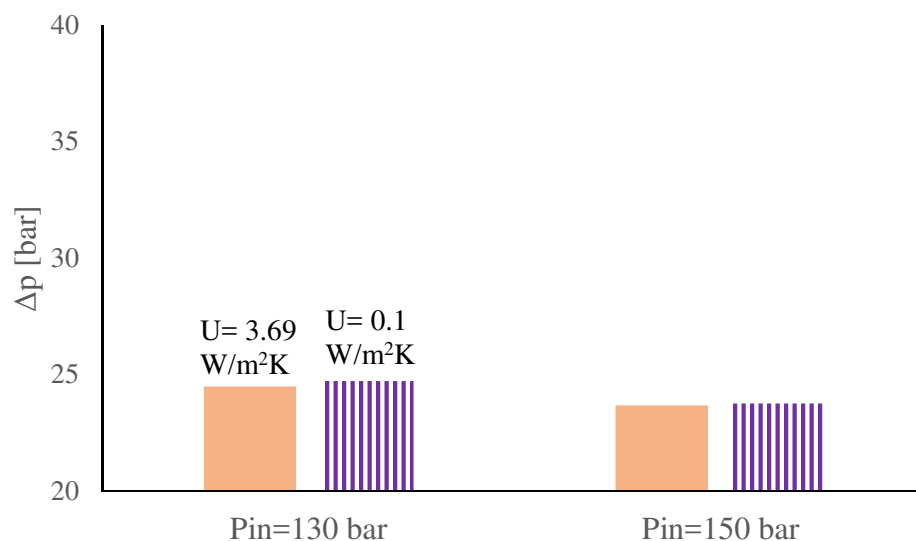


Figure 65) Pressure drop with inlet temperature equal to 323,15 K with different values of $U_{onshore}$

Figure 66 displays the results for the temperature drop along the pipeline with different values of the Overall Heat Transfer Coefficient for the non-isothermal cases. The onshore trunk without insulation ($U_{\text{onshore}}=3.69 \text{ W/m}^2\text{K}$) shows a 30 K temperature drop reaching the soil temperature. In contrast, the insulated pipeline ($U_{\text{onshore}}=0.1 \text{ W/m}^2\text{K}$) has a temperature drop of approximately 10-12 K.

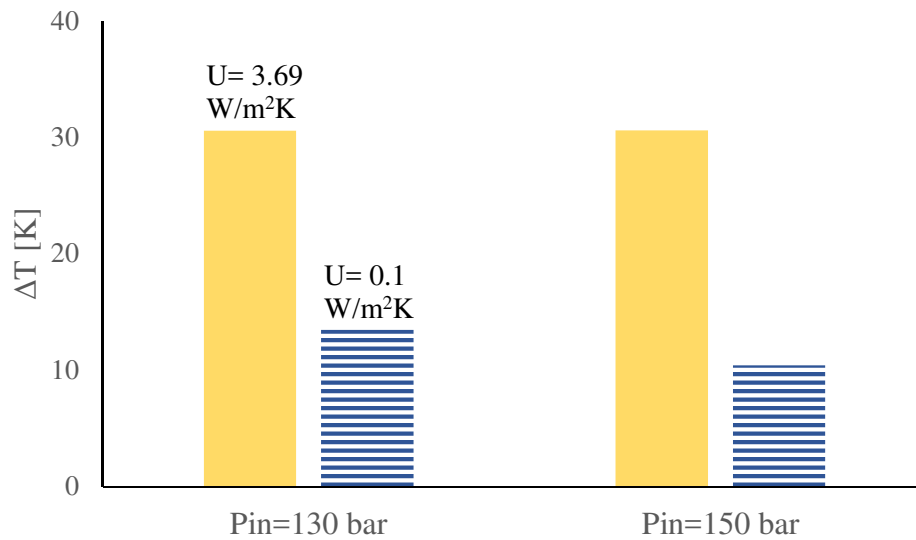


Figure 66) Temperature drop with inlet temperature equal to 323,15 K with different values of U_{onshore}

Effects of soil temperature

The aim of this sensitivity analysis is to understand the effects on pressure and temperature profile of an onshore trunk with different soil temperatures.

Figure 67 shows the results obtained varying the soil temperature from 283,15 to 323,15 K with a pipeline inlet temperature equal to 323,15.

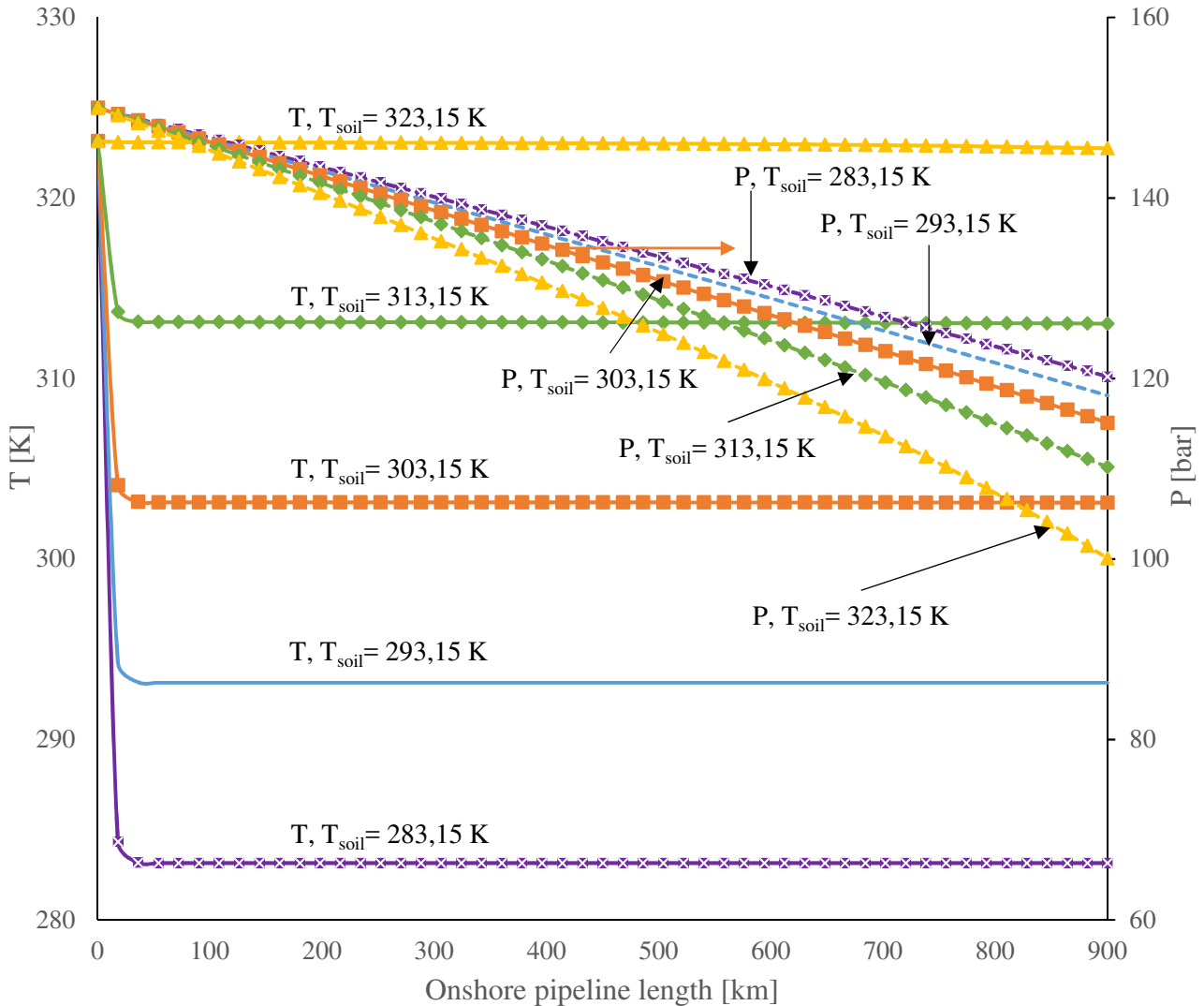


Figure 67) Temperature and pressure variations along the onshore length with different values of soil temperature

The results show that the fluid temperature reaches the soil temperature, independently on its value, after about 20 km and then it remains constant for the rest of the onshore length. This is due to the high heat transfer between the carbon dioxide flowing in the pipeline and the surroundings area determined by high value of the isobaric heat capacity and Joule-Thomson coefficient.

The pressure profile is almost linear for every value of soil temperature with the amount of pressure drop increasing as the soil temperature increases. This arises due to a higher fluid velocity

and internal energy as stated by the Bernoulli's Principle. Figure 65 shows that the pressure drop increases from 30 to 50 bar if the soil temperature increases from 298,15 to 323,15 K. For this reason, during very hot summer days, it is advisable to have a higher inlet pressure in order to avoid a decrease below the critical value and, consequently, a gas-phase transport.

Considering the higher pressure drop when the soil temperature increases, it may be possible in very hot areas to cover the pipeline with an innovative material, such as Phase Changing Materials (PCMs), which are able to cool the pipes down when the external temperature are high. This will have benefit of reducing the likely pressure drop.

A Phase Change Material (PCM) is a substance classified as "latent heat storage" (LHS) with a high heat of fusion which, melting and solidifying at a certain temperature, is capable of storing and releasing large amounts of energy. Heat is absorbed or released when the material changes from solid to liquid. When it reaches the melting temperature, it absorbs large amounts of heat at an almost constant temperature. The PCM continues to absorb heat without a significant rise in temperature until all the material is transformed to the liquid phase. When the ambient temperature falls, the PCM solidifies, releasing its stored latent heat. A large number of PCMs are available in any required temperature range from 268 up to 463 K, as stated by PCM Products [80].

5. Conclusions

The work presented in this thesis evaluate pressure and temperature profiles in carbon dioxide pipelines. CO₂ transportation was modelled non-isothermally in order to investigate the heat transfer between the pipeline and the environment (soil for onshore trunks and sea water for offshore trunks). The analysis conducted in this thesis provides insights into understanding the behaviour of the carbon dioxide pipelines under different inlet conditions. These results can be used to assist in the development of a Carbon Capture and Storage (CCS) pipeline transportation roadmap, providing valuable information in the design and operating of transport networks.

A one-dimensional, steady state, non-isothermal, multi-component model for a natural gas network was adapted for carbon dioxide to enable the accurate evaluation of the pressure and temperature profile along the pipeline. The pressure and temperature profile were calculated non-isothermally in two loop cycles, the fluid-dynamic (flow equation) and the energy problem (energy equation). Different ambient temperatures (from 283,15 to 323,15) were considered to understand changes in terms of pressure and temperature variations. Additionally, single trunk and whole network cases were modelled to understand the differences and the possible use of booster station. Results from the developed model were also used for the cost calculation. The pressure profile was also calculated in a network composed by two power plants with variable flow-rate profiles connected to a single storage site. A sensitivity analysis was conducted to understand the effects of diameter, flow-rate, length, inlet pressure and temperature, Overall Heat Transfer Coefficient and soil temperature on the pressure and temperature profile along the pipeline.

The temperature profile along the pipeline was investigated and it was found that when the inlet temperature is 323,15 K, the pipeline temperature did not to reach the ambient value for onshore trunks (almost 3 K above the soil temperature in 100 km) even if the fluid temperature experiences a rapid temperature drop at the beginning due to the higher difference with respect to the surroundings. However, if the inlet temperature is 298,15 K, the pipeline temperature undergoes a slower decrease along the same length, but it reaches the soil value after almost 60 km. A faster drop in the fluid temperature was achieved in the offshore trunk due to the higher heat transfer coefficient for offshore transportation.

Having a lower inlet temperature results in a lower velocity of the carbon dioxide particles and a decrease of the pressure drop due to less turbulences in the pipeline. The pressure profile along the pipeline was shown to be linear regardless of the temperature profile. The results also show that

there is a bigger slope in the onshore trunk when the temperature difference between the fluid and the environment is higher. In the offshore trunk, pressure has a slight decrease (approximately 2 bar over 20 km).

The heat transfer between pipeline and the environment (soil for onshore pipelines and sea water for offshore transportation) was also analysed for different ambient values and pipeline inlet temperatures. Modelling carbon dioxide transportation isothermally was showed to lead to an overestimation of the pressure drop along the pipeline by approximately 5% on average. The results show that this difference is particularly marked when the inlet temperature is high (323,15 K compared to 298,15 K). This is because at higher temperatures, the level of turbulence is higher due to the higher fluid temperature leading to a higher friction factor and Joule-Thomson coefficient.

The results also showed that the Overall Heat Transfer Coefficient has minimal effect on the pressure drop. This highlights that a possible insulated pipeline does not lead to an increase in the pressure drop along the length and, consequently, does not need a higher inlet pressure to avoid the phase changing. The onshore trunk without insulation ($U_{\text{onshore}}=3.69 \text{ W/m}^2\text{K}$) shows a 30 K temperature drop reaching the soil temperature. In contrast, the insulated pipeline ($U_{\text{onshore}}=0.1 \text{ W/m}^2\text{K}$) has a temperature drop of approximately 10-12 K.

This thesis also investigated key parameters affecting the pipeline pressure and temperature. It was found that the nominal outer diameter was a key parameter for CO₂ transportation. Increasing the diameter of about 30 % from the determined value of 650 mm showed that there was negligible pressure drop along the pipeline because of a lower friction factor. In contrast, a small decrease in the diameter size resulted to an important increase in the pressure drop. Hence, the diameter of the pipeline has to be kept as small as possible for economic reasons, but the higher pressure drop should be avoided to ensure that the CO₂ does not undergo phase change.

The flow-rate was found to be another key parameter. Results showed that an increase of approximately 60% (from 5 to 8 Mt/y) determines a very high increase in the pressure drop. If the flow-rate increases to 9 Mt/y, the results showed that carbon dioxide undergoes the phase change along the pipeline with an outlet pressure below the critical value (73,8 bar). For this reason, carbon dioxide pipelines are usually oversized to avoid the line packing of the link if the mass flow rate has to be increased.

The pipeline length was showed to be the less significant parameter of the three. Hence, doubling the length increases the pressure drop by approximately 24%. The variation in the length was found not to create a higher turbulence level in the pipe compared to the diameter and flow-rate.

The results on the effects of soil temperature showed that the fluid temperature reaches the soil value after about 20 km and then it remains constant for the rest of the onshore length. The pressure profile was found to be almost linear for every value of soil temperature with the amount of pressure drop increasing as the soil temperature increases. The results showed that the pressure drop increases from 30 to 50 bar if the soil temperature increases from 298,15 to 323,15 K in a 1000-km pipeline. For this reason, during very hot summer days, it is advisable to have a higher inlet pressure in order to avoid a decrease below the critical value and, consequently, a gas-phase transport.

The steady-state model described in this paper is the first step approximation in the development of a more general “dynamic” model incorporating time effects. The results from this analysis may be used as the starting point and basis for comparison for later “dynamic” non-isothermal model results.

A future model development may include CO₂-rich mixtures to evaluate the pressure and temperature profiles of “real” flows coming from carbon capture sites.

The design optimisation of the network based of different parameters (flow-rate, diameter and cost) could also be achieved in further studies.

6. References

- 1) The Intergovernmental Panel on Climate Change (IPCC) (2007). IPCC Fourth Assessment Report: Climate Change.
https://www.ipcc.ch/publications_and_data/ar4/wg1/en/tssts-3-1-1.html
- 2) M. Mohitpour, P. Seevam, K.K. Botros, B. Rothwell, C. Ennis (2012). Pipeline transportation of carbon dioxide containing impurities. New York, ASME Press
- 3) J.R. Ehleringer, T. E. Cerling, M.D. Dearing (2005). A history of atmospheric CO₂ s and its effects on plants, animals, and ecosystems. New York, NY, Springer
- 4) International Energy Agency (2011). CO₂ Emissions from Fuel Combustion.
<https://www.iea.org/media/statistics/CO2highlights.pdf>
- 5) IEAGHG (2009). Safety in Carbon Dioxide Capture, Transport and Storage, Technical Study. Cheltenham, UK.
- 6) W. Mallon, L. Buit, J. van Wingerden, H. Lemmens, N. H. Eldrup (2013). Costs of CO₂ transportation infrastructures. KEMA Nederland B.V.
- 7) The Callide Oxyfuel Project (2014). Australian Reservoirs.
<http://www.callideoxyfuel.com/How/CarbonStorage/tabid/77/Default.aspx>
- 8) R. Span and W. Wagner (1996). A New Equation of State for Carbon Dioxide Covering the Fluid Region from Triple-Point Temperature to 1100 K at Pressures up to 800 MPa. Journal of Physical and Chemical Reference Data.
- 9) Y. Kim (2007). Equation of State for Carbon Dioxide. Journal of Mechanical Science and Technology.
- 10) Cooperative Research Centre for Greenhouse Gas Technologies (CO2CRC) (2015). Australian Power Generation Technology Report.
http://www.co2crc.com.au/wp-content/uploads/2016/04/LCOE_Report_final_web.pdf
- 11) G. A. Fimbres Weihs, D. E. Wiley (2012). Steady-state design of CO₂ pipeline networks for minimal cost per tonne of CO₂ avoided. The University of New South Wales, Sydney, Australia 2052.
- 12) S. Pellegrino, A. Lanzini, P. Leone (2016). Greening the gas network – The need for modelling the distributed injection of alternative fuels. Energy Department, Politecnico di Torino.
- 13) O. Kunz, W. Wagner (2012). The GERG-2008 Wide-Range Equation of State for Natural Gases and Other Mixtures: An Expansion of GERG-2004. Lehrstuhl für Thermodynamik, Ruhr-Universität Bochum, D-44780 Bochum, Germany.
- 14) J. A. Swaffield, S. Bridge (1983). Applicability of the Colebrook-White Formula to Represent Frictional Losses in Partially Filled Unsteady Pipeflow. Brunel University, Uxbridge, Middlesex, U.K.
- 15) E. Heidaryan, T. Hatami, M. Rahimi, J. Moghadasi (2011). Viscosity of pure carbon dioxide at supercritical region: Measurement and correlation approach. Kermanshah, Iran.
- 16) The World Bank (2017). CO₂ Emissions (metric tons per capita).
<https://data.worldbank.org/indicator/EN.ATM.CO2E.PC?end=2014&start=1960>
- 17) A. Feitz (2014). An overview of CCS in Australia.
<http://www.pucrs.br/cepac/download/ccsavancado/10.Overview CCS Australia Feitz.pdf>
- 18) J. Barrie, K. Brown, P. Hatcher, H. Schellhase (2004). Carbon dioxide pipelines: a preliminary review of design and risks. Vancouver, Canada.
- 19) J. G. Serna (2016). Peng-Robinson Equation of State.
<https://au.mathworks.com/matlabcentral/fileexchange/4519-peng-robinson-eos>
- 20) M. W. Chase Jr (1998). NIST-JANAF Thermochemical Tables, Fourth Edition. The Journal of Physical and Chemical Reference Data (American Institute of Physics).

- 21) C. M. Colina, K.E. Gubbins (2003). Choosing and evaluating equations of state for thermophysical properties. North Carolina State University.
- 22) N. J. Wise (2012). Experimental Determination of the Joule-Thomson Coefficient of Nitrogen, Carbon Dioxide and Oxygen. Bob Jones University, Division of Science, Department of Chemistry, Greenville, South Carolina.
- 23) L. Ouyang (2012). New Correlations for Predicting the Thermodynamic Properties of Supercritical Carbon Dioxide. Chevron Corporation, Bellaire, Texas.
- 24) E. Heidaryan, A. Jarrahan (2013). Modified Redlich–Kwong Equation of State for Supercritical Carbon Dioxide. The Journal of Supercritical Fluids.
- 25) M. Mazzocchi, B. Bosio, E. Arato (2012). Analysis and comparison of Equations-of-State with p-p-T experimental data for CO₂ and CO₂-mixture pipeline transport. University of Genoa.
- 26) J. Morbee, J. Serpa, E. Tzimas (2010). The evolution of the extent and the investment requirements of a trans-European CO₂ transport network. European Commission, Joint Research Centre, Institute for Energy, Petten, The Netherlands.
- 27) E. Aursand, P. Aursand, T. Berstad, C. Dørum, M. Hammer, S. T. Munkejord, H. O. Nordhagen (2013). CO₂ pipeline integrity: A coupled fluid-structure model using a reference equation of state for CO₂. Trondheim, Norway.
- 28) M.M.J. Knoope, A. Ramírez, A.P.C. Faaij (2013). Economic optimization of CO₂ pipeline configurations. Utrecht University, The Netherlands.
- 29) X. Luo, M. Wang, E. Oko, C. Okezue (2014). Simulation-based techno-economic evaluation for optimal design of CO₂ transport pipeline network. The University of Hull, United Kingdom.
- 30) W. Mallon, L. Buit, J. v. Wingerden, H. Lemmens, N. H. Eldrup (2013). Costs of CO₂ transportation infrastructures. Groningen, The Netherlands.
- 31) R. Simon, H. E. Skontorp, J. J. Poplsteinova (2013). Multi-criteria Analysis of Two CO₂ Transport Technologies. Trondheim, Norway.
- 32) Global CCS Institute (2015). CO₂ Pipeline Design - an Australian perspective. <http://www.globalccsinstitute.com/insights/authors/ChrisConsoli/2015/09/23/co2-pipeline-design-australian-perspective>
- 33) S. T. McCoy, E. S. Rubin (2005). Models of CO₂ Transport and Storage Costs and Their Importance in CCS Cost Estimates. Carnegie Mellon University.
- 34) M. Drescher, Ø. Wilhelmsen, P. Aursand, E. Aursand, G. d. Koeijer, R. Held (2013). Heat Transfer Characteristics of a Pipeline for CO₂ Transport with Water as Surrounding Substance. Trondheim, Norway.
- 35) S. T. Munkejord, C. Bernstone, S. Clausen, G. d. Koeijer, M. J. Mølnevik (2013). Combining thermodynamic and fluid flow modelling for CO₂ flow assurance. Trondheim, Norway.
- 36) S. Brown, S. Martynov & H. Mahgerefteh (2015). Modelling heat transfer in flashing CO₂ fluid upon rapid decompression in pipelines. Department of Chemical Engineering, University College London, UK.
- 37) S. Liljemark, K. Arvidsson, M.T.P. Mc Cann, H. Tummescheit, S. Velut (2011). Dynamic simulation of a carbon dioxide transfer pipeline for analysis of normal operation and failure modes. Goteborg, Sweden.
- 38) P. Aursand, M. Hammer, S. T. Munkejord, Ø. Wilhelmsen (2012). Pipeline transport of CO₂ mixtures: Models for transient simulation. NORDICCS Technical Report.
- 39) H. Mahgerefteh, S. Brown, S. Martynov (2012). A study of the effects of friction, heat transfer, and stream impurities on the decompression behavior in CO₂ pipelines. Greenh.
- 40) G. d. Koeijer, J. H. Borch, M. Drescher, H. Li, Ø. Wilhelmsen, J. Jakobsen (2011). CO₂ Transport - Depressurization, Heat Transfer and Impurities. Trondheim, Norway.
- 41) J.O. Valderrama (1990). A generalized Patel-Teja equation of state for polar and non-polar fluids and their mixtures. Journal Chemical Engineering Japan.

- 42) D. Avlonitis, A. Danesh, A. C. Todd (1994). Prediction of VL and VLL Equilibria of Mixtures Containing Petroleum Reservoir Fluids and Methanol with a Cubic EOS. Journal of Fluid Phase Equilibria.
- 43) J.H. Van der Waal, J.C. Platteeuw (1959). Clathrate solutions. Advances in Chemical Physics.
- 44) W.R. Parrish, J.M. Prausnitz (1972). Dissociation pressures of gas hydrate formed by gas mixture. Industrial & Engineering Chemistry Process Design and Development.
- 45) G.D. Holder, G. Corbin, K.D. Papadopoulos (1980). Thermodynamic and molecular properties of gas hydrate from mixtures containing methane, argon and krypton. Industrial & Engineering Chemistry Fundamentals.
- 46) T. Kihara (1953). Virial Coefficient and Models of Molecules in Gases. Reviews of Modern Physics.
- 47) K. Li, X. Zhou, R. Tu, Q. Xie, X. Jiang (2014). The flow and heat transfer characteristics of supercritical CO₂ leakage from a pipeline. University of Science and Technology of China, Hefei, Anhui.
- 48) A. Witkowski, M. Majkut, S. Rulik (2014). Analysis of pipeline transportation systems for carbon dioxide sequestration. Silesian University of Technology, Institute of Power Engineering and Turbomachinery, Konarskiego, Poland.
- 49) S. T. Munkejord, M. Hammer, S. W. Løvseth (2016). CO₂ transport: Data and models – A review. SINTEF Energy Research, Trondheim, Norway.
- 50) Z.X. Zhang, G.X. Wang, P. Massarotto, V. Rudolph (2006). Optimization of pipeline transport for CO₂ sequestration. Energy Conversion and Management.
- 51) B.I. Lee, M.G. Kesler (1975). A generalized thermodynamic correlation based on three-parameter corresponding states. AIChE Journal.
- 52) U. Plocker, H. Knapp (1978). Calculation of High-Pressure Vapor-Liquid Equilibria from a Corresponding-States Correlation with Emphasis on Asymmetric Mixtures. Industrial & Engineering Chemistry Process Design and Development.
- 53) D.Y. Peng, D.B. Robinson (1976). A New Two-Constant Equation of State. Industrial & Engineering Chemistry Fundamentals.
- 54) M. Benedict, G.B. Webb, R.C. Louis (1940). An Empirical Equation for Thermodynamic Properties of Light Hydrocarbons and Their Mixtures: I. Methane, Ethane, Propane, and n-Butane. Journal of Chemical Physics.
- 55) K.E. Starling (1973). Fluid Properties for Light Petroleum Systems. Gulf Publishing Company, Houston.
- 56) W.C. Edmister, B.I. Lee (1984). Applied Hydrocarbon Thermodynamics. Gulf Publishing Company, Houston.
- 57) K.H. Lüdtke (2004). Process centrifugal compressors. Springer, Berlin Heidelberg.
- 58) W.A. Maxey (1974). Fracture initiation, propagation and arrest. Fifth Symposium on Line Pipe Research, American Gas Association.
- 59) International Energy Agency (2016). 20 Years of Carbon Capture and Storage. Paris, France.
- 60) O. Redlich, J.N.S. Kwong (1949). On the Thermodynamics of Solutions. Chemical Reviews.
- 61) S. Clausen, A. Oosterkamp, K. L. Strøm (2012). Depressurization of a 50 km long 24 inches CO₂ pipeline. Energy Procedia.
- 62) H. Sick, D. Manderson (2016). CarbonNet Knowledge Product: development of a CO₂ specification for a CCS hub network. The State of Victoria, Australia.
- 63) B. Prah, R. Yun (2017). Heat transfer and flow characteristics of CO₂-hydrate mixture in pipeline. Hanbat National University, Republic of Korea.
- 64) P.R. Neal, M. Ong (2009). An update on the Integrated CCS Economics Model. CO₂CRC Research Symposium, Australia.
- 65) M. Mohitpour, H. Golshan, A. Murray (2003). Pipeline design and construction: a practical approach. American Society of Mechanical Engineers, New York.

- 66) C. Teh, A. Barifcania, D. Packa, M. O. Tade (2015). The importance of ground temperature to a liquid carbon dioxide pipeline. Cooperative Research Centre for Greenhouse Gas Technologies (CO2CRC), Clean Gas Technology, Australia.
- 67) J.A. Lake, I. Johnson, D.D. Cameron (2016). Carbon Capture and Storage (CCS) pipeline operating temperature effects on UK soils: The first empirical data. University of Sheffield, UK.
- 68) G.S. Campbell, J.M. Norman (1998). An Introduction to Environmental Biophysics. Springer-Verlag New York.
- 69) B. Wetenhall, J.M. Race, H. Aghajani, J. Barnett (2017). The main factors affecting heat transfer along dense phase CO₂ pipelines. Newcastle University, University of Strathclyde, West Midlands, UK.
- 70) Government of Western Australia, Department of Mines and Petroleum (2012). South West CO₂ Geosequestration Hub. East Perth, Western Australia.
http://www.ceg.uwa.edu.au/__data/assets/pdf_file/0008/2186846/South-West-Hub.pdf
- 71) Chevron Australia (2016). Carbon dioxide injection project. Perth, Western Australia.
<https://www.chevronaustralia.com/docs/default-source/default-document-library/gorgon-co2-injection-project.pdf?sfvrsn=0>
- 72) K. Kang, Y. Seo, D. Chang, S.G. Kang, C. Huh (2015). Estimation of CO₂ Transport Costs in South Korea Using a Techno-Economic Model. Offshore CCS Research Unit, Korea Research Institute of Ships and Ocean Engineering, Korea.
- 73) R. Haghbakhsh, H. Hayer, M. Saidi, S. Keshtkari, F. Esmaeilzadeh (2013). Density estimation of pure carbon dioxide at supercritical region and estimation solubility of solid compounds in supercritical carbon dioxide: Correlation approach based on sensitivity analysis. Shiraz University, Iran University of Science and Technology(IUST), Iran.
- 74) Z. Wang, B. Sun, J. Wang, L. Hou (2014). Experimental study on the friction coefficient of supercritical carbon dioxide in pipes. China University of Petroleum, China.
- 75) Department of Primary Industries, NSW Government (2017). Soil Temperature Data. New South Wales, Australia.
<http://www.tocal.nsw.edu.au/farms/Tocals-e-farm/the-climate-of-tocal/temperature,-frost,-humidity-and-clouds/soil-temperature-data>
- 76) World Sea Temperatures (2017). Australia Sea temperatures.
<https://www.seatemperature.org/australia-pacific/australia/>
- 77) J. Wang, Z. Wang, B. Sun (2017). Improved equation of CO₂ Joule–Thomson coefficient. China University of Petroleum (East China).
- 78) D. L. McCollum, J. M. Ogden (2006). Techno-Economic Models for Carbon Dioxide Compression, Transport, and Storage. Institute of Transportation Studies, Davis University of California.
- 79) Kazuaki Katayama (2018). Steel pipeline cost. Personal communication.
- 80) PCM Products Ltd (2011). Phase Change Material. Cambridgeshire, United Kingdom.
http://www.pcmproducts.net/files/eutectic_catalogue-2011-1.pdf

APPENDIX A: Matlab model

The developed MATLAB model for the evaluation of pressure and temperature profile in carbon dioxide pipelines is presented in this section. The inlet pressure and temperature were fixed as guess value (boundary condition).

```
clear all
close all
clc
% TOLERANCE
tolNR=1e-9; % NEWTON-RAPHSON METHOD
tolFLUID=1e-9; % FLUID PROBLEM LOOP
tolFRAC=1e-6; % MASS FRACTION LOOP
tolTHER=1e-2; % NODE TEMPERATURE LOOP
tolMAIN=1e-6; % AVERAGE TEMPERATURE LOOP
% WEIGHT
a=0; % FLUID PROBLEM LOOP
b=0; % MASS FRACTION LOOP
c=0; % NODE TEMPERATURE LOOP
d=0; % AVERAGE TEMPERATURE LOOP
%% Branch Input*****
[INPUT_b] = xlsread('Input_pipelines_Test');
Ainput = INPUT_b(:,1:3); % Network topology (column1:BRANCH;column2:IN-
NODE;;column2:OUT-NODE)
D = INPUT_b(:,4)/1000; % INSIDE DIAMETER, m %%Branch long
LL = INPUT_b(:,5)*1000; % Branches length, m %%Branch long
epsi = INPUT_b(:,6)/1e6; % Rugosity, m %%Branch long
%U = INPUT_b(:,10); % Linear Heat Transfer Coefficient, W/m/K %%Branch long
Text= INPUT_b(:,8)+273.15; % External Temperature (Soil), K %%Branch long
G = INPUT_b(:,7)*31.69; % Branches flow rate (GUESS VALUE) %%Branch long
%kg/s
PIPE=find(INPUT_b(:,9)==1); % Indicates branches which are pipes
L_tot=sum(LL)/1000; %total length km
node=max(max(Ainput(:,2:3))); % Number of nodes of the network
%% Node Input*****
[INPUT_n] = xlsread('Input_nodes_Test');
Gext = INPUT_n(:,1)*31.69; % Mass flow-rate exchanged with the environment, kg/s %%Node
long
KNOWN = find(Gext>0); % Sets the node with known pressure (usually the inlet ones)
UNKNOWN = find(Gext<=0); % Sets the nodes with unknown pressure
P = INPUT_n(:,2)*1e6; % Nodes pressure (GUESS VALUE), Pa %%Node long
T = INPUT_n(:,3)+273.15; % Nodes temperature (GUESS VALUE), K %%Node long
% BOUNDARY CONDITION (NODE KNOWN)
PRESSURE=P(KNOWN); % Pa
UGC=8.314413; % Universal Gas Constant J/molK
AREA=pi*(D.^2)/4; % Pipeline cross sectional area
```

```

% OVERALL LINEAR HEAT TRANSFER COEFFICIENT
UL=zeros(length(PIPE),1);
Tsoil=19.5+273.15;
for dd=1:length(PIPE)
    if Text(dd)==Tsoil
        U=3.69;      % W/m2/K
    else
        U=39.6;      % W/m2/K
    end
    UL(dd)=U*pi*D(dd);    % W/m/K
end
ENT=find(Gext>0);    % Nodes with flow rates entering the network from the external
EXT=find(Gext<0);    % Nodes with flow rates exiting the network to the external
T_ent=zeros(node,1); % Temperature of the flow rates entering the network from the external
(INITIALIZATION)
T_ent(ENT)=T(ENT);
%% *****MATRIX*****
% A=INCIDENCE MATRIX
for i=1:max(Ainput(:,1))
    for j=1:max(max(Ainput(:,2:3)))
        if j==Ainput(i,2)
            A(j,i)=1;
        else if j==Ainput(i,3)
            A(j,i)=-1;
        end
    end
end
end
Aplus=A;
Aminus=A;
Aplus(A==1)=0; % Positive part of the incidence matrix
Aminus(A==1)=0; % Negative part of the incidence matrix
Aminus=abs(Aminus);
MGext=diag(Gext);
MGexta=diag(abs(Gext));
IE=zeros(length(Gext));
for i=1:length(Gext)    % Matrix IE
    if Gext(i)>0
        IE(i,i)=-1;
    elseif Gext(i)<0
        IE(i,i)=1;
    end
end
IEplus=0.5*(abs(IE)+IE);    % Matrices IEpos
IEminus=0.5*(abs(IE)-IE);    % Matrices IENeg
Tm = 0.5*abs(A)*T; % Branches average temperature (GUESS VALUE) %%Branch long
T_out = Aminus*T; % Branches output temperature (GUESS VALUE) %%Branch long
T_in=Aplus*T; % Branches input temperature (GUESS VALUE) %%Branch long
%% *****PURE CARBON DIOXIDE*****
% PROPERTIES OF THE GAS
M_W=0.04401; %Molar Weight kg/mol

```



```

R=(UGC./M_W); %J/kg/K
T_c=304.15; %Critical Temperature [K]
p_c=7.38e6; %Critical Pressure [Pa]
w=0.224; %acentric factor
%% *****MODEL SOLUTION*****
PP=size(P(2:end),1); % NUMBER OF PIPES
if length(KNOWN(:,1))>1
    PP=PP-(length(KNOWN(:,1))-1);
end
Gext_ENT=zeros(size(Gext));
Gext_EXT=zeros(size(Gext));
Gext_EXT(EXT)=Gext(EXT);
Gext_ENT(ENT)=Gext(ENT);
yy=0;
kkk=0;
Niter1=0;
ver1=0;
errorMAIN=NaN;
S1='SOLVING....NITER: ';
S3='...ERROR: ';
while ver1==0
    S2=num2str(Niter1);
    S4=num2str(errorMAIN);
    display(strcat(S1,S2,S3,S4));
    Niter3=0;
    ver3=0;
    errorFLUID=NaN;
    while ver3==0
        S1=' FLUID-DYNAMIC PROBLEM....NITER: ';
        Niter3=Niter3+1;
        S2=num2str(Niter3);
        S4=num2str(errorFLUID);
        display(strcat(S1,S2,S3,S4));
        Pm=2/3*(Aplus'*P+Aminus'*P-
            (Aplus'*P).*(Aminus'*P)./((Aplus'*P)+(Aminus'*P)));
        X=1; %pure CO2
        gas.R=8.314;
        gas.M=44.01;
        gas.Tc=T_c;
        gas.Pc=p_c;
        gas.Vc=0.000094;
        gas.cCp_degC = [7.464e-9 -2.887e-5 0.04233 36.11];
        gas.w=w;
        gas.eosID= 5; %PENG-ROBINSON EOS
        gas.cAlpha=[0.37464,1.54226,-0.26992,2];
        gas.epsilon=1-sqrt(2);
        gas.sigma=1+sqrt(2);
        gas.OmegaA= 0.457235;
        gas.OmegaB= 0.077796;
        gas.Zc=0.274;
        for ii=1:PP

```

```

Pmi=Pm(ii);
Tmi=Tm(ii);
x.P_atm= Pmi*9.8692e-6; %atm
x.T_degC= Tmi -273.15; %Celsius
x.ID = 1; %Pure CO2
x;
props=source_props(x);
Zm(ii) = getfield(props,'Z'); %Compressibility PR
Rhom(ii)=getfield(props,'dens'); %Density kg/m3
viscosity(ii)=getfield(props,'visc')*0.001; % [Pa*s]
Gi=G(ii);
Di=D(ii);
epsii=epsi(ii);
velocity(ii)=Gi/Rhom(ii)/AREA(ii);
Re(ii)=Rhom(ii)*velocity(ii).*Di/viscosity(ii);
f(ii)=Frictionfactoraverage(Pmi,Tmi,epsii,Gi,Di);
end
RR=R*ones(PP,1);
    Y_P=AREA(PIPE).*(((abs(A(:,PIPE))*P).^0.5)./
        ((A(:,PIPE)*P).^0.5)).*((D(PIPE)./(Zm(PIPE)'.*RR.*Tm(PIPE).*f'.*LL(PI
        PE))).^0.5);
    temp=(AREA(PIPE).^2).*(((abs(A(:,PIPE))*P))./
        ((A(:,PIPE)*P))).*((D(PIPE)./(Zm(PIPE)'.*RR.*
        Tm(PIPE).*f'.*LL(PIPE)))));
Y_P(temp>=0)=sqrt(temp(temp>=0));
Y_P(temp<0)=sqrt(abs(temp(temp<0)));
% FLUID DYNAMIC PROBLEM*****
    nleq=@(INC)(A(UNKNOWN,PIPE)*diag(Y_P)*A(UNKNOWN,PIPE)*
        INC(1:PP)+A(UNKNOWN,PIPE)*diag(Y_P)*
        A(KNOWN,PIPE)*PRESSURE-Gext_ENT(UNKNOWN)-
        Gext_EXT(UNKNOWN));
    options=optimset('TolX',tolNR,'MaxIter',1000,'Display',
        'off');
INCmeno1=[P(UNKNOWN)];
[INC, resnorm, erre, exitflag, output, jacob] =
    newtonraphson(nleq, INCmeno1, options);
Pmeno1=P;
Pnew(KNOWN,1)=PRESSURE;
Pnew(UNKNOWN,1)=INC(1:PP);
if max(abs((Pnew-Pmeno1)./Pmeno1))<=tolFLUID
    ver3=1;
else if max(abs((Pnew-Pmeno1)./Pmeno1))>tolFLUID
    errorFLUID=max(abs((Pnew-Pmeno1)./Pmeno1));
    P=Pmeno1*(a)+Pnew*(1-a);
else if Niter3>1000
    ver3=1;
    disp('***FLUID PROBLEM LOOP: Max number of
        iterations***');
    end
    end
end

```

```

end
P=Pnew;
Pm=0.5*(Aplus'*P+Aminus'*P);
for kk=1:PP
    Pmk=Pm(kk);
    Tmk=Tm(kk);
    x1.P_atm= Pmk/101000; %atm
    x1.T_degC = Tmk -273.15; %Celsius
    x1.ID = 1; %Pure CO2
    x1;
    props1=source_props(x1);
    Zm(kk) = getfield(props1,'Z'); %Compressibility
    Rhom(kk)=getfield(props1,'dens'); %Density kg/m3
    viscosity(kk)=getfield(props1,'visc')*0.001; %[Pa*s]
end
Niter4=0;
ver4=0;
S1=' THERMAL PROBLEM....NITER: ';
errorTHERMAL=NaN;
Tm_meno1=Tm;
while ver4==0
    yy=yy+1;
    kkk=kkk+1;
    Niter4=Niter4+1;
    S2=num2str(Niter4);
    S4=num2str(errorTHERMAL);
    display(strcat(S1,S2,S3,S4));
    cp_ent=zeros(node,1);
    JT_ent=zeros(node,1);
    cp_ent(ENT)=Cp_calc(P(ENT),T_ent(ENT),X,gas)*1e3; %J/kg/K
    JT_ent(ENT)=Joulethomson_new(P(ENT),T_ent(ENT))*1e-6;%K/Pa
    cp_ext=zeros(node,1);
    JT_ext=zeros(node,1);
    cp_ext(EXT)=Cp_calc(P(EXT),T(EXT),X,gas)*1e3;
    JT_ext(EXT)=Joulethomson_new(P(EXT),T(EXT))*1e-6;
    for jj=1:PP
        Pmj=Pm(jj);
        P_in=Aplus'*P;
        P_in_j=P_in(jj);
        P_out=Aminus'*P;
        P_out_j=P_out(jj);
        Tin_j=T_in(jj);
        Tout_j=T_out(jj);
        Tmj=Tm(jj);
        cp_in(jj,1)=Cp_calc(P_in_j,Tin_j,X,gas)*1e3;
        cp_out(jj,1)=Cp_calc(P_out_j,Tout_j,X,gas)*1e3;
        cp_branches(jj,1)=Cp_calc(Pmj,Tmj,X,gas)*1e3;
    end
end

for ll=1:PP
    P_in=Aplus'*P;

```

```

P_in_1=P_in(11);
P_out=Aminus'*P;
P_out_1=P_out(11);
T_in_1=T_in(11);
T_out_1=T_out(11);
Pml=Pm(11);
Tml=Tm(11);
JT_in(11,1)=Joulethomson_new(P_in_1,T_in_1)*1e-6;
JT_out(11,1)=Joulethomson_new(P_out_1,T_out_1)*1e-6;
JT_branches(11,1)=Joulethomson_new(Pml,Tml)*1e-6;
end
    for hh=1:node
        Ph=P(hh);
        Th=T(hh);
        cp(hh)=Cp_calc(Ph,Th,X,gas)*1e3;%J/kg/K
        JT(hh)=Joulethomson_new(Ph,Th)*1e-6;
    end
beta=UL(PIPE)./cp_branches(PIPE)./G(PIPE);
    gamma=JT_branches(PIPE).*Zm(PIPE)'.*f(PIPE)'.*RR.*G(PIPE).*
        abs(G(PIPE))./2./Pm(PIPE)./D(PIPE)./(AREA(PIPE).^2);
L=diag(cp_in);
K=-(JT_in.*cp_in).*P_in;
diagM=zeros(size(Ainput,1),1);
N=zeros(size(Ainput,1),1);
diagM(PIPE,1)=cp_out(PIPE).*exp(-(beta+gamma).*LL(PIPE));
M=diag(diagM);
    N(PIPE,1)=cp_out(PIPE).*(beta(PIPE)./(beta(PIPE)+
        gamma(PIPE))).*(Text(PIPE)-Text(PIPE).*
        exp(-(beta(PIPE)+gamma(PIPE)).*LL(PIPE)))-
        (JT_out(PIPE).*cp_out(PIPE)).*P_out(PIPE);
Vent=diag(cp_ext);
Went=diag(cp_ext.*JT_ext);
V=diag(cp_ext);
W=diag(cp_ext.*JT_ext);
E=Aplus*diag(abs(G))*L*Aplus'-
    Aminus*diag(abs(G))*M*Aplus'+
    IEplus*diag(abs(Gext))*V;
E(ENT,:)=zeros(length(ENT),node);
for zz=1:length(ENT)
    E(ENT(zz),ENT(zz))=1;
end
F=Aplus*diag(abs(G))*K-Aminus*diag(abs(G))*N-
    IEminus*diag(abs(Gext))*(Vent*T_ent-Went*P)-
    IEplus*diag(abs(Gext))*W*P;
F(ENT)=-T_ent(ENT);
T_meno1=T;
T=E\F;
    Tm(PIPE)=(1./LL(PIPE)).*((beta./(beta+gamma)).*Text.*
        LL(PIPE)+(Aplus'*T-Text)./(beta+gamma).*
        (1-exp(-(beta+gamma).*LL(PIPE))));
if max(abs(T-T_meno1)./T_meno1)<tolTHER

```

```

    ver4=1;
else if max(abs(T-T_meno1)./T_meno1)>=tolTHER
    errorTHERMAL=max(abs(T-T_meno1)./T_meno1);
    T=T_meno1*c+T*(1-c);
    T_in=Aplus'*T;
    T_out=Aminus'*T;
else if Niter3>1000
    ver4=1;
    disp('***NODE TEMPERATURE LOOP: Max number of
            iterations***');

end
end
end
end
if max(abs(Tm-Tm_meno1)./Tm_meno1)<tolMAIN
    ver1=1;
else if max(abs(Tm-Tm_meno1)./Tm_meno1)>=tolMAIN
    errorMAIN=max(abs(Tm-Tm_meno1)./Tm_meno1);
    Tm=Tm_meno1*d+Tm*(1-d);
    Niter1=Niter1+1;
else if Niter1>1000
    ver1=1;
    disp('***AVERAGE TEMPERATURE LOOP: Max number of
            iterations***');

end
end
end
end
%%% *****PROPERTIES CALCULATION AT FINAL CONDITIONS*****
for tt=1:node
    Pt=P(tt);
    Tt=T(tt);
    x2.P_atm= Pt*9.8692e-6; %atm
    x2.T_degC = Tt-273.15; %Celsius
    x2.ID = 1; %Pure CO2
    x2;
    props2=source_props(x2);
    Z(tt)= getfield(props2,'Z'); %Compressibility PR
    Rho(tt)=getfield(props2,'dens'); %Density kg/m3
end
Press=P./1e5; %bar
OUTPUT=[Press,T];

figure
lengthP=zeros(node,1);
LLkm=LL./1000;
for ii=1:length(LL)
    lengthP(ii+1)=sum(LLkm(1:ii));
end
LengthP=lengthP';
nodes=(1:node);

```

```

Text1=[Tsoil Text'];
ax=plotyy(LengthP,T,LengthP,P./100000)
hold on
plot(LengthP,Text1,'-.')
xlim(ax(1),[LengthP(1),LengthP(end)])
xlim(ax(2),[LengthP(1),LengthP(end)])
XtickP=linspace(0,L_tot,11);
xticks([XtickP])
xlabel('Pipeline Length [km]')
title('Temperature & Pressure profile along the pipe')
set(gca,'FontSize',20)
set(ax(2),'FontSize',20)
set(ax(1),'YLim',[288 325])
set(ax(2),'YLim',[100 118])
ylabel(ax(1),'T [K]')
ylabel(ax(2),'P [bar]')
set(ax(1),'Box','off')
set(ax(1),'YTick',[288:5:328])
set(ax(2),'YTick',[100:2:118])
legend('Temperature','Ambient Temperature','Pressure')
grid on
box on

```

APPENDIX B: Network model validation

The network described in 3.2. composed by two sources (Latrobe Valley and South New South Wales) and one sink (Gippsland) was modelled as three separated single trunks or as a whole network. The top-hole pressure (trunk C outlet pressure) was set 100 bar as stated by the CO2CRC [10]. The booster station at the Junction was not considered.

In Table 28, a comparison of the results obtained is presented as a model validation to highlight possible differences.

Table 28) Results comparison between modelling as a network or as single pipelines

	A	B	C
Network modelling			
Pipeline Inlet Pressure [bar]	138	138	118
Pipeline Inlet Temperature [K]	298,15	298,15	294,42
Single pipeline modelling			
Pipeline Inlet Pressure [bar]	139	137	118
Pipeline Inlet Temperature [K]	298,15	298,15	294,45

As can be seen from Table 28, only a slight difference is showed in the outlet temperature. The results highlight a good capability of the model to adapt to single pipeline or network calculation of pressure and temperature profiles during carbon dioxide transportation.